POLY(2,6-DIMETHYL-1,4-PHENYLENE OXIDE)-BASED SEMI-INTERPENETRATING POLYMER NETWORK PROTON EXCHANGE MEMBRANES FOR DIRECT METHANOL FUEL CELLS

FANG CHUNLIU

(M. Sc., University of Science and Technology of China)

A THESIS SUBMITTED

FOR THE DEGREE OF DOCTOR OF PHILOSOPHY

NUS GRADUATE SCHOOL FOR INTEGRATIVE SCIENCE AND

ENGINEERING

NATIONAL UNIVERSITY OF SINGAPORE

2012

DECLARATION

I thereby declare that the thesis is my original work and it has been written by me in its entirety. I duly acknowledged all the sources of information which have been used in the thesis.

This thesis has also not been submitted for any degree in any university previously.

_____

Fang Chunliu

25 January 2013

ACKNOWLEDGEMENT

TABLE OF CONTENT

SUMMARY

One of the barriers in the commercialization of direct methanol fuel cells (DMFCs) is the high methanol permeability of proton exchange membranes (PEMs) based on Nafion® or other perflurosulfonate polymers. This limitation prompted the development of alternative PEMs with high proton conductivity but lower methanol permeability. However, the tradeoff between proton conductivity and methanol permeability is often observed in the alternative PEMs. This thesis focuses on refining the use of a semi-interpenetrating polymer network (SIPNs) structure to mitigate the tradeoff.

A new SIPN design was proposed where ion pairs were used to reinforce the SIPN structure. The SIPN was synthesized by the covalent cross-linking of brominated poly(2,6-dimethyl-1,4-phenylene oxide) (BPPO) with ethylenediamine (EDA) in the presence of linear sulfonated PPO (SPPO). Ion pairs were formed during covalent cross-linking and strengthened the attachment of SPPO to the BPPO/EDA network in addition to the classical mechanical interlocking mechanism. The chemical resistance and dimensional stability of the membranes were consequently improved. The ion pairs also contributed to the more uniform distribution of SPPO in the cross-linked BPPO network, thereby increasingly the formation of connected hydrophilic channels upon water absorption to facilitate proton transport.

The relation between SIPN structure and membrane morphology was investigated next to optimize the application performance. The polymer network host structure was modified by using cross-linkers with different length and size (bulkiness). It was found that shorter or smaller cross-linkers were more capable than longer or bulky

cross-linkers in forming narrow and well-connected hydrophilic channels. The narrow and well-connected hydrophilic channels are not prohibitive to proton transport, but can increase the resistance to the transport of the larger methanol molecules, thereby increasing the selectivity in proton-to-methanol transport.

In this study of ion pair-reinforced SIPN membranes, the formation of ion pairs between acidic $-SO_3H$ groups and the basic amine moieties in the cross-links depleted some of the free $-SO_3H$ groups which would otherwise be used for proton conductivity. The effect is inevitable but there may exist an acid-base combination which could minimize the adverse effect of ion pair formation on proton conduction. Hence we investigated the proton transport mechanisms in several PPO-based PEMs cross-linked by acid-base complexes only. It was found that the protons were transferred through the water bridges between the acid and base sites in acid-base complexes by the Grotthuss mechanism. The average length of the water bridges controlled the proton transfer rate. Acid-base cross-linked membranes formed with acid-heterocyclic amine complexes were found to be more effective in proton transport than membranes formed with acid-aliphatic amine complexes.

LIST OF TABLES

LIST OF FIGURES

LIST OF SYMBOLS

AA	Acrylic Acid
AMPS	2-acrylamido-2-methyl-1-propanesulphonic acid)
APTES	3-Aminopropyl-triethoxysilane
BADE	Bisphenol A Diglycidyl Ether
BDE	1,4-Butanediol Diglycidyl ether
BPE4	2,2-bis(4-(acryloxydiethoxy)phenyl)propane
BPPO	Brominated Poly(2,6-dimethyl-1,4-phenylene oxide)
CCM	Catalyst-Coated membrane
CCS	Catalyst-Coated substrate
DAB	1,4-Diaminobutane
DAD	1,10-Diaminodecane
DAO	1,8-Diaminooctane
DEA	Diethylamine
DMA	Dynamic Mechanical Analysis
DMF	Dimethyl Formamide
DMFC	Direct Alcohol Fuel Cell
DMSO	Dimethyl Sulfoxide
DSC	Differential Scanning Calorimetry
DVB	Divinylbenzene
EDA	Ethylene Diamine
EMA	Ethyl Methacrylate
FPI	Fluorine-Containing Polyimide
GDL	Gas diffusion layer
HMDA	Hexamethylenediamine
HPDA	1,6-Hexanediol Propoxylate Diacrylate
ID	Imidazole
IEC	Ion Exchange Capacity
LBL	Layer-by-Layer
MEA	Membrane Electrode Assembly
MID	Methylimidazole
NMP	N-Methyl-2-Pyrrolidone
OCV	Open Circuit Voltage

PA	Propylamine
PAEEK	Poly(aryl ether ether ketone)
PAES	Poly(arylene ether sulfone)
PANI	Protonated polyaniline
PATBS	Poly(acrylamide-*tert*-butyl sulfonic acid)
PBAE	Poly(bisphenol A-co-epichlorohydrin)
PBI	Poly(benzimidazole)
PEEK	Poly(ether ether ketone)
PEM	Polymer Exchange Membrane
PEMFC	Polymer Exchange Membrane Fuel Cell
PES	Poly(ether sulfone)
PPO	Poly(2,6-dimethyl-1,4-phenylene oxide)
PPY	Polypyrrole
PS	Poly(styrene)
PSf	Polysulfone
PSSA	Poly(styrene sulfonic acid)
PSSA-MA	Poly(styrene sulfonic acid-*co*-maleic acid)
Pt	Platinum
PTFE	Polytetrafluoroethylene
PVA	Poly(vinyl alcohol)
PVDF	Poly(vinylidene fluoride)
PVP	Poly(vinyl pyrrolidone)
PWA	Phosphotungstic Acid
RDE	Resorcinol Diglycidyl Ether
Ru	Ruthenium
SAXS	Small Angle X-ray Scattering
SD	Sulfonation Degree
SIPN	Semi-interpenetrating Polymer Network
SPAEK	Sulfonated Poly(arylene ether ketone)
SPEEK	Sulfonated Poly (ether ether ketone)
SPEK	Sulfonated Polyetherketone
SPES	Sulfonated Polyether sulfone
SPI	Sulfonated Polyimide
SPPO	Sulfonated Poly(2,6-dimethyl-1,4-phenylene oxide)

SPS   Sulfonated Polysulfone

SPSE   Poly(styrene-ran-ethylene)

SiO$_2$ Silicon dioxide

SSA   Sulfosuccinic Acid

TEM   Transmission Electron Microscopy

TMBP   4, 4'-Diglycidyl (3, 3', 5, 5'-tetramethylbiphenyl) Epoxy Resin

VI   1-Vinylimidazole

XPS   X-ray Photoelectron Spectroscopy

CHAPTER 1

INTRODUCTION

1.1   Problem Statement

The phenomenal growth of portable electronic market in the last several decades presents a pressing need for clean and advanced power sources. The direct methanol fuel cells (DMFCs), where electrical energy is generated by oxidizing a liquid fuel ("methanol") at relatively low temperatures; have drawn considerable interest as a competing alternative to rechargeable batteries (Kerres, J. *et al.* 2002; Deluca, N. W. *et al.* 2006; Song, S. Q. *et al.* 2006). The advantages of DMFC are many: continuous operation (as long as methanol is available), high efficiency and energy density (in comparison with batteries), low environmental impact at the point of use, instantaneous refueling and the potential to use methanol from renewable sources (Kamarudin, S. K. *et al.* 2009). However, DMFCs also face tremendous challenge in the market. One of the major impediments is the high cost of a critical, lifetime-determining component of all DMFCs – the proton exchange membrane (PEM) (Shuqin, S. *et al.* 2007).

The PEM for DMFCs is a polymer electrolyte with ionizable groups which can support the transport of protons and water from the anode to the cathode while inhibiting selectively the crossing of methanol (Jagur-Grodzinski, J. 2007; Neburchilov, V. *et al.* 2007). The properties of PEM therefore have a deterministic influence on the fuel cell power output. A good PEM for DMFCs should satisfy several requirements, such as a sufficiently high proton conductivity, low methanol

permeability, good dimensional stability in both dry and hydrated states, and cost-effectiveness (Hickner, M. A. *et al.* 2004). The Nafion$^®$ membranes, which are perfluorosulfonate polymers with high proton conductivity, good dimensional stability and chemical resistance (Neburchilov, V. *et al.* 2007), satisfy many of the functional requirements, and are presently the most extensively used PEM. Nafion$^®$ membranes are however very expensive because of the high cost of polymer synthesis and membrane fabrication (Dunwoody, D. C. *et al.* 2006). Furthermore, Nafion$^®$ membranes also perform rather poorly in blocking methanol passage (Song, S. *et al.* 2005; Shuqin, S. *et al.* 2007).

The high proton conductivity and high methanol permeability of Nafion$^®$ membranes can be understood in terms of the large hydrophobic/hydrophilic difference between the fluorocarbon polymer backbone and pendent sulfonic acid groups. In the presence of water, microphase separation occurs between the hydrophilic and hydrophobic constituents: the sulfonic acidic groups associate to form a network of connected ionic domains (also known as the "hydrophilic channels"). This cluster network model was first proposed by Hsu and Gierke (Hsu, W. Y. *et al.* 1983). The hydrophilic channels in Nafion$^®$ are wide and extensively connected, allowing protons and methanol molecules to diffuse easily alongside the water molecules. The facile transport of protons and methanol gives rise to the observed high proton conductivity and methanol permeability (Wojciech, K. *et al.* 1992; Saito, M. *et al.* 2006).

The drawbacks of Nafion$^®$ have prompted a lot of efforts to develop alternative PEMs. One way to reduce the PEM cost is to replace the expensive fluorocarbon with lower cost hydrocarbon polymers. Among many of the proposed Nafion$^®$ alternatives,

membranes which are based on aromatic polymers, such as sulfonated poly(arylene ether ketone) (SPAEK) (Lin, H. D. *et al.* 2009), sulfonated poly (ether ether ketone) (SPEEK) (Lin, C. K. *et al.* 2009), sulfonated polysulfone (SPS) (Li, W. *et al.* 2010), sulfonated poly (phenylene)s (Wu, D. *et al.* 2008), and sulfonated polyimide (SPI) (Hu, Z. X. *et al.* 2009), exhibit the low methanol permeability needed for DMFC applications (Kreuer, K. D. 1997). In comparison with Nafion[®], the aromatic backbone of sulfonated aromatic polymers has a weaker affinity for methanol than a fluorocarbon backbone (Kundu, P. P. *et al.* 2007). This gives rise to some intrinsic methanol rejection properties of the membranes. In addition, the less flexible aromatic backbone, and the small hydrophilic/hydrophobic difference between the backbone and the pedant sulfonic acid groups, result in the formation of narrow and less-connected hydrophilic channels (Kreuer, K. D. 2001) where methanol passage is more hindered. However, proton transport is also affected by the narrow width and low connectivity of the hydrophilic channels; and low proton conductivity has become the Achilles heel of aromatic polymer membranes.

Integrating two conflicting yet critically important properties – high proton conductivity and low methanol permeability – in a single PEM is necessary for the development of high-performance PEMs for DMFCs (Higashihara, T. *et al.* 2009). Previous studies of Nafion[®] and sulfonated aromatic polymer membranes have highlighted the importance of the polymer main chain structure on hydrophilic channel formation. Structure-morphology studies have also indicated changes in the side chain structure could be used to modify the size and connectivity of the hydrophilic channels and hence the resultant membrane morphology (Peckham, T. J. *et al.* 2010). Consequently the proton conductivity-methanol permeability conundrum

can be mitigated by membrane morphology control. One obvious solution is to develop narrow but well-connected hydrophilic channels which can block off the larger methanol molecules while allowing the small protons to pass through freely. This requires a high-level of morphology control and a comprehensive understanding of the relationships between polymer chain structure, membrane morphology and application performance.

1.2   Objective and Scope of Thesis

The design of PEMs with narrow and well-connected hydrophilic channels is the particular interest of this thesis study as it has the greatest potential to address the proton conductivity/methanol permeability conundrum. Currently, PEMs with such morphologies are mostly prepared from specialty block/graft copolymers. The complex and multi-step synthesis of the block/graft copolymers is not amenable to large scale production and is a hindrance to market penetration (Higashihara, T. *et al.* 2009).

The primary objective of this PhD study is therefore to fabricate PEMs with both narrow and well-connected hydrophilic channels by using easily accessible commercial polymers, and by understanding and optimizing the structure-morphology-property relationships in membrane fabrication. Poly(2,6-dimethyl-1,4-phenylene oxide) (PPO) has been chosen as the base material as it has good mechanical strength and excellent hydrolytic stability. More importantly for the same degree of sulfonation, sulfonated PPO (SPPO) can provide higher proton conductivity than sulfonated aromatic polymers such as SPEEK, SPAEK and SPS. The aryl and benzyl positions of PPO are easily modifiable by bromination, sulfonation, and

carboxylation (Xu, T. W. *et al.* 2008). A semi-interpenetrating polymer network (SIPN) architecture was used to deliver the target morphology of narrow and well-connected hydrophilic channels. SIPN is a special class of polymer composites where a linear or branched polymer percolates extensively into a network of other polymers. The interpenetrating structure can provide better mixing of hydrophilic and hydrophobic segments at the molecular level. This results in a more uniform distribution of the hydrophilic domains within the hydrophobic polymer network; thereby increasing the probability and the number of connections between the hydrophilic domains (Gitsov, I. *et al.* 2003; Rohman, G. *et al.* 2005; Wu, X. *et al.* 2007). The hydrophobic segments were additionally cross-linked to restrain the aggregation of hydrophilic domains so that only narrow hydrophilic channels could be formed. These efforts were carried out in four specific projects:

1.2.1 Ion Pair-Reinforced Semi-interpenetrating Polymer Network for Direct Methanol Fuel Cell Applications

Ion pair-reinforced SIPNs were synthesized by immobilizing SPPO, a linear polymer proton source, in a brominated PPO (BPPO) network covalently cross-linked by ethylenediamine (EDA). The immobilization of SPPO in the SIPN network was accomplished not only by the usual means of mechanical interlocking, but also by ion pair formation between the sulfonic acid groups of SPPO and the amine moieties formed by the cross-linking reaction of BPPO with EDA. Through ion pair interactions, the immobilization of SPPO polymer in the BPPO network was made more effective resulting in a greater uniformity of sulfonic acid cluster distribution in the membrane. The hydrophilic amine-containing cross-links also compensated for some of the decrease in proton conductivity caused by ion pair formation. The SIPN

membranes prepared as such showed good proton conductivity low methanol permeability, good mechanical properties and dimensional stability. Consequently the PPO based SIPN membranes were able to deliver higher maximum power density than Nafion®, demonstrating the potential of the SIPN structure for PEM design.

1.2.2 Ion Pair-Reinforced Semi-interpenetrating Polymer Networks for Direct Methanol Fuel Cell Applications: Effects of Cross-linker Length

The primary function of cross-linker in any PEM design is to provide a mechanical stable hydrophobic network. The mesh width of the network may also affect other performance-related membrane properties. In order to evaluate the effects of network structure on the SIPN membrane morphology and properties, BPPO was thermally cross-linked by a series of aliphatic α,ω-diamines in the presence of SPPO. The length of the aliphatic α,ω-diamine cross-linker was varied to adjust the mesh width and hydrophobicity of the cross-linked network. The effects of such adjustments were investigated by examining the morphology of hydrophilic domains, water absorption, and PEM-related properties such as proton conductivity and methanol permeability. Increase in mesh width and hydrophobicity by long cross-linkers resulted in scattered hydrophilic domains and fewer contiguous water channels for proton conduction. On the contrary, short cross-linkers increased the proximity of hydrophilic domains in the membrane and promoted proton transport. Changes in the hydrophobicity of the network also strongly affected dimensional swelling and methanol permeability of the membrane.

1.2.3 Ion Pair-Reinforced Semi-interpenetrating Polymer Networks for Direct Methanol Fuel Cell Applications: Effects of Cross-linker Bulkiness

The effects of cross-linker bulkiness on the size and connectivity of the hydrophilic domains were investigated next. Four epoxides with different bulkiness, i.e., 1,4-butanediol diglycidyl ether (BDE), resorcinol diglycidyl ether (RDE), bisphenol A diglycidyl ether (BADE) and poly(bisphenol A-co-epichlorohydrin) (PBAE), were deployed as cross-linkers for the comparative study. The SIPN membranes were fabricated by thermally cross-linking aminated BPPO and the epoxide cross-linker in the presence of linear SPPO. It was found that the cross-linker bulkiness and hydrophobicity were particularly important in determining the membrane morphology, namely SIPN membranes with small (less bulky) and more hydrophobic BDE cross-links contained narrower and better-connected hydrophilic channels than other SIPN membranes formed with bulky and less hydrophobic cross-links.

1.2.4 Proton Transfer through Acid-base Complexes in Proton Exchange Membrane

Ion pair formation in the SIPN-based PEMs consumes free sulfonic acid groups. The depletion of proton source leads naturally to lower proton conductivity. In order to search for possible solutions that could reduce the adverse outcome of ion pair formation on proton conductivity, it is necessary to first understand the proton transport mechanism in membranes cross-linked only by acid-base pairs. Hence the final part of this thesis study was focused on the investigation of proton transfer through acid-base complexes. PPO was aminated by various aliphatic and heterocyclic amines (i.e., propylamine, diethylamine, imidazole and methylimidazole) and mixed with SPPO to form different acid-base cross-linked membranes. The

relationships between the basicity of the nitrogen group, state of water and proton transport mechanism in these membranes were determined. It was found that the proton conductivity of the membranes was dependent on the length of the water bridge between the acid and base sites of the complex, especially at low humidity levels.

1.3 Organization of Thesis

This PhD dissertation contains seven chapters. Chapter 1 (this chapter) outlines the motivations behind this thesis project, defines the scope of work and introduces the organization of the thesis topics. Chapter 2 provides a concise literature review of PEMs for the DMFCs; including their synthesis and properties. The preparation of ion pair-reinforced SIPN membranes is presented in Chapter 3. Chapter 4 and Chapter 5 focus on the study of the structure-morphology-property relationships of the ion pair-reinforced SIPN membranes. Chapter 6 examines the proton transport through the ion pairs in acid-base cross-linked PEMs. Chapter 7 is the conclusion chapter of this thesis study, which also includes some recommendations for future work.

CHAPTER 2

LITERATURE REVIEW

2.1   Scope of the Review

PEMs with high proton conductivity and low methanol permeability are necessary for the DMFCs. This chapter presents a concise review of PEMs for DMFCs in two sections. The first section introduces the technical background of DMFCs with emphasis on the membrane electrode assembly (MEA), the transport mechanisms in PEMs, and the current progress in PEM development. The literature survey will focus on developments which mitigate the conundrum between proton conductivity and methanol permeability of PEMs. The second section of this chapter scrutinizes the use of a particular polymer structure – the semi-interpenetrating polymer networks (SIPNs), for the PEM design in greater detail, in particular the synthesis and morphology control of SIPNs. It is believed that the nanoscale co-continuous phase morphology of SIPNs has the most potential for keeping proton conductivity high and methanol permeability low at the same time.

2.2   Direct Methanol Fuel Cells

2.2.1   Construction and Basic Operations of DMFCs

The DMFCs, working at relatively low temperatures (25-120 ^{o}C) and utilizing liquid methanol as the fuel directly, have been considered as an alternative to rechargeable batteries for mobile power generation for portable electronic products and electric

vehicles (Arico, A. S. *et al.* 2001). Quick refueling has been the most salient advantage. DMFCs convert the chemical energy in the fuel molecules continuously into electrical energy by the redox reactions on the anode and cathode, which are spatially separated by a PEM. Figure 2.1 is a schematic of a typical DMFC. Methanol is oxidized at the anode to CO_2 and protons, and oxygen is reduced at the cathode to water. A PEM maintains current flow in the cell by transporting protons from the anode to the cathode (Kamarudin, S. K. *et al.* 2009).
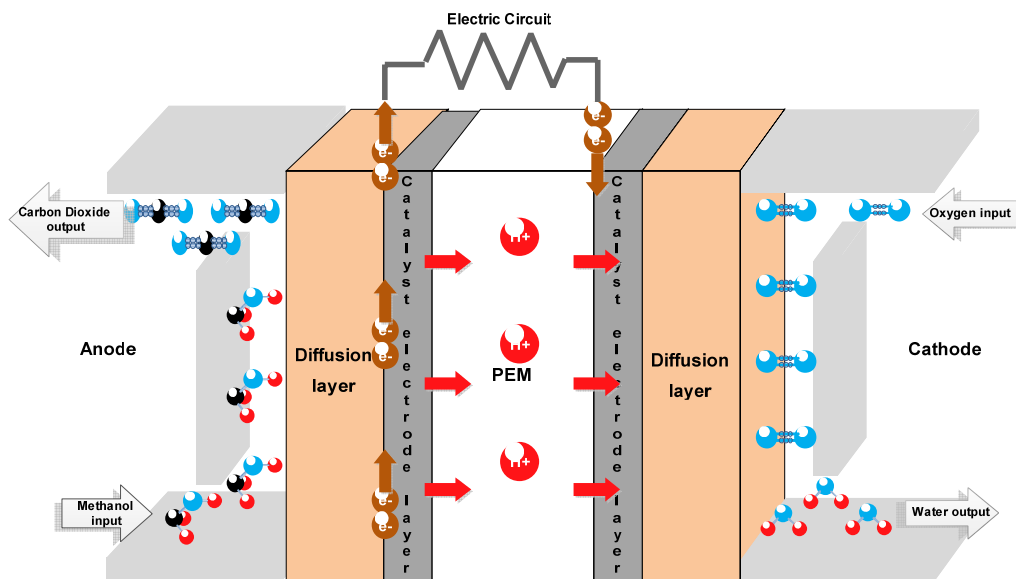
Figure 2.1 Schematic of a typical DMFC.

Anode reaction:

$$CH_3OH + H_2O \rightarrow CO_2 + 6H^+ + 6e^-$$

Cathode reaction:

$$\frac{3}{2}O_2 + 6H^+ + 6e^- \rightarrow 3H_2O$$

Overall reaction:

$$CH_3OH + \frac{3}{2}O_2 \rightarrow CO_2 + 2H_2O$$
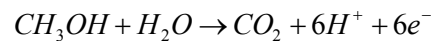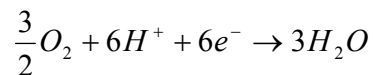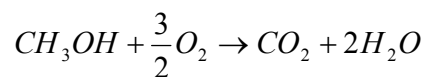
DMFCs are theoretically superior to rechargeable batteries because they are five to ten times higher in energy density, and are continuous in operation (batteries by comparison are batch systems). However, there is still a significant technology gap between the current state of development and commercialization such as the ineffective electro-oxidation of methanol and the crossover of methanol through the PEM (Lamy, C. *et al.* 2001; Song, S. Q. *et al.* 2006). The accumulation of unreacted methanol at the anode due to the low activity of the anode catalyst (especially at low temperatures) is the driving force for methanol diffusion through the PEM (Ren, X. *et al.* 2000). Methanol molecules are also transported by electro-osmotic drag in the PEM. A mixed potential is created at the cathode due to the interference of methanol oxidation with the oxygen reduction reaction. As a result the cell voltage and the cell performance (Gurau, B. *et al.* 2002; Qi, Z. *et al.* 2002; Song, S. *et al.* 2005) are lowered. Due to the irreversibility of the electrode reactions and methanol crossover, less than 30% of the chemical energy in methanol is convertible into electricity (Nakagawa, N. *et al.* 2009; Wan, C. H. *et al.* 2009). The DMFC efficiency can however be improved by (1) enhancing the activity of the anode catalyst for methanol oxidation; and/or (2) developing PEMs with good proton conductivity and methanol resistance (Bai, Y. *et al.* 2005; Mann, J. *et al.* 2006; Vigier, F. *et al.* 2006; Antolini, E. 2007; Wang, H. *et al.* 2007). Nafion$^{®}$, the ubiquitous PEM for the hydrogen fuel cells, is unsuitable for the DMFCs because of a high methanol permeability.

The fabrication of MEAs can also be a challenge for the DMFCs. Currently MEAs are fabricated by bonding the anode, the PEM, and the cathode into a hetero layer structure using Nafion$^{®}$ as the binder. The use of PEM materials other than Nafion$^{®}$

may introduce interfacial incompatibility between the catalyst layers and the PEM, as will be shown in the next section.

2.2.2 Membrane Electrode Assembly

In DMFCs, the PEM is sandwiched between two catalyst layers and two gas diffusion layers (GDLs) to form a MEA. Good fuel cell performance depends critically on the quality of the MEA. The fabrication of a good MEA is therefore key to the DMFC construction.
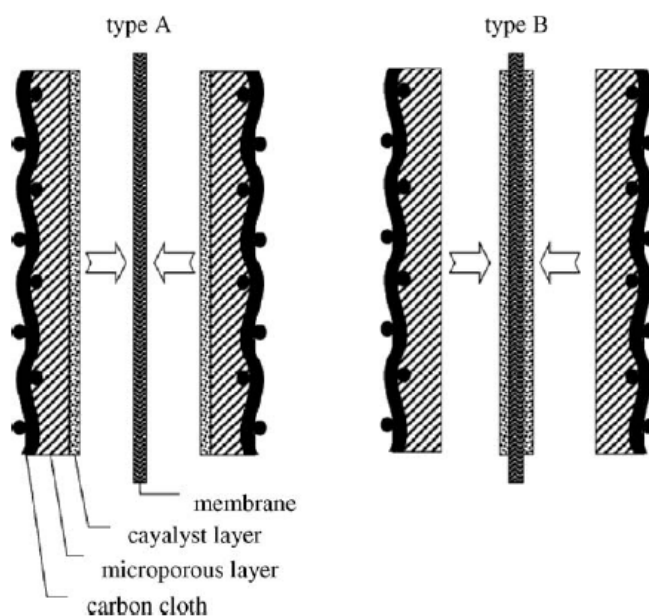
Figure 2.2 MEA fabrications (Qian, W. M. *et al.* 2006).

The interface between the PEM and the catalyst layer in a MEA establishes the triple-phase boundary where electrolyte, catalyst particles and fuel molecules are in intimate contact. There are two conventional MEA fabrication methods: the catalyst-coated substrate (CCS) method and the catalyst-coated membrane (CCM) method (Cho, J. H. *et al.* 2009). In the CCS method (Figure 2.2 type A), the GDLs, which are made from

carbon paper, cloth or felt, are first coated with the catalysts and then hot-pressed with the PEM to form an integrated sandwich structure. In the CCM method (Figure 2.2 type B), the opposing sides of membrane are coated with the catalysts by sputtering, physical or chemical vapor deposition, and then hot-pressed with the GDLs.
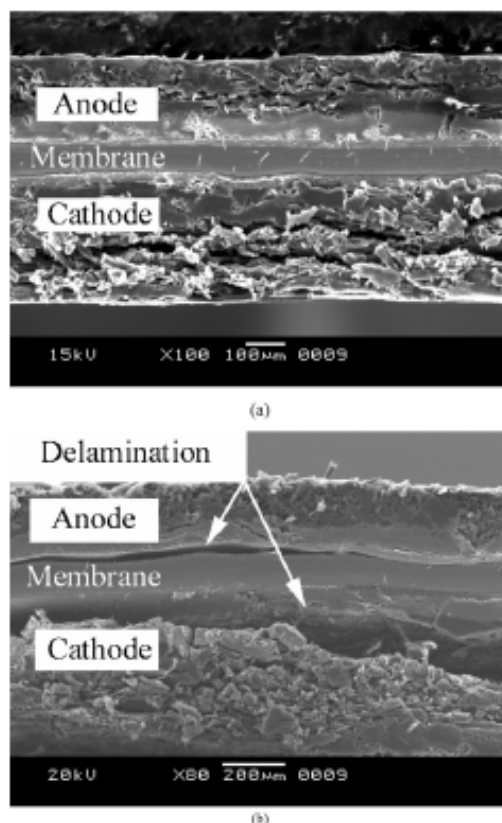
Figure 2.3 SEM images of MEA cross-section: (a) before and; (b) after 75 h of operation (Liu, J. G. *et al.* 2004).

From the processing perspective the CCS method is more suitable for the mass production of MEAs. However, the catalyst-coated GDLs may not integrate well with the membrane by hot-pressing. In particular, non-Nafion® MEAs prepared by this method often encounter interfacial degradation and delamination after prolonged operations. The cause is the incompatibility between Nafion® (which is used in the catalyst ink and as a binder) and the PEM material due to the significant differences in their physicochemical properties (Liang, Z. X. *et al.* 2006). Degradation normally

appears as a gradual increase of the fuel cell resistance with time. For example, severe delamination was detected in the MEA at the PEM-electrode interface after a DMFC was operating for 75 hours (Figure 2.3) (Liu, J. G. *et al.* 2004). The compatibility issue has to be carefully examined before a non-Nafion® PEM, which may have good properties on its own, can be adopted for the DMFCs.

This delamination problem is especially acute for the PEMs of aromatic polymers because the physicochemical properties and hence swelling characteristics of aromatic polymers are very different from Nafion® (Liang, Z. X. *et al.* 2006). Hence the MEAs of aromatic polymer PEMs are often fabricated by the CCM method. The MEAs made by this method have shown a stronger catalyst/membrane interface and better utilizations of the catalysts (Tang, H. L. *et al.* 2007; Cho, J. H. *et al.* 2009). There were also compatibilization methods such as introducing a Nafion® layer between the PEM and the electrodes (Lee, G. *et al.* 2007), roughening the PEM surface in order to increase the interfacial contact area and the interaction between the membrane and the catalyst layers (Wang, S. *et al.* 2005), optimizing the hot-pressing parameters, and etc. Other approaches include using Nafion® solution to bind the PEM and the catalyst-containing electrodes, or by replacing Nafion® with an alternative binder (Liang, Z. X. *et al.* 2006). Eason *et al.* fabricated MEAs using a SPEEK/dimethyl formamide (DMF) (or dimethyl sulfoxide, DMSO) solution as the binder (Easton, E. B. *et al.* 2005). The decrease in the interfacial resistance was however compensated by more easily flooding. Krishnan *et al.* examined the effects of sulfonated poly (ether sulfone) (PES) and partially fluorinated PES binders in the catalyst layer on fuel cell performance (Krishnan, P. *et al.* 2006). The fuel cell performance is generally poorer with these alternative binders than with Nafion® binder. Hence the integration of

alternative PEMs with the Nafion®-based binder system remains a challenging

problem.

2.2.3 Proton Exchange Membranes

DuPont's Nafion® membranes, with chemical structure shown in Figure 2.4, have

been the most ubiquitous PEM in the market today (Mauritz, K. A. *et al.* 2004).

However, their inherently high material cost, complex manufacturing process, and

high methanol crossover are significant challenges for the DMFCs, hindering their

commercial acceptance on a large scale (Neburchilov, V. *et al.* 2007).

$$—[(CFCF_2)(CF_2CF_2)_m]—$$
$$OCF_2CFOCF_2CF_2SO_3H$$
$$CF_3$$
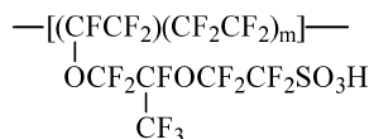
Figure 2.4 Chemical Structure of Nafion® (Mauritz, K. A. *et al.* 2004).

The limitations of Nafion® membranes have prompted extensive research efforts to

search for cost effective Nafion® substitutes. Many alternatives with sulfonic acid (–

SO_3H), phosphonic acid (–$PO(OH)_2$) and carboxylic acid (–COOH) functional groups

as the proton source have been proposed (Liu, J. G. *et al.* 2004; Easton, E. B. *et al.*

2005; Krishnan, P. *et al.* 2006). These alternative PEMs can be categorized into two

main groups: partially fluorinated membranes and non-fluorinated membranes. The

former includes blends of fluoropolymers and block and graft copolymers of

fluoropolymers (Sankir, M. *et al.* 2007; Kim, D. S. *et al.* 2008) such as

poly(vinylidene fluoride) (PVDF)/SPEEK blend membranes (Jung, H. Y. *et al.* 2009),

PVDF-co-hexafluoropropylene/poly vinyl alcohol (PVA) membranes (Kumar, G. G.

et al. 2009), and PVDF-g-poly(styrene sulfonic acid) (PSSA) membranes (Saarinen,

V. *et al.* 2007). The second group is dominated by sulfonated aromatic polymer membranes by virtue of their good mechanical and chemical stability, which are highly valuable for fuel cell applications.

The interest in sulfonated aromatic polymer membranes is mainly based on cost consideration and methanol permeability (Liu, J. G. *et al.* 2004; Rohman, G. *et al.* 2005). The use of relatively inexpensive fluorine-free hydrocarbon monomers is expected to lead to some cost reduction in membrane production (Neburchilov, V. *et al.* 2007; Kamarudin, S. K. *et al.* 2009). Hence a large variety of sulfonated aromatic polymer membranes have been developed over the years by different groups. Summaries of these works are nicely documented in the review articles of Neburchilov *et al.*, Jagur-Grodzinski *et al.*, Hickner *et al.*, Borup *et al.* and Harrison *et al.* (Hickner, M. A. *et al.* 2004; Harrison, W. L. *et al.* 2005; Hickner, M. A. *et al.* 2005; Borup, R. *et al.* 2007; Jagur-Grodzinski, J. 2007; Neburchilov, V. *et al.* 2007). A survey of the polymers in these reviews indicates that sulfonated aromatic polymer membranes generally have lower methanol crossover issues than Nafion[®] membranes. For example, the nitrated SPEEK membrane of Lin *et al.* has a methanol permeability of 1.76×10^{-7} cm^2 s^{-1}, which is about one order of magnitude lower than that of Nafion[®] (Lin, C. K. *et al.* 2009).

Although the sulfonated aromatic polymer membranes have strong methanol barrier properties and good mechanical and thermal stability, the weaker acidity of their sulfonic acid groups often results in a proton conductivity substantially lower than that of Nafion[®] membranes (Hickner, M. A. *et al.* 2005). While this can in principle be compensated by increasing the degree of sulfonation (Nakagawa, N. *et al.* 2009), a

heavily sulfonated aromatic polymer membrane is mechanically weak, and swells excessively in water especially at elevated temperatures (Di Vona, M. L. *et al.* 2005). The excessive swelling induces polymer disentanglement in the membrane matrix, decreasing the resistance to methanol crossover and hence a loss of proton/methanol selectivity (Kang, M. S. *et al.* 2005). Therefore, the tradeoff between proton conductivity and methanol permeability is a major deficiency of the aromatic polymer PEMs. Several strategies have been developed in the last two decades to address this deficiency. They can be classified according to the PEM structure as: (i) application of methanol barrier layer, (ii) doping with small inorganic particles, and (iii) ionic or covalent cross-linking, and (iv) membranes of highly ordered block/graft copolymers (Deluca, N. W. *et al.* 2006; Jagur-Grodzinski, J. 2007; Neburchilov, V. *et al.* 2007). The effectiveness of these solution strategies and current progress will be reviewed after some understanding of the transport mechanisms in PEMs, which is given in the next section.

2.2.3.1 Transport of Protons and Methanol in PEM

The transport mechanisms in PEMs have been studied most extensively for the Nafion® membrane. The popularity of this perfluorosulfonate membrane in fuel cell and other electrochemical engineering applications may be attributed to its unique microstructure. Several models based on experimental observations have been proposed to relate the transport properties of Nafion® to its structure. Among them the "cluster network" model (Figure 2.5) is the best known and provides a fundamental understanding of the existence of hydrophilic ionic clusters (Hsu, W. Y. *et al.* 1983); their structure and their contributions to the transport properties of Nafion® membranes. In simple terms, microphase separation occurs when Nafion® is hydrated

– the sulfonic acid groups aggregate to form interconnected clusters. The sulfonic acid clusters and surrounding water molecules form a continuous network of hydrophilic domains known collectively as the hydrophilic channels. The fluoropolymer backbone also assimilates into a continuous hydrophobic phase – a bicontinuous structure is therefore established in the membrane.
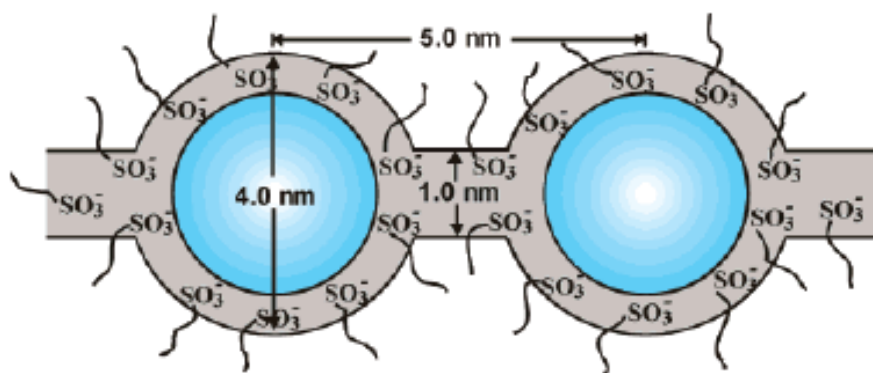
Figure 2.5 Cluster-network model for the morphology of hydrated Nafion$^{®}$ (Hsu, W. Y. *et al.* 1983).
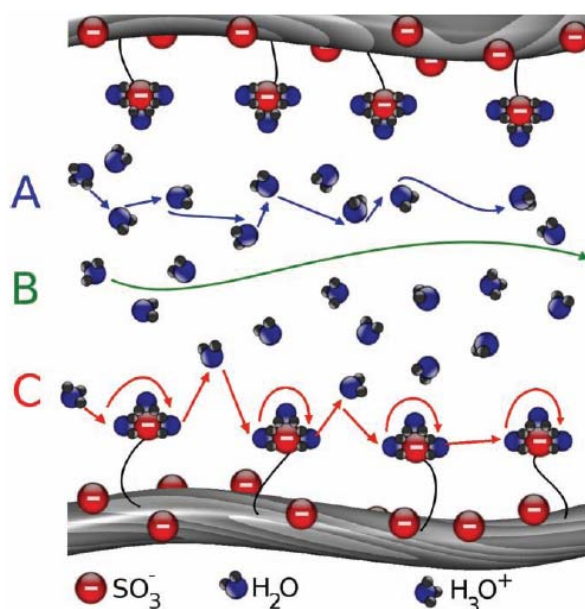
Figure 2.6 Schematic illustration of three mechanism of proton transport in a PEM where A= Grotthus; B=vehicular; C=surface mechanisms (Choi, P. *et al.* 2005).

Proton transport in hydrophilic channels is believed to occur by three mechanisms depending on the water environment (Figure 2.6). In the surface water region of the hydrophilic channels, proton transfer occurs by a surface diffusion mechanism through a series of hops between adjacent $-SO_3^-$ groups on the channel surface (Peckham, T. J. *et al.* 2010). In the bulk water region of the hydrophilic channels, proton transfer occurs by two complementary mechanisms: the Grotthuss mechanism and the vehicular mechanism (Kreuer, K. D. *et al.* 1982). The former involves the breaking and making of hydrogen bonds between proton-donating hydronium ions (e.g., $H_5O_2^+$ or $H_9O_4^+$) and proton-accepting water molecules and molecular reorientation (structure diffusion) (Eikerling, M. *et al.* 2001). The vehicular mechanism, on the other hand, involves the movement of proton-water aggregates in a process similar to molecular diffusion. The overall proton conductivity is the sum of the contributions from these three mechanisms. Previous studies have indicated that the relative contributions could be identified by the hydration number λ (the number of water molecules per sulfonic acid group in the membrane). The dominant proton conduction mechanism is Grotthuss diffusion at high water content ($\lambda > 14$), and the vehicular mechanism at moderately water content ($\lambda = 6\sim13$) (Paddison, S. J. *et al.* 2002; Kreuer, K. D. *et al.* 2004). As the water content decreases further ($\lambda < 6$), the strong association between SO_3^- and H_3O^+ makes it difficult for protons to transfer by the vehicular mechanism; and the surface mechanism becomes increasingly important (Eikerling, M. *et al.* 2001).

In addition to the water content, the connectivity of the hydrophilic channels is another critical factor in proton transport. Based on the results of small angle X-ray scattering (SAXS) measurements, Kreuer proposed the microstructures of hydrated Nafion® and sulfonated polyetherketone (SPEK) as shown in Figure 2.7 (Kreuer, K.

D. 2001). The most salient difference between the two PEM structures is the wider and better connected hydrophilic channels in Nafion[®]. This is the result of the extensive hydrophilic/hydrophobic microphase separation in Nafion[®] due to the presence of an extremely hydrophobic flexible tetrafluoroethylene (Teflon) backbone and hydrophilic sulfonic acid side groups. The resulting bicontinuous structure is highly conducive to fast proton transport. In sulfonated aromatic polymers, on the contrary, the acid groups are attached to a stiffer and less hydrophobic backbone which decreases the driving force for phase separation. The less extensive phase separation results in hydrophilic channels which are more branched and tortuous for proton transport, and consequently low proton conductivity.
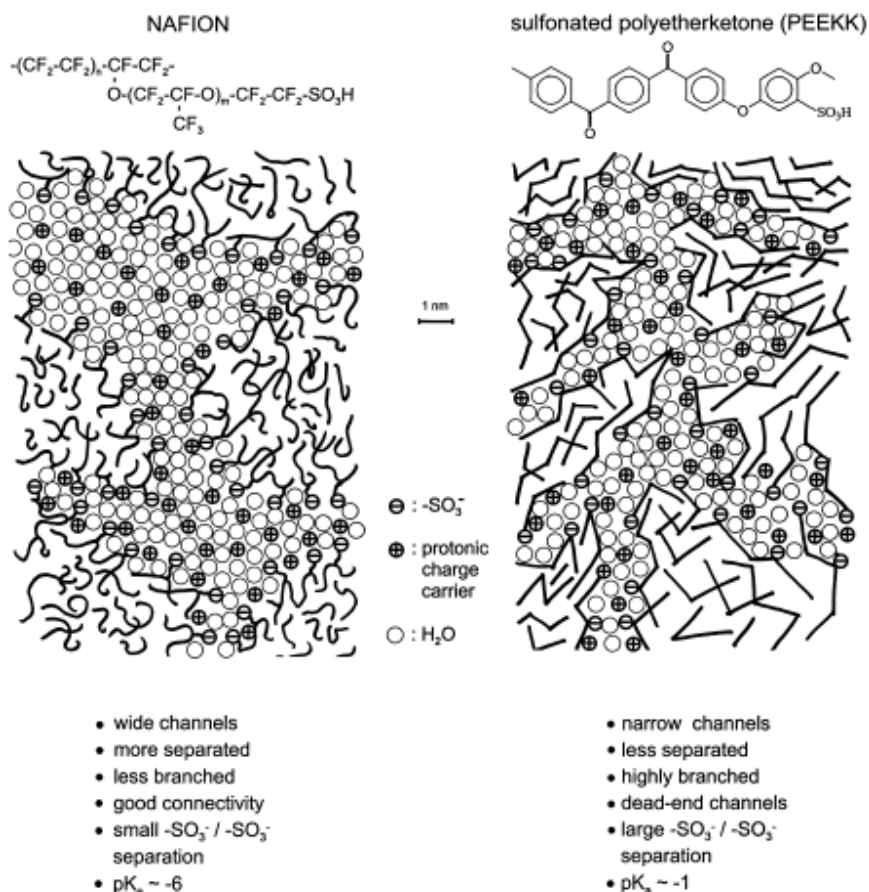
Figure 2.7 A schematic representation of the microstructures of Nafion[®] and SPEEK PEMs (Kreuer, K. D. 2001).

Methanol can exist in a variety of forms in a PEM: as self-associated clusters, $(CH_3OH)_a$, as complexes hydrogen-bonded to water, $(CH_3OH)_m(H_2O)_n$, and as proton bound complexes $H^+(CH_3OH)_b$. Therefore, methanol can be transported through the PEM by concentration gradients and electro-osmotic forces (Carrette, L. *et al.* 2001). Since methanol transport occurs alongside water molecules and protons in the hydrophilic channels, the methanol resistance of PEMs can also be altered by changing the size and the connectivity of the hydrophilic channels.

2.2.3.2 Mitigating the Tradeoff between Proton Conductivity and Methanol Permeability

The balance between high proton conductivity and low methanol permeability is the biggest challenge in the design of PEMs for the DMFCs. A number of methods have been proposed for mitigating the tradeoff between these two functional properties, most notably coating the membranes with various thin methanol barrier layers. For instance, a multilayer sulfonated poly(arylene ether ketone) (SPAEK)-based membrane was fabricated by coating SPAEK with alternating layers of oppositely charged polypyrrole (PPY) and phosphotungstic acid (PWA) formed by a layer-by-layer (LBL) construction (Lin, H. D. *et al.* 2009). The lowest methanol permeability of the SPAEK-(PPY/PWA) membranes was 0.73×10^{-8} cm^2 s^{-1}, which is more than one order of magnitude lower than that of Nafion$^®$ 117. A trilayer construction consisting of a central methanol barrier layer (Nafion$^®$-PVDF polymer blend) and two proton-conducting outer-layers (Nafion$^®$ or a mixture of Nafion$^®$ and $Zr(HPO_4)_2$ or SiO_2) was proposed by Si and coworkers (Si, Y. C. *et al.* 2004). Methanol permeability was found to depend on the PVDF content and the thickness of the barrier layer. Protonated polyaniline (PANI) has also been used as a methanol-

blocking layer for the Nafion$^®$ 117 membrane (Wang, C. H. *et al.* 2009). The composite membrane could reduce the methanol crossover in Nafion$^®$ 117 by as much as 59%. Although the effectiveness for methanol blocking was confirmed by these experimental results, the mutually compensating effect of methanol permeability and proton conductivity is still very rampant especially with increasing thickness of the barrier layer (Argun, A. A. *et al.* 2008; Wang, C. H. *et al.* 2009).

Inorganic particles have also been deployed as "obstructors" to decrease methanol permeation in the membrane (Staiti, P. *et al.* 2001; Li, Q. F. *et al.* 2003; Liu, F. Q. *et al.* 2003; Ainla, A. *et al.* 2007; Tay, S. W. *et al.* 2008; Sahu, A. K. *et al.* 2009). A variety of small inorganic particles have been tested including silica (Dimitrova, P. *et al.* 2002; Li, T. *et al.* 2010; Roelofs, K. S. *et al.* 2010; Zhong, S. L. *et al.* 2010), zirconium phosphate (Silva, V. S. *et al.* 2005), silane-derivatives (Kim, H. *et al.* 2009; Zhang, G. W. *et al.* 2009), titanium oxide (Yang, C. C. *et al.* 2010), montmorillonite (Gosalawit, R. *et al.* 2008) and zeolites (Herring, A. M. 2006; Wu, H. *et al.* 2007). These inorganic particles were originally used to overcome the membrane de-humidification problem in proton exchange membrane fuel cell (PEMFC) operating at high temperatures but were later found to be suitable for blocking methanol passage in the DMFCs. PEMs doped with the inorganic filler are effective in decreasing methanol permeation but at the great expense of proton conductivity. Hence they are not really useful for DMFCs. New filler designs were introduced including modifying the inorganic particles with acid functional groups and adding hydroscopic moieties to increase water retention. For example, PEMs based on poly(vinyl alcohol) (PVA)/silica inorganic-organic composites were prepared by a sol-gel method. – PO_3H_2 groups were then introduced to the inorganic constituent of the composites by

phosphorylation with phosphonic acid (Binsu, V. V. *et al.* 2005). The proton conductivity of the resulting membranes was derived from the phosphoric acid groups. Other acid functionalized inorganic particles have also been reported, including the heteropolyacid-functionalized silica (Kim, H. *et al.* 2007), sulfonic acid functionalized Y zeolite (Wu, H. *et al.* 2007), sulfonated oligomeric ionomer coated silica particles (Tay, S. W. *et al.* 2008), and etc. These composite membranes are definitely an improvement over the unmodified membranes in terms of methanol resistance and proton conductivity. However, they tend to be brittle with the increase in the loading of the inorganic phase.

The basic idea of cross-linking is to introduce specific interactions between the polymer molecules such as electrostatic interaction (ionic cross-linking) or chemical bonds (covalent cross-linking) to decrease methanol crossover. Many different types of ionically and covalently cross-linked membranes have been prepared and shown to be effective in lowering methanol permeability and restraining membrane swelling in water and methanol solutions (Kerres, J. A. 2001; Fu, R. Q. *et al.* 2008; Ye, Y. S. *et al.* 2009). Ionically cross-linked membranes are usually prepared from two polymers containing acid and base functionalities respectively, e.g., SPAEK and poly(benzimidazole) (PBI) (Feng, S. G. *et al.* 2010), SPPO and PBI (Kosmala, B. *et al.* 2002), sulfonated polysulfone (SPSf) and aminated PSf (Kerres, J. A. 2005), SPEEK and 5-amino-benzotriazole tethered PSf (Li, W. *et al.* 2010), sulfonated polyimide and pyridine-containing polyimide (Jang, W. *et al.* 2006), SPAEK and naphthyl group-containing PAEK (Guo, M. M. *et al.* 2009), just to name a few. Ionic cross-linking can also be achieved by using cross-linkers with basic groups. For example, Xue *et al.* synthesized a series of ionically cross-linked SPEEK-based

membranes using 3-aminopropyltriethoxy silane (APTES) (Xue, Y. *et al.* 2010). Through the hydrolysis and condensation of APTES, dispersed aminated silica was formed and immobilized in the membrane by the electrostatic interactions between the (basic) amine groups and the (acidic) sulfonic groups of SPEEK. The silica phase contributed to the suppression of methanol permeation in the membrane. Relative to ionic cross-linking, covalent cross-linking is stronger in restraining membrane swelling in water and alcohol solutions. In a previous report, a covalently cross-linked SPPO membrane was formed simply by the condensation reaction between sulfonic acid groups at high temperature (Wu, D. *et al.* 2010). This method, however, can lead to the loss of the sulfonic acid groups and consequently considerable decrease of proton conductivity. In addition, the sulfonic acid ester linkages formed are sensitive to hydrolysis under fuel cell operating conditions. Therefore, other functional group, such as carboxylic acid groups (Zhang, Y. *et al.* 2010) and bromomethyl groups (Zhang, G. *et al.* 2011), were introduced to the polymer backbone (e.g., PAEK and PEEK) to allow direct cross-linking between the polymer main chains. The carboxylic acid groups (or bromomethyl groups) can undergo Friedel-Crafts reaction with the phenyl rings of the polymer backbone to form inter- or intra-polymer covalent bonds (Zhang, Y. *et al.* 2010; Zhang, G. *et al.* 2011). The resulting membranes showed very substantial reduction of methanol permeability. The esterification reaction between the carboxyl acid groups of poly(aryl ether ether ketone) (PAEEK) and the hydroxyl groups of PVA has also been used to synthesize covalently cross-linked membranes (Liu, B. J. *et al.* 2008).

However, the cross-linked membranes also exhibit some major drawbacks. Ionic cross-linking lacks mechanical robustness, whereas covalently cross-linked

membranes tend to be brittle in the dry state (Kerres, J. A. 2005). Therefore, the synthesis of ionically-covalently cross-linked membranes was proposed. For example, Kerres *et al.* blended a sulfonated polymer, a sulfinate polymer, a polymer base and a dihalogeno cross-linker into ternary ionically-covalently cross-linked membranes (Kerres, J. *et al.* 2002). The dihalogeno cross-linker was used to alkylate the sulfinate groups to establish covalent cross-linking while the sulfonic acid groups interacted with the polymer base to form ionic cross-linking. This method combines the flexibility of ionically cross-linked membranes and the hydrolytic stability of covalently cross-linked membranes. Measurements showed lower water uptake and dimensional swelling in these membranes than ionically cross-linked membranes. However, macro phase-separation also occurred in the membrane because of the incompatibility between the sulfinate polymer and the polymer base. Later the authors overcome the incompatibility problem by developing binary ionically-covalently cross-linked blend membranes consisting of a sulfonated polymer and a polymer with both sulfinate and basic functional groups, or consisting of a base-modified polymer and a sulfonate-sulfinate polymer (Kerres, J. *et al.* 2003; Kerres, J. 2006). However, the synthesis of the acid- or base-modified polymers is rather time and labor intensive. It poses significant scalability challenges for volume production unless the steps can be greatly simplified.

Pore-filling electrolyte membranes were proposed by Yamaguchi to decrease the methanol crossover (Yamaguchi, T. *et al.* 2003). A pore-filling membrane generally contains two components: a porous substrate to provide mechanical strength and a filling polymer that occupies the pores of the substrate to provide proton conductivity (see Figure 2.8). A suitable substrate should satisfy two requirements: i) high

mechanical strength and no swelling even with the filled electrolyte under fully hydrated conditions; ii) uniform porosity. In pore-filling membranes, the mechanically robust substrate constrains the swelling of the filling polymer, thereby decreasing methanol crossover which would otherwise be caused by a freely swollen polymer. Many types of substrate have been examined including polyimide films (Yamaguchi, T. *et al.* 2005), porous silica (Moghaddam, S. *et al.* 2010), polytetrafluoroethylene (PTFE) (Liu, F. Q. *et al.* 2003; Wang, L. *et al.* 2007) and cross-linked polyethylene (Yamaguchi, T. *et al.* 2005). The selection of the filling polymer should be based on high proton conductivity and good compatibility with the porous substrate. Examples include poly(acrylamide-*tert*-butyl sulfonic acid (PATBS) (Yamaguchi, T. *et al.* 2003), sulfonated polyether sulfone (SPES) (Yamaguchi, T. *et al.* 2007), and poly(styrene-ran-ethylene) (SPSE) (Nguyen, T. H. *et al.* 2009), and etc.
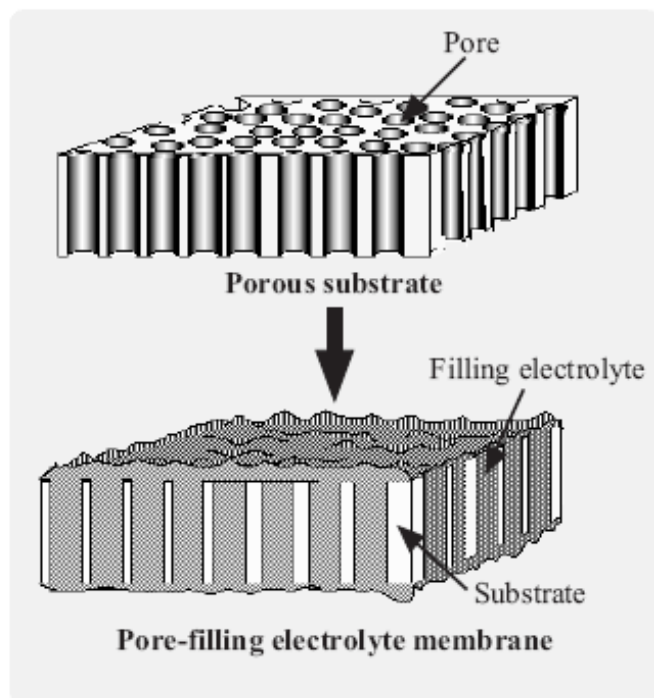
Figure 2.8 Concept of pore-filling electrolyte membranes (Yamaguchi, T. *et al.* 2007).

In practice, in addition to the requirements mentioned above, the substrate should also have pores on the sub-micrometer scale or lower. Yamaguchi *et al.* selected commercial porous polyimide as the substrate (Yamauchi, A. *et al.* 2007). Nguyen *et al.* fabricated the porous substrate by a wet phase inversion method (Nguyen, T. H. *et al.* 2009). As the filling polymer must completely occupy all the pores; the impregnation polymerization method is normally used to achieve this. Specifically, the pores of the substrate are first impregnated with a monomer solution, and then the substrate is put under the condition which can complete the pore-filling polymerization reaction. Direct impregnation of the pores with a dilute polymer solution was also attempted (Nguyen, T. H. *et al.* 2009). In that work the polymer was dissolved in a mixture of DMF and ethanol to lower the viscosity and to decrease the contact angle between the substrate and filling polymer. The polymer solution was infiltrated into the pores of the substrate by gravity. Although pore-filling membranes can reduce methanol crossover over a wide range of methanol concentrations, the demanding requirements on the various components and processes (a uniformly porous substrate, high conductivity and compatibility of filling polymers, and impregnation homogeneity) make the pore-filling membranes less well studied than cross-linked membranes and membranes doped with inorganic particles.

There have been some research papers on suppressing methanol permeation while preserving high proton conductivity by controlling the size and the connectivity of the hydrophilic channels in the membrane. Such membranes are mostly prepared from block/graft copolymers (Peckham, T. J. *et al.* 2010; Elabd, Y. A. *et al.* 2011). These studies suggest that methanol permeation can be suppressed by decreasing the channel size, while high proton conductivity can be maintained by ensuring that the

hydrophilic channels are well-connected. The channel size and channel connectivity can be altered by the constituents of the block/graft polymers such as increasing the size of the hydrophobic constituent in the block copolymer (Bae, B. *et al.* 2009), lowering the molecular weight of the copolymer (Jha, A. K. *et al.* 2011), and increasing the chain length of the block or the graft (Ding, J. F. *et al.* 2002; Lee, M. *et al.* 2009; Roy, A. *et al.* 2009). An ideal morphology was also proposed in the course of these studies: during microphase separation of the hydrophilic/hydrophobic constituents, narrow and interconnected channels formed by the hydrophilic polymers can provide a better selectivity of protons over methanol. The complement hydrophobic polymer segments provides the requisite mechanical properties to prevent excessive swelling in water (Higashihara, T. *et al.* 2009). Although block/graft copolymers have shown good tailorability and greater potential in addressing the tradeoff between proton conductivity and methanol permeability, their complex and multi-step synthesis is not easily amenable to mass production (Higashihara, T. *et al.* 2009).

2.3   Semi-interpenetrating Polymer Network

SIPN is a polymer comprising one or more polymer networks and one or more linear or branched polymers characterized by the penetration on a molecular scale of at least one of the networks by at least some of the linear or branched macromolecules (IUPAC definition) (Chikh, L. *et al.* 2011). The polymer constituents in SIPN are more entangled than in simple polymer blends, leading to forced miscibility and the formation of mechanically strong membranes. SIPNs are therefore useful for improving the membrane performance in a wide range of applications such as gas/liquid separation (Saimani, S. *et al.* 2010; Singha, N. R. *et al.* 2010), electrolyte

for the polymer lithium-ion batteries (Li, W. L. *et al.* 2012), drug-delivery; just to name a few (Liu, C. H. *et al.* 2010; Mundargi, R. C. *et al.* 2010).

2.3.1 Synthesis of Semi-interpenetrating Polymer Networks: *in situ* synthesis and impregnation synthesis
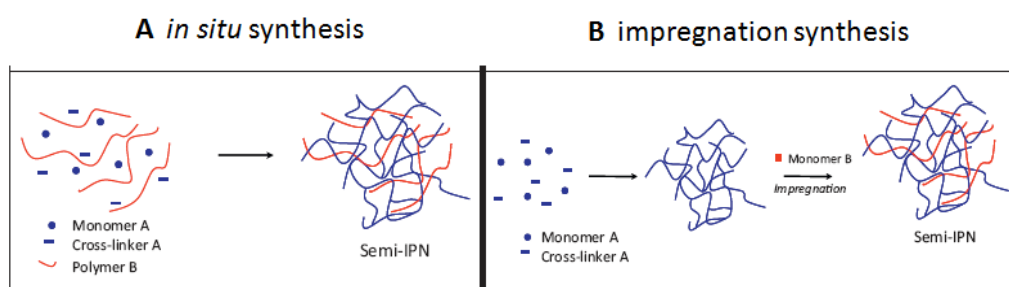
Figure 2.9 Schematics of *in situ* and impregnation synthesis of SIPN polymers (Chikh, L. *et al.* 2011).

SIPNs can generally be prepared by two synthetic pathways: *in situ* synthesis and impregnation synthesis (Figure 2.9). In the former all of the reactants are mixed in one-pot before the polymerization or cross-linking reaction. For impregnation synthesis a host polymer network is formed first followed by the polymerization of impregnated guest monomers in the network. For *in situ* synthesis, the synthesis of the polymer network and the linear (or branched) guest polymer may or may not be initiated at the same time, leading either to simultaneous or sequential formation of the SIPN structure (Kim, Y. S. *et al.* 1999). Therefore, the mechanisms of formation of the network polymer and the linear (or branched) polymer should be different in nature so as to prevent cross-reactivity resulting in copolymer formation. On the other hand, since the polymerization of the linear (or branched) polymer occurs within the confine of the host polymer network in impregnation synthesis, membrane

morphology is primarily controlled by the host polymer network. In addition, the extent to which the linear (or branched) polymer can be accommodated in the host polymer is determined by the swelling property of the network polymer.

The cross-linked network in SIPNs can oppose the demixing of polymer constituents thereby allowing polymers with very different properties to be assimilated into a more or less homogeneous material. Relatively small domains of different compositions are formed by microphase separation instead of the common macrophase separation found in most polymer blends.

Figure 2.10 Typical morphology of SIPN (Chikh, L. *et al.* 2011).

Microphase separation in SIPNs can occur by two mechanisms: the nucleation/growth mechanism and the spinodal decomposition mechanism. The nucleation/growth mechanism forms mostly spheroidal domains with domain size increasing with time. The resulting membrane typically shows a sea-island morphology in which the spheroidal domains of one of the polymers are dispersed in a matrix ("sea") of the other polymer. The spinodal decomposition mechanism, on the other hand, tends to form interconnected cylinders. The initial growth mechanism involves an exchange of

mass across the phase boundary of two polymers, resulting in increasing purity of the phases with time. This mechanism often leads to a membrane showing co-continuous phase morphology (Figure 2.10). The mechanism at work depends on the temperature and composition of the reaction mixture, especially the proportion of the dispersed phase. The nucleation/growth mechanism predominates when the proportion of the dispersed phase by weight is low. Increase in the proportion by weight gradually shifts the mechanism of phase separation to spinodal decomposition and membranes showing the co-continuous phase morphology are formed.

2.3.2 Semi-interpenetrating Polymer Networks as Proton Exchange Membranes
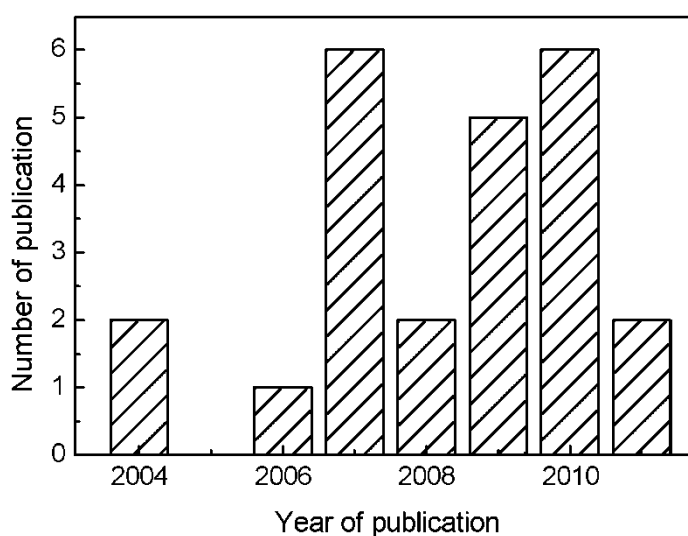
Figure 2.11 The number of papers containing the terms "SIPN" and "DMFC" published in recent years.

The good dimensional stability and homogeneity of the SIPN structure are useful for PEM fabrication (Guan, Y. S. *et al.* 2010; Pan, H. Y. *et al.* 2010; Shah, M. *et al.* 2010; Zapata, P. *et al.* 2010). In principle a linear polymer may be used as the distributed

proton source inside a cross-linked network which provides the mechanical stability.
In addition to enhancing mechanical stability through an interlocked structure, the co-
continuous matrix of SIPNs also has the greatest potential to deliver the desired
outcome of well-connected hydrophilic channels. However, only a small number of
studies have investigated the application of SIPNs as the PEMs of DMFCs in recent
years. Figure 2.11, which shows the number of papers containing the terms of "SIPN"
and "DMFC" published in recent years, is good evidence.

The synthesis of SIPNs for DMFC applications as summarized from these limited
number of studies is given in the next section. Properties of relevance to fuel cell
operations such as proton conductivity, methanol permeability, and dimensional
swelling are included and compared whenever available.

2.3.2.1 Nafion®-based Semi-interpenetrating Polymer Networks

Earlier discussion has shown that high methanol crossover is a major deficiency of the
Nafion® membranes in DMFC operation. It has been estimated that almost 40%
methanol could be loss in DMFCs with Nafion® membranes (Tricoli, V. *et al.* 2000).
In order to reduce the methanol crossover in Nafion®, some researchers have
proposed to associate Nafion® with different hydrocarbon polymer networks.
Therefore, SIPNs with entrapped Nafion® were synthesized.

Nafion®-based SIPNs can be prepared by the impregnation method, i.e., swelling the
Nafion® membrane in a monomer-containing organic solvent and then cross-linking
the monomers in the pores of the swollen Nafion® membrane photochemically or
thermally. By this means, the pores of Nafion® are filled with cross-linked polymers

to impede methanol transport. In order to maintain acceptable proton conductivity, monomers with sulfonic acid groups, such as 2-acrylamido-2-methyl-1-propanesulphonic acid) (AMPS) (Cho, K. Y. *et al.* 2004) and sulfonated styrene (Kundu, P. P. *et al.* 2007) were polymerized inside the pores of a swollen Nafion® membrane. Since sulfonated styrene is more polar and acidic than AMPS, the increased affinity for water resulted in membranes of higher water uptake and formation of some hydrophilic channels within the pores of Nafion®. The polymerized sulfonated styrene in the pores of Nafion® has shown acceptable methanol blocking capability.

The association of Nafion® with a cross-linked hydrocarbon polymer network is another approach which can be carried out by *in situ* synthesis. Here SIPN membranes are formed by casting a solution of dissolved Nafion® with other polymers such as fluorine-containing polyimide (FPI) (Figure 2.12) (Pan, H. Y. *et al.* 2010). The ethylene groups in FPI can be polymerized and cross-linked by free radical polymerization during membrane preparation to form the SIPN structure. In comparison with the pristine Nafion® membrane, the composite membranes have an improved dimensional stability. However, proton conductivity is lower in the composite membranes and the decrease in conductivity was found to increase with the fluorinated polyimide content. In another effort from the same research group, different vinyl group-containing cross-linkers including 2-propene-1-sulfonic acid sodium salt, 1-vinylimidazole (VI), acrylic acid (AA), and 1,4-divinylbenzene (DVB), were used as individual cross-linkers in the formation of Nafion®/FPI SIPN membranes (Pan, H. *et al.* 2010). FPI could react with these cross-linkers to from a host polymer network with Nafion® as the embedded linear polymer. Examination of

the properties of the resulting SIPNs suggested that the hydrophilic groups of SAS and AA induce a higher water uptake and hence could restore some of the lost proton conductivity. The conductivity is however still lower than that of the pristine Nafion® membrane. The other drawback of Nafion®/FPI SIPN membranes is the incompatibility between Nafion® and FPI when the FPI content is high (Pan, H. *et al.* 2010).
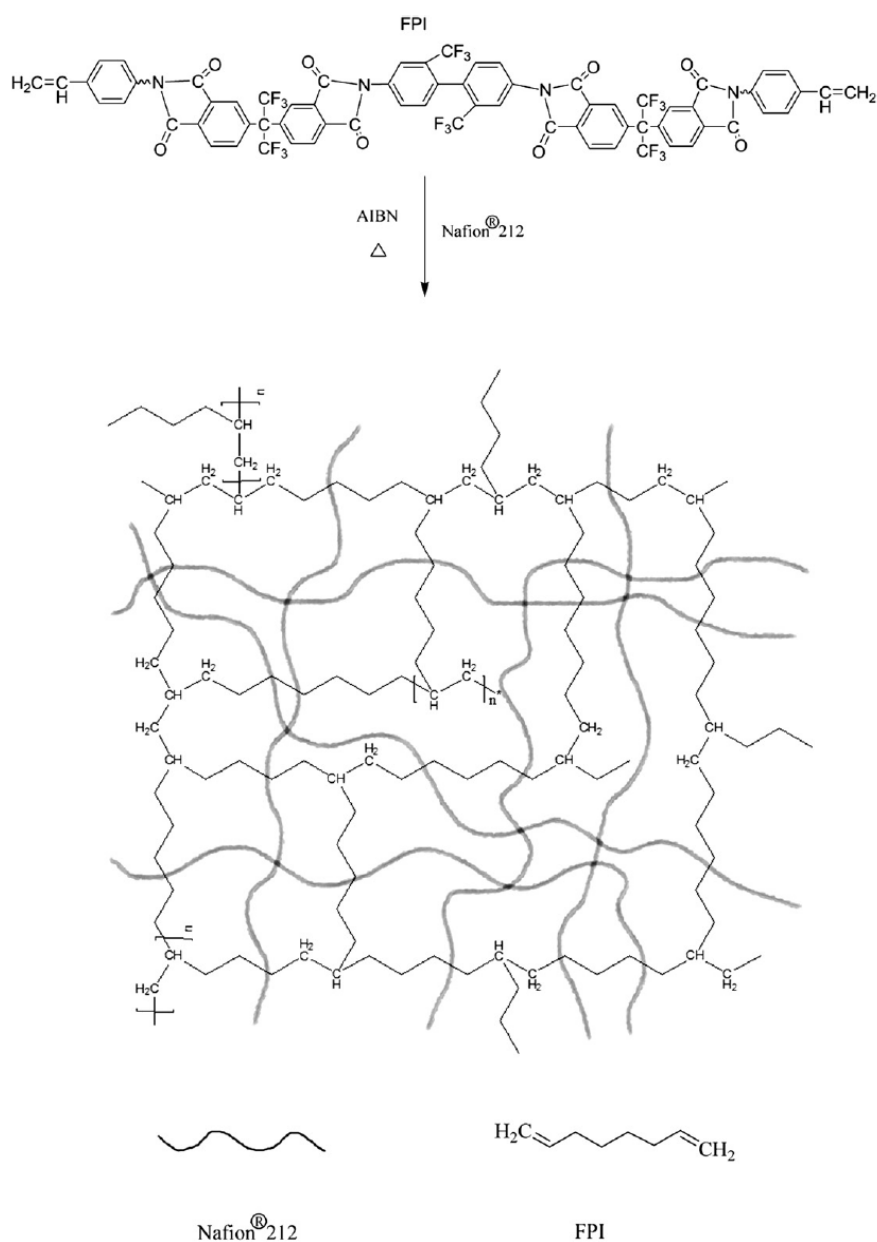
Figure 2.12 The SIPN structure of FPI/Nafion® 212 composite membrane (Pan, H. Y. *et al.* 2010).

Although the interlocking mechanism of SIPNs can improve the miscibility of different constituents to a great extent, gross phase separation can still occur in the polymer matrix (Chikh, L. *et al.* 2011), especially when the constituents differ greatly in polarity. There is a strong tendency for the more mobile linear polymer to retreat from the host polymer under certain conditions or with time, resulting in gross phase separation and the deterioration of application performance (Gitsov, I. *et al.* 2003; Lumelsky, Y. *et al.* 2008). Comparing between impregnation synthesis and *in situ* synthesis, the latter is more prone to the phase separation between Nafion® and other polymers when the proportion of one of them exceeds certain threshold values. An example is the *in situ* cross-linked divinylbenzene (DVB)/Nafion® SIPN membrane (Matsuguchi, M. *et al.* 2006). The withdrawal of Nafion® from the cross-linked DVB network was found to occur when the DVB mole ratio is higher than 0.10, resulting in reduced dimensional stability. This result indicates that *in situ* synthesis may not be a good strategy for fabricating Nafion®-based SIPN membranes because of the polarity difference between Nafion® and the cross-linked hydrocarbon polymer network.

In order to mitigate gross phase separation, Nafion® has to be entrapped by a more compatible polymer network such as poly(vinyl pyrrolidone) (PVP) (Li, T. *et al.* 2010). The strong polarity of the PVP molecule imparts good compatibility with the Nafion®. In addition, the acid-base interactions between the amine groups of PVP and the sulfonic acid groups of Nafion® could be used to stabilize Nafion® in the cross-linked network and decrease its retraction from the latter. The methanol permeability of the resulting SIPN membranes is 47% of that of Nafion® 117 while their proton conductivity is 38% higher than Nafion® 117. Although the study confirms that the Nafion®-based SIPNs is an improvement over pristine Nafion® membranes, the cost

of the PEM is likely to increase further because of the cost of post-processing the already high-cost Nafion® membranes.

2.3.2.2 Other Semi-interpenetrating Polymer Network Membranes

Poly(vinyl alcohol) (PVA)-based membranes are commonly used in the pervaporation dehydration of alcohols because they could preferentially permeate water and reject alcohol molecules (Chiang, W.-Y. *et al.* 1998). The high water/alcohol selectivity of PVA makes it a natural candidate material for the PEM of DMFCs (Huang, Y. F. *et al.* 2009; Kumar, G. G. *et al.* 2009; Higa, M. *et al.* 2010). Hence SIPN membranes combining PVA and other acidic polymers have been developed and tested. Lin *et al.* reported a series of PVA-based SIPNs with sulfosuccinic acid (SSA) as the cross-linking agent and poly(styrene sulfonic acid-*co*-maleic acid) (PSSA-MA) as the proton source (Lin, C. W. *et al.* 2007). The sulfonic acid groups in the SSA cross-linker could also contribute to proton conductivity. High proton conductivity was obtained at high PSSA-MA contents but the membranes also swelled excessively in water. The use of higher molecular weight PVA was found to be helpful in preventing the deterioration of membrane mechanical stability and reducing methanol permeability at the same time. Unfortunately, the ester linkages at the cross-linking points are easily hydrolyzed by protons under the acidic environment of DMFCs. (Tsai, C. E. *et al.* 2010).

Sulfonated aromatic polymers, with good materials properties such as low cost, high methanol resistance, outstanding thermal, chemical and mechanical stability (Hickner, M. A. *et al.* 2004) are another prime candidate for the SIPN construction. SIPNs combining sulfonated tetrmethyl PEEKs (STMPEEK), and a 4, 4'-diglycidyl (3, 3', 5,

5'-tetramethylbiphenyl) epoxy resin (TMBP)/sulfonated phenol novolac (PNBS) cross-linked network have been developed. During the formation of the cross-linked network, the epoxy groups of TMBP reacted with the phenol groups of PNBS to generate hydroxyl groups (Fu, T. Z. *et al.* 2009). As hydroxyl groups are hydrophilic, the cross-linked TMBP/PNBS network was expected to not only improve the methanol barrier property but also proton conductivity. Optimal results were obtained when the percentage of TMBP/PNBS by weight in the SIPN membrane was 14%. With the increase in the cross-linking of TMBP/PNBS, the proton conductivity of SIPNs decreased significantly due to low water content and hindrance to proton mobility from a heavily cross-linked matrix.

2.3.2.3 Morphology control of SIPN Membranes

Previous discussion suggests that hydrophilic domains well-connected to form a continuous pathway are most effective for proton transport. The size of the hydrophilic domains should also be sufficiently small to suppress methanol crossover. Many of the PEMs with both narrow and well-connected hydrophilic channels reported to date have been prepared from block/graft copolymers because the ordered microstructure of block/graft co-polymers facilitates a high-level of morphology control. However, the synthesis of block/graft copolymers is complex and not easily scalable for mass production (Higashihara, T. *et al.* 2009). Compared with the synthesis of block/graft copolymers, the fabrication of SIPNs offers the ease of preparation with equally good potential to form a desirable PEM morphology. This is because the interpenetrating structure forces a high level of intermixing of hydrophilic and hydrophobic constituents. A more uniform dispersion of the hydrophilic constituent in the hydrophobic polymer network can significantly increase the

connectivity of the hydrophilic channels (Gitsov, I. *et al.* 2003; Rohman, G. *et al.* 2005; Wu, X. *et al.* 2007). Therefore, the formation of co-continuous phase morphology is easier in SIPNs compared with the graft/block copolymer approach.

Previous studies on SIPN membranes reported co-continuous phase morphology, but only a few of them focused on decreasing the domain size. Kwon *et al.* prepared a series of SIPNs by mixing the poly(ether sulfone) with acrylate-terminated sulfonated poly(arylene ether sulfone) (SPAES) and ethylene glycol dimethacrylate (Kwon, Y. H. *et al.* 2009). The acrylate terminal groups of SPAES polymers could be cross-linked by ethylene glycol dimethacrylate under UV irradiation. In order to investigate the factors in phase separation kinetics, the authors altered the solvent-evaporation temperature and the hydrophilicity of SPAES polymers by capping the $-SO_3^-$ groups with different bulky cations such as Na^+ and tetrabutylammonium. Membrane morphology examination revealed that a smaller polarity difference between the hydrophilic and hydrophobic constituents and lower solvent-evaporation temperature could decrease the domain size and promote the formation of well-developed phase co-continuity. Jain *et al.* also studied SIPNs consisting of linear polysulfone in a cross-linked 2,2-bis(4-(acryloxydiethoxy)phenyl)propane network that was formed by addition polymerization. They found that the domain size was strongly dependent on the cross-linking degree, which could be varied by controlling the curing temperature and the radiation intensity (Jain, S. H. *et al.* 2003). However, these findings have not yet resulted in a consistent strategy for decreasing the hydrophilic domain size in practice. More understanding of the basic structure-morphology relationships is still needed in order to achieve a better control of the SIPN morphology. This thesis study is an effort in that direction.

<center>**CHAPTER 3**</center>

<center>**ION PAIR-REINFORCED SEMI-INTERPENETRATING**</center>

<center>**POLYMER NETWORK FOR DIRECT METHANOL FUEL CELL**</center>

<center>**APPLICATIONS**</center>

3.1 Introduction

In comparison to a typical polymer blend, the constituents of SIPN are more extensively interlocked to yield structures effective enough for forced miscibility between incompatible constituents and mechanical property enhancements (Wu, X. *et al.* 2007). The SIPN polymers are very adept at developing a co-continuous phase morphology for the membranes cast from them (Rohman, G. *et al.* 2005). The membrane mechanical and barrier properties, which are affected by the co-continuous phase morphology, can then be controlled through the careful design of the SIPN structure. Hence there have been studies on using SIPN membranes as the PEM for fuel cells (Kundu, P. P. *et al.* 2007; Kwon, Y. H. *et al.* 2009; Pan, H. *et al.* 2010). In these studies the proton source is often the linear polymer penetrant in a cross-linked polymer network which provides the mechanical properties.

Despite the promising prospects, SIPN membranes for PEM applications have yet to deliver satisfactory practical performance (Lin, C. W. *et al.* 2007; Huang, Y. F. *et al.* 2009; Tsai, C. E. *et al.* 2010). In many of the studies, the network polymer was cross-linked by ester linkages. The instability of ester linkages to hydrolysis under acidic and alkaline pH conditions (which are prevalent in fuel cells) can degrade the online

performance of these SIPNs. In addition, a common drawback of SIPNs is the high mobility of the linear constituent which may lead to the leaching of the linear polymer from the network host by swelling in an appropriate solvent. The result is a loose structure with gradually deteriorating application performance (Gitsov, I. *et al.* 2003; Lumelsky, Y. *et al.* 2008). A potential solution to this problem is offered in this study, which uses ion pair interactions between the functional groups of the linear polymer and the host network to strengthen their attachment. Through these interactions, the linear polymer can also be made more extended in the host polymer network to increase the distributed presence of the ionic clusters.

For PEMs, there is a known tradeoff between two important application properties – proton conductivity and mechanical properties – while strong hydrophilicity is preferred for proton conductivity, it also induces significant swelling to undermine the membrane integrity. There have been a number of ways to reduce this tradeoff and strengthen the membrane mechanical properties (Chang, H. Y. *et al.* 2003; Kerres, J. A. 2005; Xue, Y. *et al.* 2010). Among them, ionic cross-linking and covalent cross-linking are commonly applied. However, ionic cross-linking often lacks mechanical strength (Kerres, J. A. 2005) and covalent cross-linking often gives rise to brittleness of the membrane in the dry state and a marked decrease in proton conductivity (Kerres, J. 2006; Feng, S. *et al.* 2010). The SIPN structure may be the best solution to the conundrum – providing simultaneously good mechanical stability (through ion pair-reinforced interlocking) and effective proton conduction (through an extensive network of hydrophilic channels established by the uniform distribution of ionic clusters in an SIPN structure)

This chapter describes a new SIPN design where ion pairs are used to reinforce a covalently cross-linked network. Through the ion pair interactions, the immobilization of the linear polymer in the network can be is made more uniform. Furthermore the ion pair interactions also complement the covalent cross-linking to increase the membrane hydrolytic stability. More specifically the SIPN was synthesized from linear sulfonated SPPO, BPPO, and ethylenediamine (EDA) cross-linker by a one-pot thermal cross-linking procedure. PPO was chosen because it is a thermally and mechanically stable aromatic polymer with good chemical resistance. Its ease of processability and sulfonation are particularly suited for PEM fabrications (Xu, T. W. *et al.* 2008). Ion pairs were formed during cross-linking and strengthened the attachment of SPPO to the BPPO/EDA network. The SIPNs prepared as such contain more chemically resistant linkages to endure the DMFC operation. Measurements of membrane dimensional changes and hydrolytic stability confirmed the improvements made to the PPO membranes for DMFCs.

3.2   Experimental Section

3.2.1   Materials

PPO (M_w=30000, T_g=211 ^{o}C), chlorosulfonic acid (99.0~99.4%), N-methyl-2-pyrrolidone (NMP, 99%), EDA were purchased from Sigma-Aldrich. BPPO (59.1% benzyl bromide and 40.9% aryl bromide as analyzed by ^{1}H NMR spectrometry) was obtained from Tianwei Membrane Corporation Ltd. of Shandong (People's Republic of China). Chloroform (99%) and methanol (99.8%) were supplied by Merck. Nafion[®] 117 films were provided by Sigma-Aldrich.

3.2.2   Preparation of SPPO/BPPO/EDA SIPN Membranes

SPPO was synthesized by a published procedure using chlorosulfonic acid as the sulfonation reagent (Huang, R. Y. M. *et al.* 1984). Specifically, 3.5 mL chlorosulfonic acid was added to a PPO solution in chloroform (5 g of PPO per 100 mL of chloroform) at room temperature over a period of 30 min under vigorous stirring. The reaction was allowed to continue for 30 more minutes after the addition. The precipitate from the reaction was filtered off and dissolved in NMP and dried in an oven at 80 $^{\circ}$C for solvent removal. The oven-dried solid was washed with deionized water until the rinsewater was pH 6-7 and then vacuum-dried. The ion exchange capacity (IEC) of the SPPO synthesized as such was determined to be 2.58 mmol g^{-1}, or 39.1% degree of sulfonation according to the relation given in the literature (Kruczek, B. *et al.* 1998). BPPO and the synthesized SPPO were separately dissolved in NMP to a concentration of 30 mg mL^{-1} each. A predetermined amount of EDA cross-linker was added to the BPPO solution. After stirring for 12 h, the two solutions were mixed. The mixture was cast onto a glass Petri dish and cured at 80 $^{\circ}$C for 48 h and then at 100 $^{\circ}$C for 2h in vacuum. The resultant membrane was acidified in 1.0 M HCl for 24 h, washed several times with distilled water and air-dried.

The optimal SPPO to BPPO ratio, which is critical for the balance between various membrane properties such as dimensional swelling and proton conductivity, was determined first. Consequently, all the membranes in this study were prepared with this SPPO/BPPO ratio and variable EDA contents. These membranes are designated as EDA-5/1/x, where 5/1/x is the mole ratio of the functional groups ($-SO_3H/-CH_2Br/-NH_2$) used in the preparation. For example, EDA-5/1/0.15 is the membrane prepared from SPPO, BPPO and EDA in the functional group mole ratio of 5:1:0.15.

A membrane without the EDA cross-linker, EDA-5/1/0, was also prepared as the control.

3.2.3   Characterizations

Transmission electron microscopy (TEM) images were obtained from a JEOL JEM-2010 microscope operating at 200 kV accelerating voltage. The membrane samples for TEM examination were first treated with a saturated solution of $Pb(NO_3)_2$ for 24 h to enhance the imaging contrast between ionic and nonionic domains. The treated samples, after rinsing with distilled water and drying in a vacuum, were encapsulated in an epoxy embedding medium (Sigma-Aldrich) and sectioned to 50 nm slices by a Leica ultramicrotome. The slices were then placed on 100 mesh copper grid for TEM analysis. The thermal properties of the membranes were evaluated by differential scanning calorimetry on a METTLER TOLEDO DSC 822e in N_2 atmosphere. The membrane samples were heated from 25 to 270 ^{o}C at the rate of 10 ^{o}C min^{-1}. Dynamic mechanical analysis (DMA) of the membranes was performed on a TA Instruments DMA 2980. The analysis was carried out in air from 50 to 270 ^{o}C at 1 Hz frequency. Solid state ^{13}C NMR measurements were performed on a Bruker DRX-400 MHz NMR spectrometer operating at 100 MHz. X-ray photoelectron spectroscopy (XPS) spectra were collected from a Kratos Axis Ultra DLD spectrometer. All binding energies were referenced to the C1s carbon peak at 284.6 eV. Small angle X-ray scattering (SAXS) measurements were conducted on a Panalytical-PW 3830 equipped with two-dimensional wire detector and a Cu (λ=1.542 Å) rotating anode operating at 40 kV and 50 mA.

The water uptake (WU) by a membrane was determined by the difference in weights between dry (W_{dry}, g) and water-saturated states (W_{wet}, g). Water uptake was calculated as the wt% of the dry sample, i.e., WU = $((W_{wet} - W_{dry})/W_{dry}) \times 100\%$. The dimensional changes of a membrane were estimated by equilibrating a strip of sample in water at a prescribed temperature for 24 h, and then measuring the changes in length: $\Delta l = ((l_w - l_d)/ l_d) \times 100\%$ (where l_w and l_d are the lengths of the wet and dry membranes, respectively). The IEC of a membrane was determined by acid-base titration. First, a membrane in its native H^+ form was equilibrated in 1.0 M NaCl for 24 h to fully exchange the protons with sodium cations. The acidity in the NaCl solution was then titrated with 0.01M NaOH. IEC (mmol g^{-1}) was calculated as the moles of exchangeable protons per gram of the dry weight. Methanol permeability measurements were carried out using a two-compartment diffusion cell (Fu, R. Q. *et al.* 2008). One of the compartments was filled with 2.0 M methanol solution; and the other with deionized water. A membrane fully hydrated with deionized water was inserted between the two compartments. The increase in methanol concentration in the water compartment with time was monitored by gas chromatography (Shimadzu GC2010 with flame ionization detector). Methanol permeability (P, cm^2 s^{-1}) was calculated from the slope of the $C_B(t)$ vs. $t-t_0$ plot by the relation $C_B(t)= (A/V_B)(P/L)C_A(t-t_0)$, where C_A is the initial methanol concentration, $C_B(t)$ is the methanol concentration in the water compartment at time t, V_B is the volume of deionized water in the water compartment, L is the membrane thickness, and A is the effective diffusional area. Membrane proton conductivity was determined by the standard four-point probe technique. Impedance measurements in the frequency range 1 MHz to 50 Hz were taken by an Autolab PGSTAT 30 (Eco Chemie, Netherlands) potentiostat/galvanostat equipped with a FRA2 module (Frequency Response

Analysis). The membrane resistance (R, Ω) was obtained from impedance measurements by an established procedure (Sone, Y. *et al.* 1996). Proton conductivity (σ, S cm^{-1}) was then calculated from the equation $\sigma = L/RWd$, where L is the distance between the potential-sensing electrodes and W and d are the width and thickness of the sample, respectively.

3.2.4   Fabrication of Membrane Electrode Assembly and DMFC testing

Membrane electrode assemblies (MEAs) were prepared by the hot-pressing technique using the following electrodes from Alfa Aesar: unsupported Pt:Ru alloy (1:1) anode with 3.0 mg cm^{-2} total metal loading and unsupported Pt cathode with 2.0 mg cm^{-2} total metal loading. Nafion solution was used as the binder on both electrodes, and the active cell area was 5 cm^{2}. A wet sample membrane (or the reference Nafion$^{®}$ 117 membrane) was placed between two commercial electrodes and hot-pressed at 125 °C and 60 kg cm^{-2} for 3 min. The resultant MEA was stored in a tightly sealed container. DMFC measurements were performed on a single-stack micro DMFC supplied by Fuel Cell Technologies Inc. A feed of 2.0 M methanol aqueous solution was delivered to the anode compartment at 5 cc min^{-1} through a micropump. Dry oxygen was fed to the cathode compartment at 50 cc min^{-1}. DMFC performance was evaluated at 50 °C. As part of the cell conditioning, all cells were rested in the open circuit condition for 30 min before any measurement was taken.
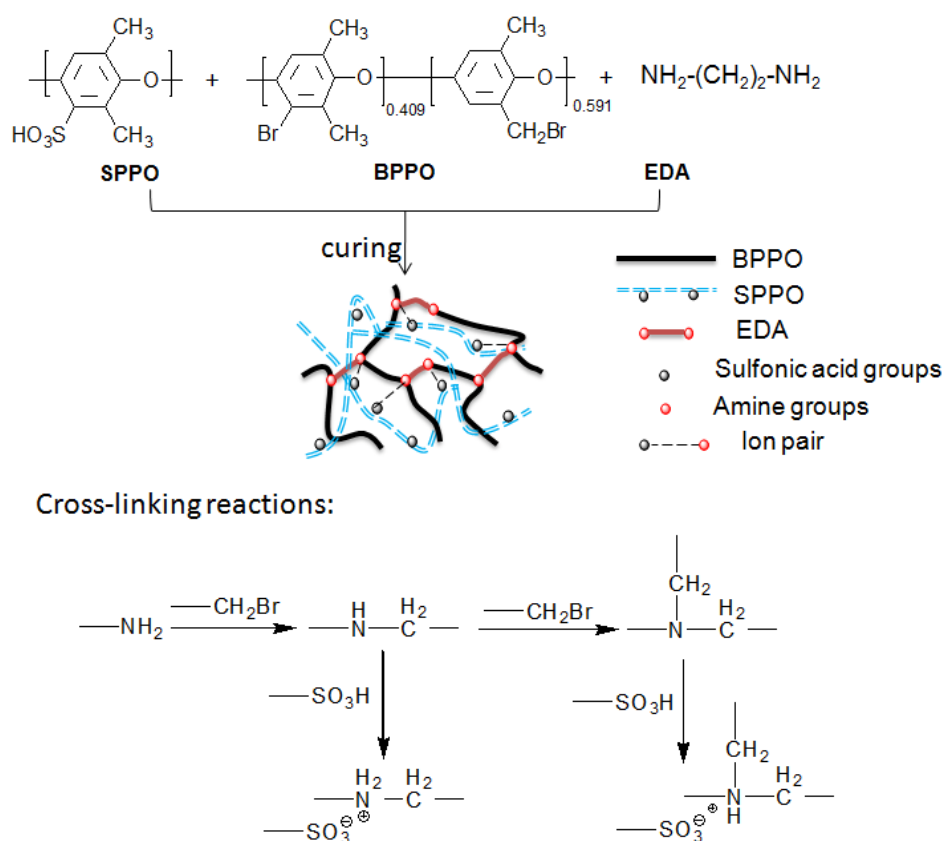
Figure 3.1 Preparation of SIPN membranes.

3.3   Results and Discussion

3.3.1   The Formation of Ion Pair-Reinforced SPPO/BPPO/EDA SIPN Structure

Figure 3.1 illustrates the main chemistry in the preparation of the SPPO/BPPO/EDA SIPN membranes where linear SPPO as the proton source was immobilized in a cross-linked BPPO/EDA network via one-pot thermal cross-linking. Since SPPO and BPPO are derived from the same PPO parent, good blending compatibility between SPPO and BPPO was assured. A covalently cross-linked BPPO network formed by the nucleophilic substitution reaction between EDA molecules and the bromomethyl groups of BPPO established the basic membrane mechanical framework. The progressive alkylation of EDA by the bromomethyl groups formed secondary and

tertiary amines in varying quantities, depending on the $-NH_2$ to $-CH_2Br$ ratio used. The quaternization of amine was however not observed under the experimental conditions (*vide infra*). Ion pairs (protonated amine-sulfonate anion) were formed by the acid-base reaction between the secondary/tertiary amines and the sulfonic acid groups of SPPO (Figure 3.1), which strengthened the attachment of SPPO to the BPPO/EDA network. The direct protonation of EDA by the sulfonic acid groups of SPPO (Kerres, J. A. 2005; Wu, D. *et al.* 2009) was also likely to occur during the mixing of SPPO and BPPO solutions initially.

$$\text{---}NH_2 \xrightarrow{\text{---}SO_3H} \text{---}SO_3^{\ominus} \ \ H_3\overset{\oplus}{N}\text{---}$$
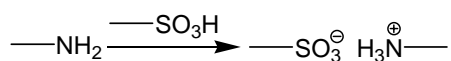
However, this acid-base reaction was soon superseded by the above-mentioned nucleophilic substitution reactions especially during curing of the membrane (*vide infra*).

The presence of different amine and ammonium moieties in the membranes was confirmed by ^{13}C solid-state NMR spectroscopy. Figure 3.2a and 3.2b show the ^{13}C NMR spectra of BPPO and an EDA-5/1/0.75 membrane, respectively. The six primary peaks (C_1-C_6) from 113 to 154 ppm could be assigned to the carbon atoms of the phenyl ring (Bonfanti, C. *et al.* 1994). The peaks at around 16 ppm and 28 ppm are characteristic of the aliphatic carbon in the methyl ($-CH_3$) and bromomethyl groups, respectively (White, D. M. *et al.* 1990). Figure 3.2b shows that amination of the bromomethyl group gave rise to new peaks at 37 and 49 ppm (C_7-C_8). The chemical shifts are typical of the decrease in electron density when aliphatic carbons are in close vicinity of secondary and tertiary amines, respectively (Sarneski, J. E. *et al.* 1975). This is an indirect indication that the EDA $-NH_2$ groups had reacted with the BPPO $-CH_2Br$ groups to form secondary and tertiary amine moieties.
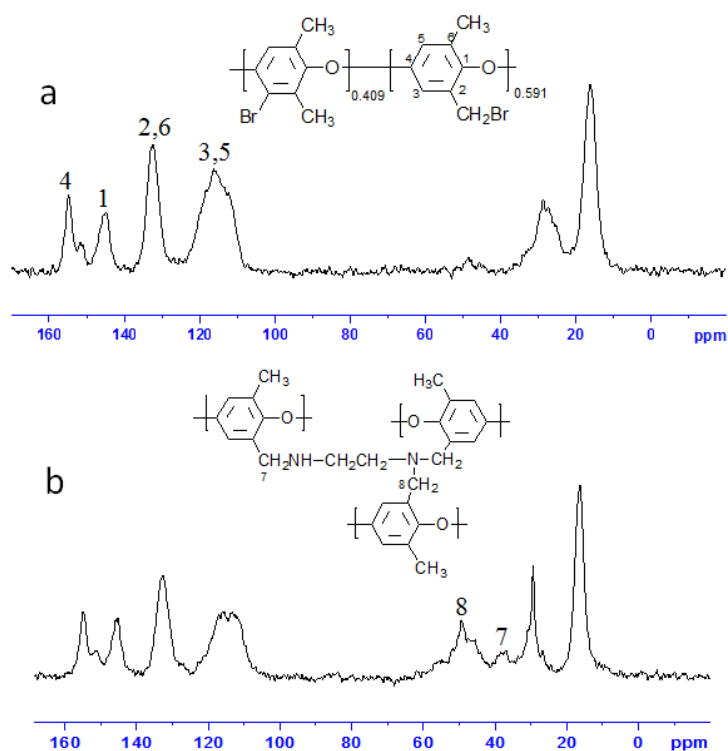
Figure 3.2 ^{13}C NMR spectra of BPPO and EDA-5/1/0.75 membrane.
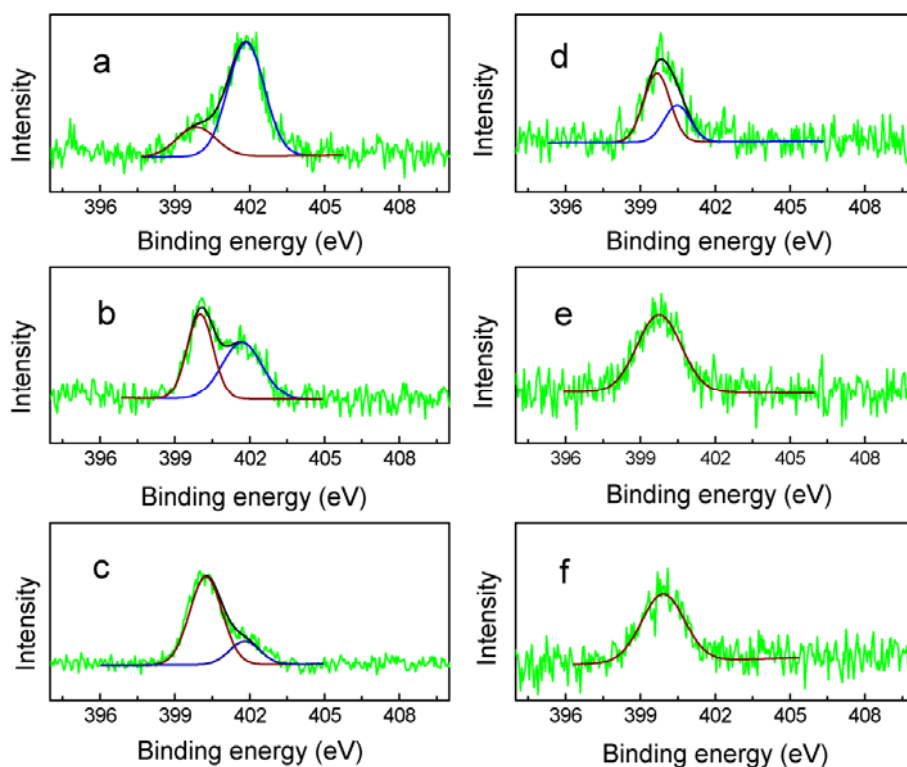
Figure 3.3 XPS spectra of SIPN membranes, (a) EDA-5/1/0.15, (b) EDA-5/1/0.45, (c) EDA-5/1/0.75, (d) EDA-5/1/0.15 after KOH treatment, (e) EDA-5/1/0.45 after KOH treatment, (f) EDA-5/1/0.75 after KOH treatment.

The amine and ammonium moieties (protonated amines) in the SIPN membranes were also characterized by XPS (Figure 3.3). There were two N1s peaks centering at about 399.9 eV and 401.8 eV for all SIPN membranes, which could be assigned to secondary (or tertiary) amines and positively charged N^+ species, respectively (Cheng, Z. P. *et al.* 2006). The N^+ species in the XPS spectra could exist in two forms: as protonated amines (i.e., $-NH_3^+$, $-RNH_2^+$ and $-R_2NH^+$) or quaternary ammonium ($-R_3N^+$). However, they could be differentiated by treating the SIPN membranes in 2 M KOH aqueous solution for 2 days and XPS re-examination. After the base treatment, protonated amine groups would be converted back to uncharged amines (i.e., $-NH_2$, $-NR_2$ and $-NHR$), whereas $-R_3N^+$ groups would become $-R_3N^+OH^-$. The XPS spectra of the KOH treated membranes (Figure 3.3d-f) did not show any N^+ peak, thereby ruling out the existence of quaternary ammonium groups $-R_3N^+OH^-$. Quaternization did not occur mostly due to steric hindrance. It should also be noted that no primary amine peak was identifiable in Figure 3.3d-f. Hence, the initial acid-base reaction between EDA and SPPO was replaced by subsequent substitution reactions between $-CH_2Br$ and EDA, which obliterated the existence of primary amines. This could be attributed to the presence of the $-CH_2Br$ group: CH_2 in the CH_2Br group is a reactive electrophile which could weaken the stability of $-SO_3^-\dots\ ^+NH_3-$ interaction to shift the equilibrium in the acid-base reaction towards ion pair dissociation. The elevated temperature used in curing could also improve the kinetics of the benzyl bromide attack on $-NH_2$ to form secondary or tertiary amines by nucleophilic substitution.
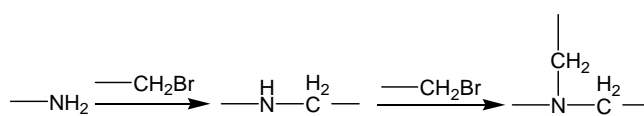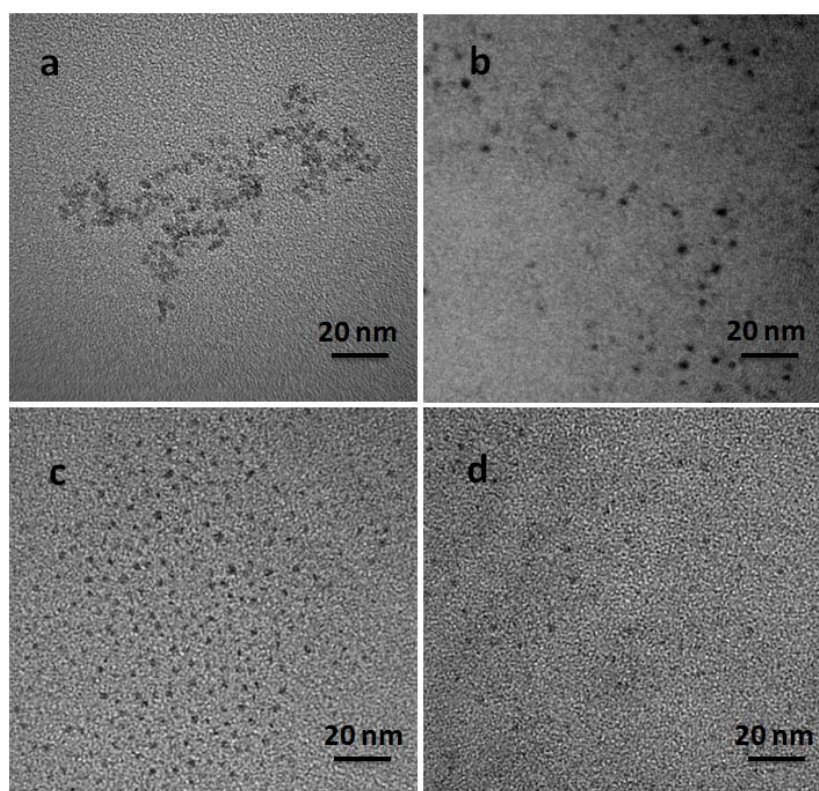
Figure 3.4 TEM images of the cross sections of (a) EDA-5/1/0 (b) EDA-5/1/0.15 (c) EDA-5/1/0.45 (d) EDA-5/1/0.75.

For membranes formed with a low EDA content, such as EDA-5/1/0.15, the peak intensity at 401.8 eV was significantly stronger than that at 399.8 eV (Figure 3.3a), suggesting that most of the amine groups were protonated and formed ion pairs with the sulfonic acid groups. With the increase in the EDA content (the EDA-5/1/0.45 and EDA-5/1/0.75 membranes), the prominence of the N1s peak at 401.8 eV diminished (Figure 3.3b and c). The decreasing proportion of positively charged N^+ species suggests the increase in steric hindrance when EDA cross-linking became more pervasive. Fewer $-SO_3H$ groups were sufficiently close to the amine groups to form ion pairs. The two N1s peaks of the KOH-treated EDA-5/1/0.15 membrane at 399.8 eV and 400.4 eV are characteristic of secondary and tertiary amines, respectively (Cheng, Z. P. *et al.* 2006). The EDA-5/1/0.45 and EDA-5/1/0.75 membranes, on the

other hand, showed only secondary amine peaks (Figure 3.3e and f). Hence, tertiary amines were not formed when the $-NH_2$ groups became abundant. This is because $-NH_2$ groups could only cross-link with proximal $-CH_2Br$ groups. An increase in the concentration of the $-NH_2$ groups depleted the $-CH_2Br$ groups locally. The likelihood of generating tertiary amines (which require a larger number of proximal $-CH_2Br$ groups) relative to the secondary amines therefore decreased as a result.
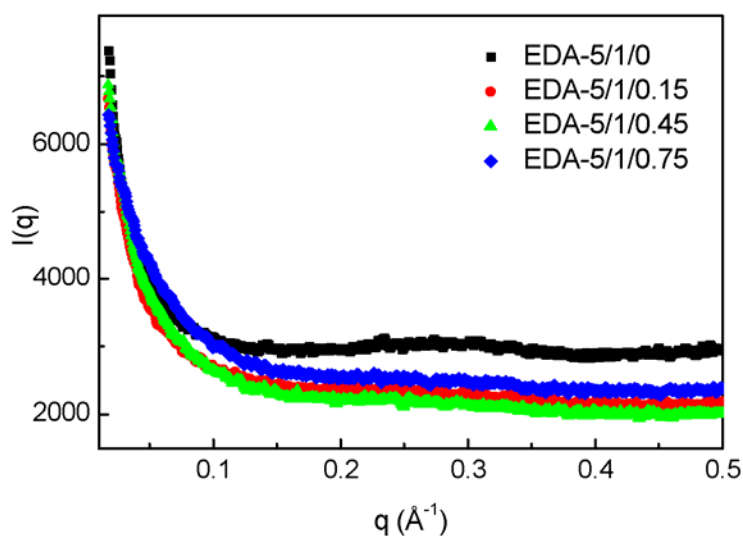
Figure 3.5 SAXS spectra of EDA-5/1/0 and various SIPN membranes.

The distribution of sulfonic acid clusters in the membrane matrix was inferred from TEM images of membrane cross-sections (Figure 3.4). The dark spots in the TEM images were sulfonic acid clusters stained by Pb^{2+} ions (as lead sulfonate) to improve the image contrast (Lee, M. *et al.* 2009). Figure 3.4a shows the cross-section of the control sample of un-cross-linked EDA-5/1/0 membrane. The Pb^{2+} stained sulfonic acid clusters spots were highly clustered and un-uniformly distributed. This is probably an indication of significant hydrophobic rejection of the $-SO_3H$ groups by the PPO backbone and the $-CH_2Br$ groups to form inverted micelle-like structures with sulfonic acid groups on the inside and hydrophobic segments (BPPO and

unsulfonated PPO) on the outside (Mauritz, K. A. *et al.* 2004; Schmidt-Rohr, K. *et al.* 2008). The dispersion of sulfonic acid clusters was significantly improved by EDA cross-linking, since all SIPN polymers showed more homogeneity of the lead sulfonate spots (Figure 3.4b-d). This could be attributed to following two contributions from cross-linking. First, the amine moieties at the cross-linking points are hydrophilic and as such decreased the hydrophobic rejection effect to result in a less pronounced microscopic phase separation. At the same time, ion pair formation between the amine moieties and the sulfonic acid groups increased the infiltration of SPPO into the cross-linked BPPO network. The more uniform distribution of the sulfonic acid clusters was also confirmed by SAXS measurements (Figure 3.5). The absence of a visible peak in the small angle region (0~0.35 Å^{-1} in scattering vector (q)) suggests a high dispersion of small sulfonic acid clusters in the polymer matrix (Essafi, W. *et al.* 2004). The uniform distribution of sulfonic acid clusters made it more likely to form a connected network of hydrophilic domains upon water absorption to facilitate proton transport. Among the SIPN membranes, the one formed with a moderate EDA content (EDA-5/1/0.45) had the most uniform distribution of the sulfonic acid clusters. It is theorized that low EDA content (e.g., EDA-5/1/0.15) formed predominantly tertiary amine cross-linking points, and high EDA content (EDA-5/1/0.75) formed a dense and excessively cross-linked network. Both were significant steric barriers to the uniform distribution of the sulfonated acid clusters. Hence an intermediate EDA content was more likely to achieve a balanced outcome for effective proton conduction through the membrane.

3.3.2 Thermal and Mechanical Properties

The results from ^{13}C NMR, XPS and TEM all hinted at the formation of an ion pair-reinforced interlocked SIPN structure. DSC and DMA measurements were subsequently used to provide further experimental evidence.

For DSC measurements, the membrane samples were subjected to two consecutive scans: an initial conditioning scan from 25-150 ^{o}C followed immediately by the measurement scan from 25-270 ^{o}C. Figure 3.6 shows the second-scan DSC thermograms of SPPO, BPPO and four SIPN membranes. Two endothermic transitions could be detected between 50 and 250 ^{o}C in the DSC thermograms of SPPO and SIPN membranes. The first endothermic peak (I) at lower temperatures has been observed for other ionomers (e.g., Nafion$^{®}$), although its assignment is still under debate. Page *et al.,* for example, considered this peak as the melting of small imperfect polymer crystals (Page, K. A. *et al.* 2005). Goddard *et al*, on the other hand, attributed this endothermic peak to enthalpy associated with water vaporization and water leaving the coordination environment of ions (Goddard, R. J. *et al.* 1994). Since the second scan in this study was run right after the first one, volatile solvent and water should all have been eliminated after the heating in the first scan. Consequently we are more inclined to attribute the first endothermic peak to the movement of short, unsulfonated PPO chain segments of SPPO. The sulfonation process placed sulfonic acid groups on the PPO chains at nearly regular intervals and increased the interchain distance between unsulfonated segments. The relaxation of the spatial constraint on the segmental motion of unsulfonated segments is shown by a glass transition temperature (T_g) which is well below that of pristine PPO (211 ^{o}C). Figure 3.6 also shows a fairly broad second endothermic peak (II) around 243 ^{o}C for SPPO indicative

of the clustering of the sulfonic acid groups due to hydrogen bonding and dipole-dipole interactions (Carbone, A. *et al.* 2006). These intra- and inter-molecular forces hindered the rotation of the sulfonated phenyl rings relative to the unsulfonated segments.
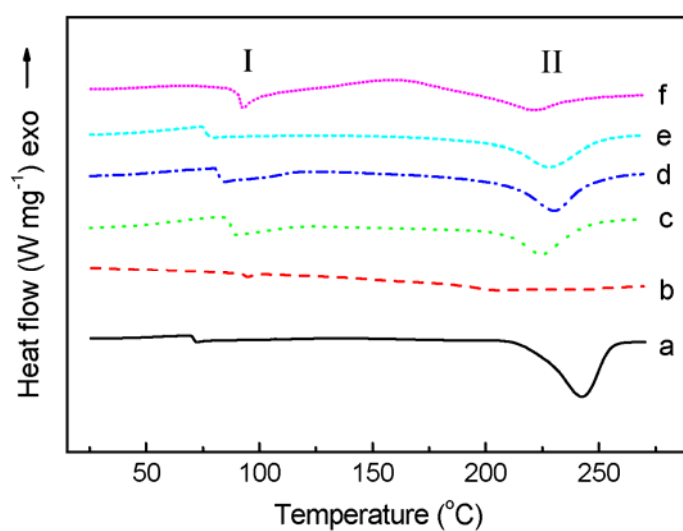
Figure 3.6 DSC curves of SPPO (a), BPPO (b), EDA-5/1/0 (c), EDA-5/1/0.15 (d), EDA-5/1/0.45 (e) and EDA-5/1/0.75 (f).
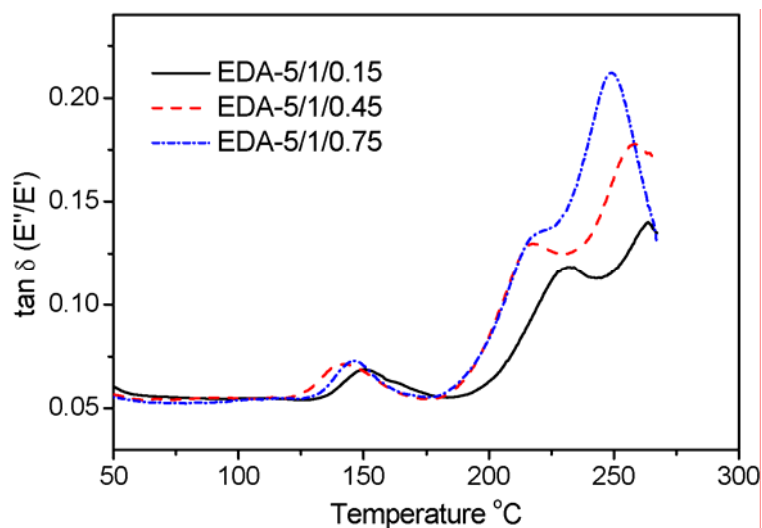
Figure 3.7 Temperature dependence of tan δ of SIPN membranes.

Different from SPPO, BPPO showed a very gentle glass transition at around 175 $^{\circ}$C. This is because the bulky bromomethyl group increased the polymer free volume,

allowing the segments to move more freely. Less energy was therefore required for glass transition.

For the EDA-5/1/0 membrane, the second endothermic peak was shifted to a lower temperature than SPPO. This could be caused by the partitioning effect of BPPO which disrupted the clustering of the sulfonic acid groups and weakened the interactions in the latter responsible for chain rotation impediment. The shape of the second endothermic peak (II) and the peak temperatures of the three SIPN membranes also display an interesting trend: with a $-CH_2Br/-NH_2$ ratio of 1/0.15, the peak temperature was about 7 ^{o}C higher than that of EDA-5/1/0, indicating the constriction effect imposed by cross-linking and protonated amine–sulfonate ion pairs. When the ratio was increased to 1/0.45, there was no increase in the peak temperature but peak broadening was observed. Further increases of the ratio to 1/0.75 resulted in a lower temperature and a broader peak. Peak broadening is an indication of a more continuous distribution of energy barriers against the thermal motion of sulfonic acid groups. The multitude of interactions between sulfonic acid groups—hydrogen bonding, dipole-dipole interactions and ion pair formation—was likely the reason. The changes in the peak temperature of the second endothermic peak (II) were also mirrored by the DMA measurements. In Figure 3.7, the $\tan\delta$-T curves show three types of relaxations in the SIPN membranes: a weak β relaxation centering about 140 ^{o}C and two intense peaks above 200 ^{o}C. The weak β relaxation could be attributed to the chain motion of short unsulfonated PPO segments (Di Noto, V. *et al.* 2010). The two intense peaks correspond well with the broad second endothermic peak (II) in the DSC thermograms. The lower temperature peak could be related to interactions such as hydrogen bonding, dipole-dipole interactions between the sulfonic acid groups, and

ion pairs, while the higher temperature peak related more to the relaxation of the entire SIPN structure. It was found that as the EDA content increased from 0.15 to 0.75, both peaks were shifted to lower temperatures. This could be caused by the weaker interactions between the ion pairs at high EDA contents, when strongly basic tertiary amines were progressively replaced by less basic secondary amines. In addition, a higher extent of EDA cross-linking also interrupted the clustering of sulfonic acid groups and confined the latter to several nanoscale domains. The interactions between the sulfonic acid groups decreased as a result. This result corroborated the previous inference that a high cross-linking degree would impede the clustering of sulfonic acid groups.
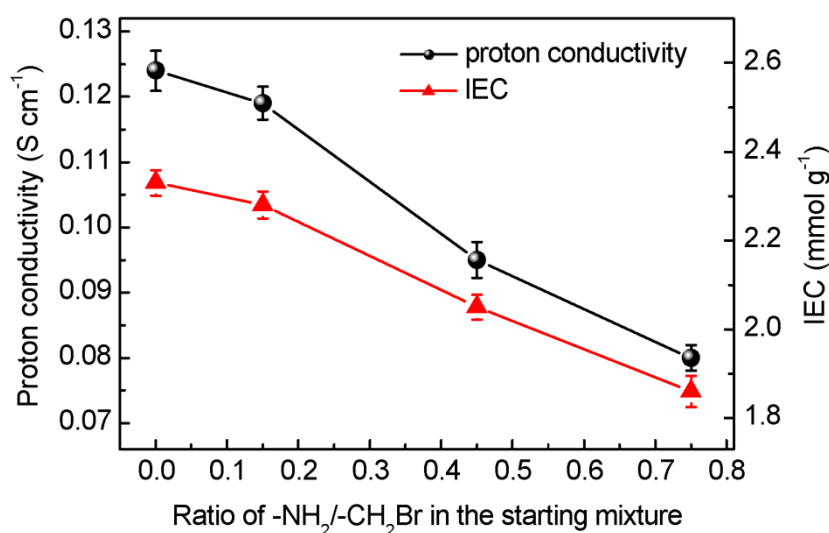
Figure 3.8 The IEC and proton conductivity of SIPN membranes.

3.3.3 Evaluation of the SPPO/BPPO/EDA SIPN Membranes for DMFC Applications

The variations in IEC and proton conductivity as functions of the EDA content are shown in Figure 3.8. The good agreement between the measured IEC of 0.95 mmol g$^-$^{1} for Nafion® 117 and the literature value validated the measurement method (Bai, Z.

W. *et al.* 2007). As expected, the IEC values correlated negatively with the EDA content of the SIPN membranes. This could be understood from the depletion of free sulfonic acid groups due to the formation of protonated amine-sulfonate ion pairs. Proton dissociation from protonated secondary/tertiary amines was a more difficult affair.

Table 3.1 Results of IEC, oxidation and hydrolytic stability tests.

Membrane	IEC (mmol g^{-1})	Protonated amine content[a] (mmol g^{-1})		Oxidative Weight loss in Fenton's test (%)	Hydrolytic stability Proton conductivity (S cm^{-1})	
					before	after
EDA-5/1/0	2.33	0		2.1	0.124	0.123
EDA-5/1/0.15	2.28	0.06	± 0.0016	1.8	0.119	0.113
EDA-5/1/0.45	2.05	0.13	± 0.0039	1.4	0.095	0.089
EDA-5/1/0.75	1.86	0.28	± 0.0043	1.3	0.080	0.079
Nafion 117	0.95	-		0.5	0.090	0.087

[a] The SIPN membranes were neutralized by KOH solution first and then equilibrated by HCl solution. The protonated amine content was then determined from the equation: protonated amine content = (number of mole of HCl equilibrated with membrane/dry mass of membrane, m_{dry}) - IEC
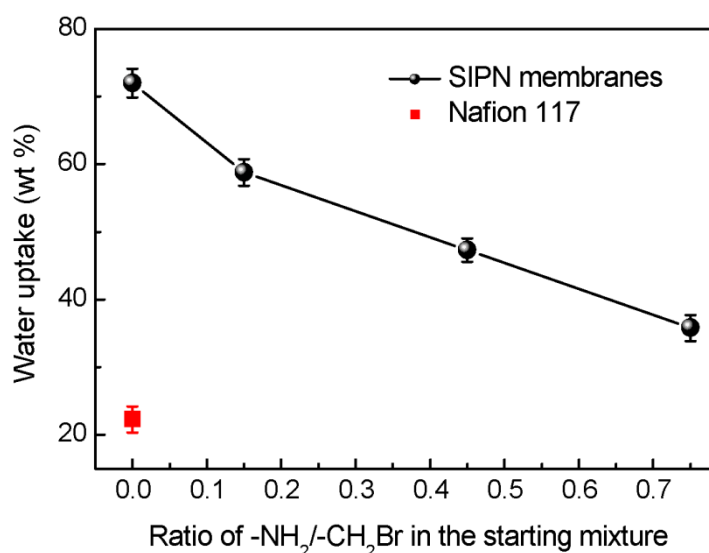
Figure 3.9 Water uptake measurements
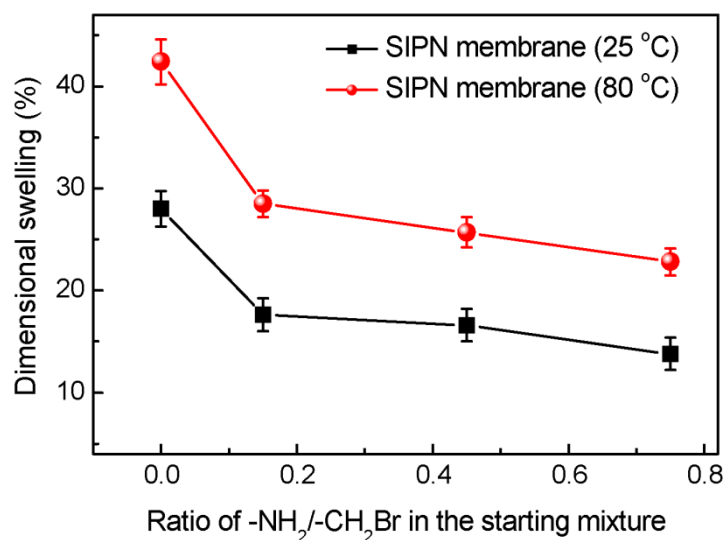
Figure 3.10 Dimensional swelling in SIPN membranes

The protonated amine moieties content of EDA-5/1/0 and three SIPN membranes were measured (Table 1). The values were 0.06, 0.13 and 0.28 mmol g^{-1} for EDA-5/1/0.15, EDA-5/1/0.45 and EDA-5/1/0.75, respectively. The increase in the number of protonated amine-sulfonate ion pairs and cross-linking degree caused a decrease in proton conductivity from EDA-5/1/0.15 to EDA-5/1/0.75. It should however be mentioned the decrease in proton conductivity was more moderate at high ion pair contents. Specifically, the proton conductivity decrease from EDA-5/1/0.45 to EDA-5/1/0.75 (15.7%) was lower than the proton conductivity decrease from EDA-5/1/0.15 to EDA-5/1/0.45 (20.2%), even though the percentage increase in ion pairs in these two cases was about the same. This could be attributed to the compensation effects of the hydrophilic cross-links which negated partially the proton conductivity decrease caused by the depletion of free sulfonic acid groups. These values also represent an improvement over our previous design of ionically cross-linked PPO-based membranes (Fu, R. Q. *et al.* 2008), indicating the more effective proton conduction in an SIPN structure than in simple ionic cross-linking. Compared with a proton conductivity of 9.0×10^{-2} S cm^{-1} for Nafion® 117, the proton conductivities of SIPN

membranes from 11.9×10^{-2} to 8.0×10^{-2} S cm^{-1} are definitely adequate for fuel cell applications.

Figure 3.9 shows the water uptake by the SIPN membranes. For comparison, the water uptake of the non-cross-linked EDA-5/1/0 membrane was also measured (72.0 wt %). The water uptake by the SIPN membranes was noticeably lower than that of the EDA-5/1/0 membrane, and decreased with the increase in the EDA content from 58.8 wt % (the EDA-5/1/0.15 membrane) to 35.8 wt % (the EDA-5/1/0.75 membrane). This was clearly a consequence of cross-linking. Increase in the EDA content increased the number of cross-links in the membrane matrix. The expansion of polymer chains under hydration conditions became more restricted. The reduction in water accommodation capability translated into a decreased water uptake. The trend in dimensional swelling (Figure 3.10) mirrored that of water uptake: the SIPN membranes underwent smaller dimensional changes than the un-cross-linked EDA-5/1/0 membrane, and swelling decreased with the increase in EDA content. The dimensional changes of 13.8% at 25 ^{o}C and 22.8% at 80 ^{o}C for EDA-5/1/0.75 were lower than the corresponding values of EDA-5/1/0 (28.0% at 25 ^{o}C and 42.4% at 80 ^{o}C), indicating the positive contribution of a cross-linked network on suppressing membrane swelling.

The methanol permeability of the SIPN membranes was then measured to evaluate the suitability of these membranes for DMFC operations. The methanol permeability of the SIPN membranes is shown in Figure 3.11. The methanol permeability of Nafion$^{®}$ 117 measured under the same experimental conditions was 2.01×10^{-6} cm^2 s^{-1}, which is consistent with the published value (Elabd, Y. A. *et al.* 2003). The pristine EDA-5/1/0

membrane without any cross-linking was 41% lower than that of Nafion® 117. Methanol permeability decreased further from 1.40×10^{-6} cm^2 s^{-1} (EDA-5/1/0) to $\sim 3.31 \times 10^{-7}$ cm^2 s^{-1} (EDA-5/1/0.75) after cross-linking. Hence an order of magnitude improvement over Nafion® 117 was possible. Especially for EDA-5/1/0.75, methanol permeability was about 6 times lower than Nafion® 117. The low methanol permeability of cross-linked SIPN membranes could be attributed to the more compact structure of a cross-linked network which is a hindrance to the transport of methanol molecules.
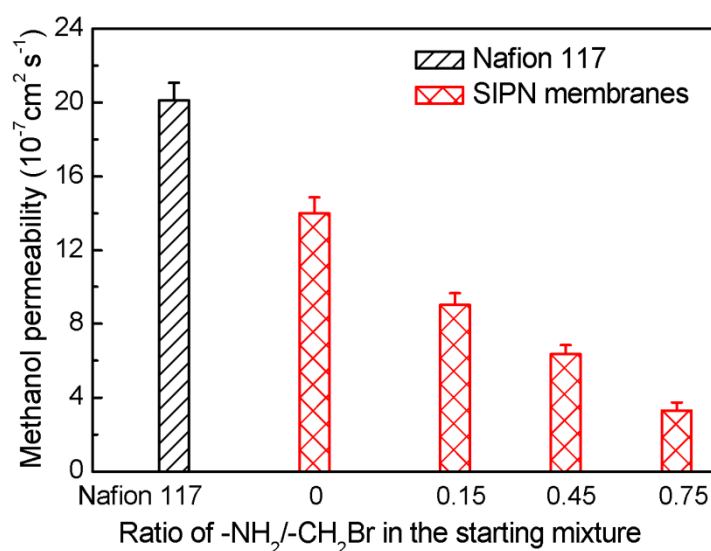
Figure 3.11 Methanol permeability of Nafion® 117 and SIPN membranes.

Proton conductivity and methanol permeability are two important transport properties of a PEM. It is desirable to have high proton conductivity together with low methanol crossover. A composite indicator may be used to evaluate the selectivity in proton and methanol transport. Selectivity has been defined as the ratio of fluxes in some published papers (Pivovar, B. S. *et al.* 1999). However, a selectivity defined as such is susceptive to external factors such as the operating conditions. Hence, we prefer the use of selectivity which is based on membrane intrinsic properties. The ratio of proton

conductivity to methanol permeability, known in the fuel cell community as the "characteristic factor", was therefore the composite indicator adopted for this study (Nasef, M. M. *et al.* 2006; Wu, D. *et al.* 2008). Figure 3.12 shows the characteristic factor of the SIPN membranes as a function of the EDA content. It is apparent that the characteristic factors of the SIPN membranes were all higher than that of Nafion® 117 and increased with increasing EDA content. Among the SIPN membranes, EDA-5/1/0.75 had the highest characteristic factor of 24.1×10^4 S s cm^{-3} which nearly doubled the value of EDA-5/1/0.
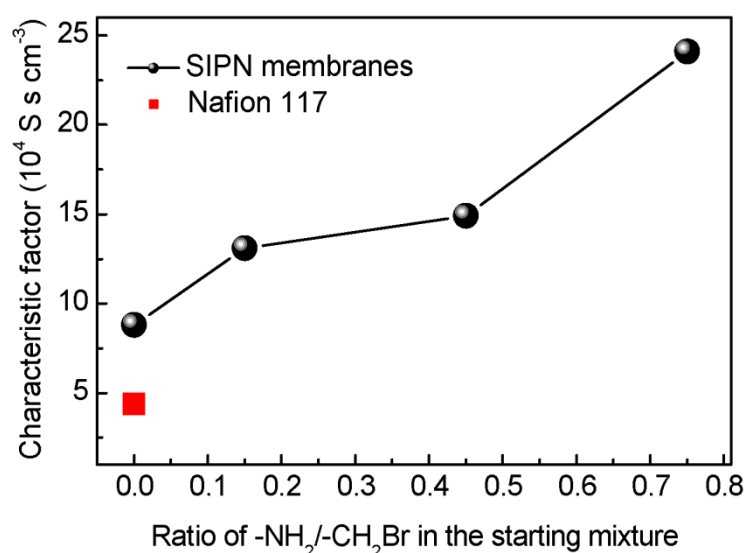
Figure 3.12 Characteristic factor of Nafion® 117 and SIPN membranes.

The oxidative and hydrolytic stability of the membranes were also measured and summarized in Table 1. Here, the oxidative stability of the membranes was evaluated by the Fenton test (chemical stability in 3 wt% H_2O_2 aqueous solution containing 3 ppm $FeCl_2 \cdot 4H_2O$) at 80 °C (Tripathi, B. P. *et al.* 2010). All membranes retained more than 97% of the initial weights after 1 h in the Fenton solution. Compared to a weight loss of 2.1% for the EDA-5/1/0 membrane, the SIPN membranes fared much better (with weight loss of 1.8%, 1.4%, 1.3% for EDA-5/1/0.15, EDA-5/1/0.45, and EDA-

5/1/0.75, respectively), showing improved stability after cross-linking. The hydrolytic stability of the membranes was investigated by comparing the proton conductivities before and after equilibrium in 80 $^{\circ}$C water for two weeks. All membranes showed negligible changes in conductivity.
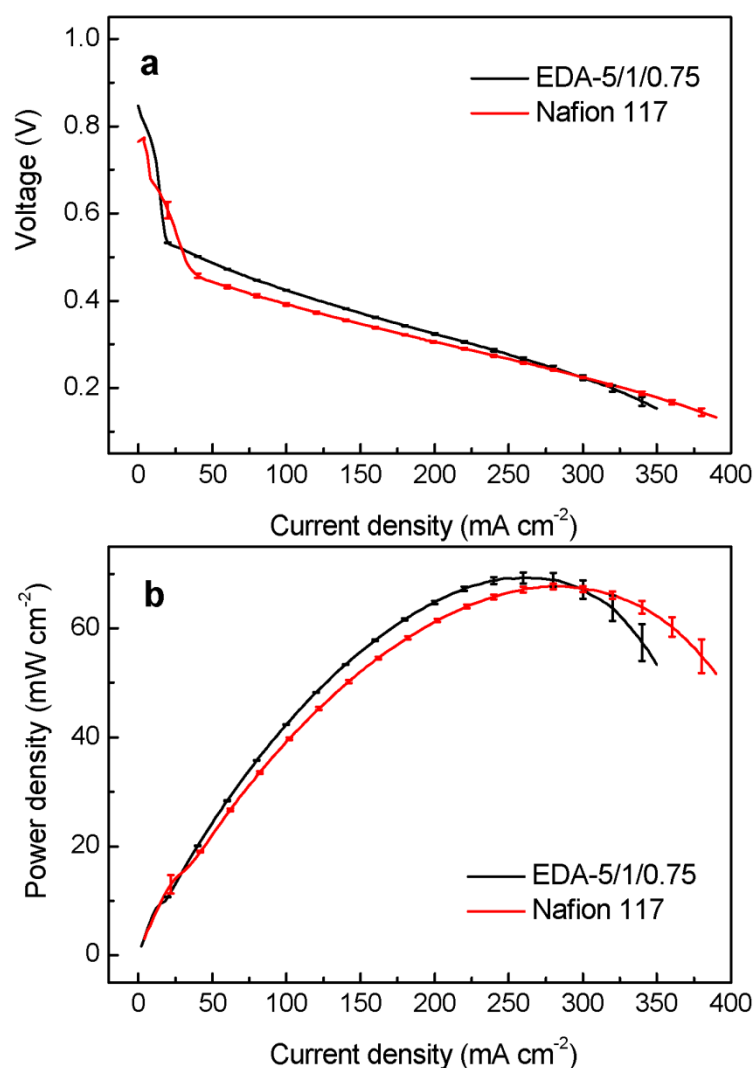
Figure 3.13 Single-stack DMFC tests of Nafion[®] 117 MEA and an EDA-5/1/0.75 MEA at 50 $^{\circ}$C with 2.0 M methanol. (a) Voltage-current density plot. (b) Power density-current density plot.

The EDA-5/1/0.75 membrane, with a high proton conductivity (8.0×10^{-2} S cm^{-1}), acceptable water uptake and dimensional swelling, and low methanol permeability (3.31×10^{-7} cm^2 s^{-1}), appears to have the best balance for DMFC applications, and was

therefore chosen for single-stack fuel cell tests. The performance of the cell is shown in Figure 3.13 alongside that of a commercial Nafion[®] 117 membrane fuel cell. The MEA fabricated from the EDA-5/1/0.75 membrane had a slightly better performance than the Nafion[®] 117 MEA. The maximum power density derivable from the EDA-5/1/0.75 MEA was about 69.3 mW cm^{-2} at 262 mA cm^{-2}, while the Nafion[®] 117 MEA delivered 67.7 mW cm^{-2} at 284 mA cm^{-2}. The open circuit voltage (OCV) was also higher for the EDA-5/1/0.75 (0.85 V) MEA than the Nafion[®] 117 MEA (0.76 V). The better performance of the EDA-5/1/0.75 MEA suggested that the SIPN membranes have great potential for DMFC applications. However, the fabrication technique has to be optimized for the SIPNs in order to fully utilize the materials advantage of the latter.

3.4   Conclusion

In this part of the study, new ion pair-reinforced SIPN membranes were prepared by thermally cross-linking EDA and BPPO in the presence of linear SPPO. The SIPN structure was deduced from ^{13}C NMR, XPS, TEM and corroborated by DSC and DMA measurements. During the *in situ* cross-linking process, different amine moieties (secondary, tertiary amines and protonated amines) were formed in quantities that depended on the amount of EDA used in the preparation. Subsequent ion pair formation between the generated amine moieties and the sulfonic acid groups of SPPO enhanced the immobilization of SPPO in the BPPO network and the uniformity of sulfonic acid cluster distribution in the membrane. It was found that the accessibility of sulfonic acid clusters, and hence the proton transport and mechanical properties of the membranes, were dependent on the EDA cross-linking degree, with a moderate cross-linking degree delivering the most desirable outcome. The ion pair-

reinforced SIPN membranes displayed good proton conductivity, good dimensional stability up to 80 ^{o}C and low methanol permeability. The greater single cell performance of EDA-5/1/0.75 MEA compared to Nafion$^{®}$ 117 MEA also demonstrated the potential of SIPN membranes for DMFC applications.

CHAPTER 4

ION PAIR-REINFORCED SEMI-INTERPENETRATING

POLYMER NETWORK FOR DIRECT METHANOL FUEL CELL

APPLICATIONS: EFFECTS OF CROSS-LINKER LENGTH

4.1   Introduction

The method of Chapter 3 was able to produce ion pair-reinforced SIPN membranes consisting of a covalently cross-linked BPPO/EDA network and distributed SPPO linear polymers. Through the ion pair interactions between the amine moieties generated in cross-linking and the sulfonic acid groups, the linear polymer SPPO could be immobilized in the BPPO/EDA network to yield stronger hydrolytic properties and dimensional stability.

The uniform distribution of sulfonic acid clusters in the SPPO/BPPO/EDA SIPN membranes was confirmed by TEM and SAXS measurements in Chapter 3. Such homogenization of the hydrophilic constituents in a hydrophobic polymer matrix is more able to support the continuity of interconnected hydrophilic domains. The importance of the connectivity of hydrophilic domains in PEM design has been deliberated in Chapters 1 and 2 – proton conductivity depends on the quality and quantity of continuous hydrophilic channels for proton transport (Higashihara, T. *et al.* 2009). The proton conductivity of the SPPO/BPPO/EDA membranes is clearly an improvement over ionically cross-linked PPO-based membranes (Fu, R. Q. *et al.* 2008), thereby confirming the contributions of an SIPN architecture in delivering

uniformly distributed hydrophilic domains. However, the synthesis of the ion pair-reinforced SIPN structure has not been optimized. The classical tradeoff between proton conductivity and methanol permeability was still prevalent at high ion pair contents. Extensive cross-linking also impeded proton mobility and a lower proton conductivity was obtained despite the improvement in methanol barrier property. Hence the next project in this thesis study was to identify and understand the important factors and control of transport properties in ion pair-reinforced SIPN membranes.

Previous studies have also revealed the importance of polymer chain structure on the formation of PEM hydrophilic domains and transport properties (Gierke, T. D. *et al.* 1981; Hsu, W. Y. *et al.* 1982; Hsu, W. Y. *et al.* 1983; Gebel, G. *et al.* 1993; Gebel, G. 2000; Gebel, G. *et al.* 2000; Kreuer, K. D. *et al.* 2000; Kreuer, K. D. 2001; Kreuer, K. D. *et al.* 2004). Hence this part of the thesis project is an attempt at deriving some basic structure-property relationships for the SIPN PEMs. In this study, we prepared a series of ion pair-reinforced SIPN membranes by thermal cross-linking the BPPO with different aliphatic α,ω-diamine cross-linkers in the presence of SPPO. The structure and properties of SIPN membranes were changed by varying the hydrophobicity and the mesh width (the average distance between two cross-linked polymer segments) of the host cross-linked network. The mesh width and the hydrophobicity of cross-linked BPPO network could be varied by changing the length of the α,ω-diamine cross-linker. All membranes were prepared in the same way to minimize the effect of solvent evaporation, and to assure that morphology was primarily determined by the formation of a cross-linked network. TEM and DMA measurements were used to characterize the changes in membrane hydrophilic

domains and the mechanical properties of the PEMs. Proton conductivity, methanol permeability, water uptake and dimensional stability of the membranes were then analyzed in terms of these changes. This then allowed us to arrive at some basic relations between the structure of the network host and the transport properties of SIPNs.

4.2 Experimental Section

4.2.1 Materials

PPO (M_w=30000, T_g=211 ^{o}C), chlorosulfonic acid (99.0~99.4%), N-methyl-2-pyrrolidone (NMP, 99%), ethylenediamine (EDA), 1,4-diaminobutane (DAB), hexamethylenediamine (HMDA), 1,8-diaminooctane (DAO), 1,10-diaminodecane (DAD), and Nafion$^®$ 117 films were supplied by Sigma-Aldrich. BPPO was purchased from Tianwei Membrane Corporation Ltd. of Shandong (People's Republic of China) and contained 59.1% benzyl bromide and 40.9% aryl bromide as analyzed by ^{1}H NMR spectroscopy. Chloroform (99%) and methanol (99.8%) were supplied by Merck.

4.2.2 Preparation of SPPO/BPPO/α,ω-diamine SIPN Membranes

A series of SPPO/BPPO/α,ω-diamine membranes with different α,ω-diamine cross-linkers were synthesized by the procedures of Chapter 3. The IEC of the SPPO was 2.07 mmol g^{-1}, or 29.8% degree of sulfonation. All of the membranes examined in this study were prepared from SPPO, BPPO and α,ω-diamine in the functional group mole ratio ($-SO_3H/-CH_2Br/-NH_2$) of 5/1/0.75, taking into account the balance between

various membrane properties such as dimensional swelling and proton conductivity. These membranes are identified by the cross-linker used in their preparation. Hence, PPO-EDA is the membrane synthesized from SPPO, BPPO and EDA; PPO-DAB is the membrane synthesized from SPPO, BPPO and DAB, and so on. An SPPO/BPPO blend membrane without any cross-linker was also prepared and used as the control.

4.2.3   Characterizations

The TEM, XPS, DMA, measurements of IEC, proton conductivity, water uptake, methanol permeability, and single stack fuel cell performance followed the same procedures given in Chapter 3.

The dimensional changes of a membrane due to water update were estimated by measuring the changes in the length, width and thicknesses of a dry membrane cut to specific dimensions after the membrane was equilibrated in water and in methanol aqueous solutions at 25 $^{\circ}$C for 24 h.

$$\Delta l = \frac{l_w - l_d}{l_d} \times 100\%$$

$$\Delta w = \frac{w_w - w_d}{w_d} \times 100\%$$

$$\Delta t = \frac{t_w - t_d}{t_d} \times 100\%$$

where l_w, w_w *and* t_w are respectively the length, width and thickness of the wet membrane. The corresponding values for the dry membrane are l_d, w_d *and* t_d.

4.3   Results and Discussions

4.3.1   Synthesis and Characterization of SPPO/BPPO/α,ω-diamine SIPNs

The SPPO/BPPO/α,ω-diamine membranes were prepared by immobilizing the linear polymer, SPPO, in a cross-linked BPPO/α,ω-diamine network. The cross-linking which occurred during membrane formation consisted of two types of cross-links. One of them was the classical covalent cross-links formed by the substitution reaction between the primary amine groups (–NH$_2$) of α,ω-diamine molecules and the bromomethyl groups (–CH$_2$Br) of BPPO, as shown in Figure 4.1. Entrapment of SPPO occurred during covalent cross-linking to result in an SIPN structure. SPPO in the proximity of the covalent cross-links reinforced their attachment to the network polymer by the formation of a second type of cross-links: ion pair interactions (ionic cross-links) between the sulfonic acid groups of SPPO and the amine moieties in the covalent cross-links. The coexistence of both covalent and ionic cross-links increased the robustness of the interpenetrated structure beyond what was possible with simple mechanical interlocking.
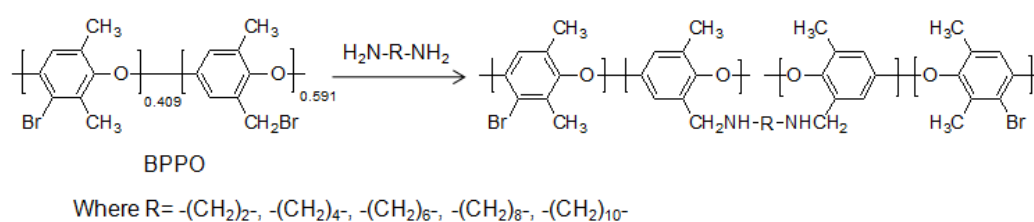
Figure 4.1 Cross-linking of BPPO by the alkylation of BPPO.

Figure 4.2 is an illustration of the possible structure which could be present in the SPPO/BPPO/α,ω-diamine SIPN membranes. There could be –SO$_3^-$…$^+$NH$_3$– ion pair interactions between the α,ω-diamine molecules and SPPO initially when the SPPO

and BPPO/α,ω-diamine solutions were mixed. However, XPS measurements showed that the initial protonation of α,ω-diamine did not inhibit the formation of $-NH-CH_2-$ linkages between α,ω-diamine and BPPO subsequently (*vide infra*), for the same reason given in Chapter 3.
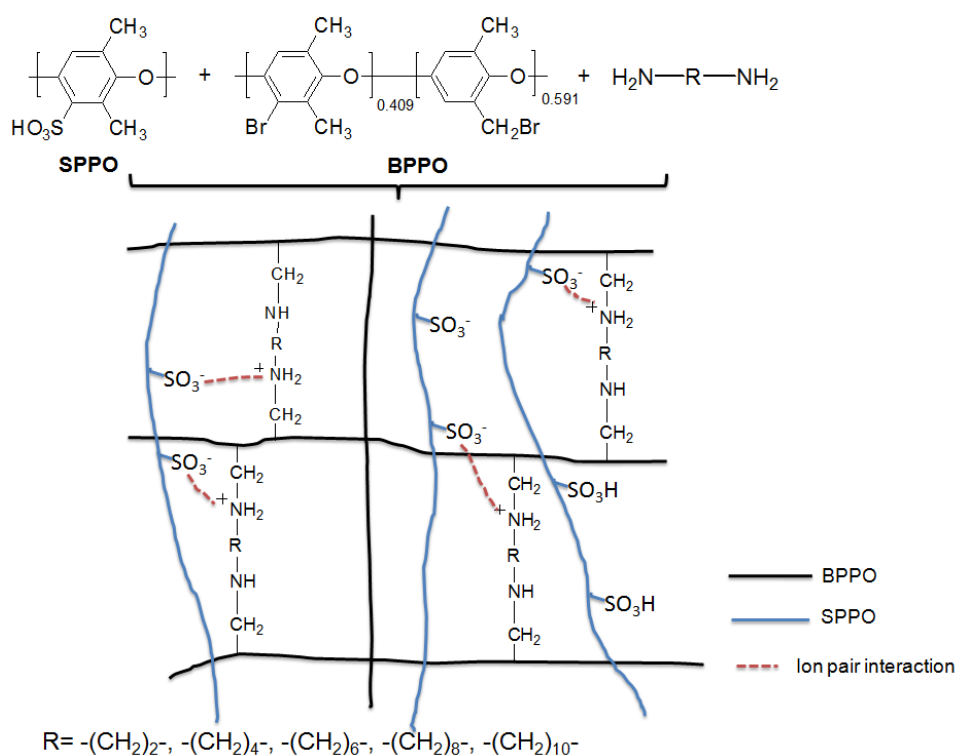
Figure 4.2 Preparation and possible structure of the SPPO/BPPO/α,ω-diamine SIPN memrbanes.

The presence of two types of cross-links (covalent and ionic) was confirmed by XPS (Figure 4.3 and Figure 4.4). The two peaks with binding energies at about 399.8 and 401.9 eV in all of the N1s XPS spectra in Figure 4.3 agree well with those of secondary amine and N^+ species, respectively (Cheng, Z. P. *et al.* 2006). The N^+ species could have been present as protonated amines (i.e., $-RNH_2^+$ from ionic cross-linking) or quaternary ammoniums ($-R_3N^+$ from covalent cross-linking). They could however be differentiated by the simple base treatment method of Chapter 3 (Fang, C. *et al.* 2012). Protonated amine groups after the base treatment would be converted to

uncharged amine groups (i.e., –NHR) whereas –R_3N^+ groups would become –$R_3N^+OH^-$. The XPS spectra of the base-treated SIPN membranes (Figure 4.4) show the complete disappearance of the N^+ peaks, thereby rejecting the existence of quaternary ammonium groups –R_3N^+. This is not surprising in view of the steric hindrance in BPPO-α,ω-diamine cross-linking reactions. The presence of secondary and protonated amine peaks in Figure 4.3 therefore substantiated the covalent cross-linking of BPPO by α,ω-diamine molecules, and the ionic cross-linking between the secondary amine moieties in the covalent cross-links and the sulfonic acid groups of SPPO, respectively.
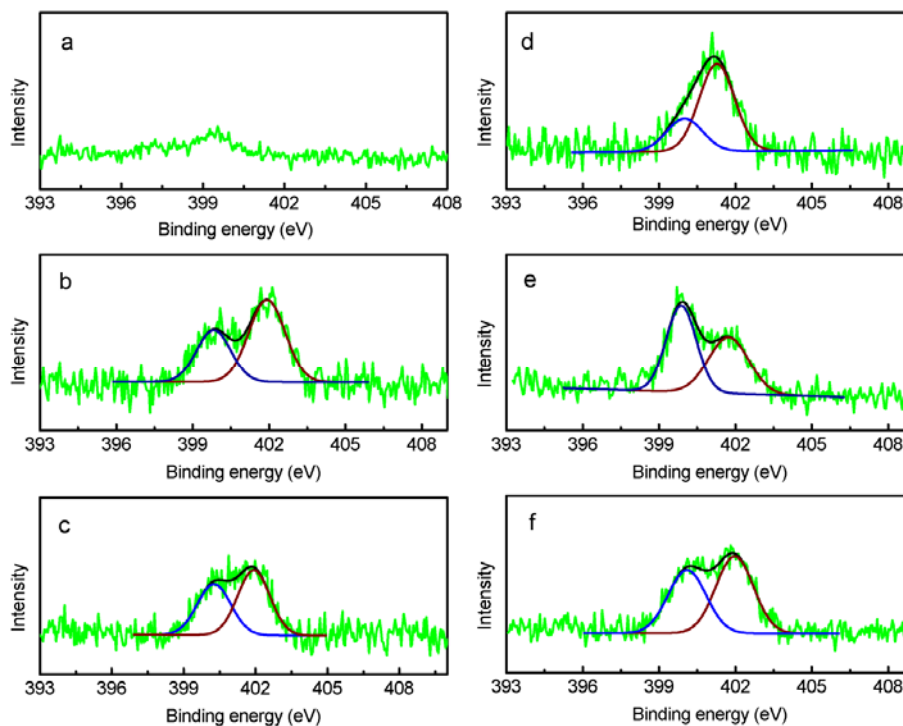
Figure 4.3 XPS spectra of SPPO/BPPO blend (a), PPO-EDA (b), PPO-DAB (c), PPO-HMDA (d), PPO-DAO (e), and PPO-DAD (f).

The absence of a primary amine peak in Figure 4.4 suggests that the α,ω-diamine cross-linkers had completely reacted with the –CH_2Br groups in BPPO. Hence, the amount of ionic cross-links in the SIPN membranes could be estimated on the basis of

the N$^+$ peak area in Figure 4.3. Among the SIPN membranes, the area of the N$^+$ peak

for PPO-HMDA was significantly larger than that of the secondary amine peak,

suggesting a higher degree of ionic cross-linking in the PPO-HMDA membrane.
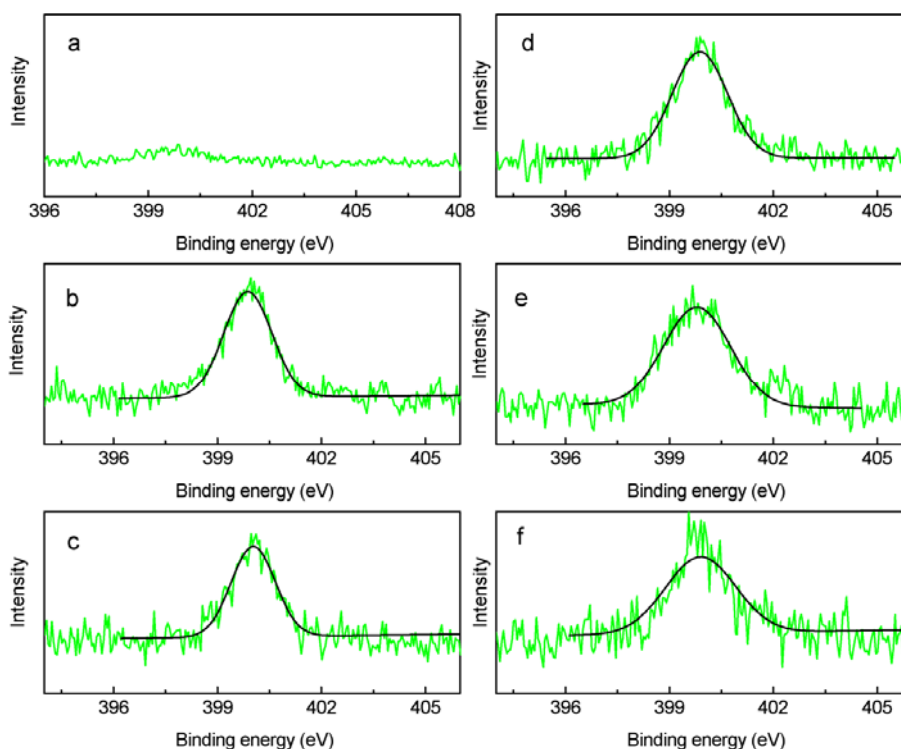
Figure 4.4 XPS spectra of base-treated SPPO/BPPO blend (a), PPO-EDA (b), PPO-DAB (c), PPO-HMDA (d), PPO-DAO (e), and PPO-DAD (f).

4.3.2 Effects of Aliphatic α,ω-Diamine Cross-linker Length on Cross-linked Network Structure and Sulfonic Acid Clustering

The presence of aliphatic α,ω-diamine-cross-linkers could lead to the increase in local

free volume between nearby polymer chains. Difference in the length of the cross-

links, which depends on the number of methylene groups in the α,ω-diamine

molecules, should therefore lead to variations in the SIPN network structure

particularly the mesh width (the average distance between two BPPO chains which

were cross-linked by α,ω-diamine). Longer cross-linkers are expected to yield a larger

mesh width and a looser cross-linked network. This could be verified by the changes in viscoelastic behavior in DMA measurements. The viscoelastic behavior of a polymer can be characterized by a storage (elastic) component and a loss (viscous) component, which are the storage modulus (E') and the loss modulus (E'') in DMA measurements, respectively. In the measurements, E' and E'' are the in-phase and out-of-phase responses of the sample to an applied oscillating stress. The ratio between the loss and storage moduli (E''/E'), also known as the mechanical damping factor (tan δ), is a measure of the deformational energy which is dissipated as heat in each measurement cycle (Sgreccia, E. *et al.* 2010). Figure 4.5 shows the temperature dependence of tan δ of the SIPN membranes in the 25~350 ^{o}C temperature range. Two types of relaxations are apparent in the tan δ -T plot: a weak relaxation centering about 200 ^{o}C and an intense peak above 250 ^{o}C. The presence of two peaks indicates two different types of polymer chain motions (Bai, Z. W. *et al.* 2007). The lower temperature peak may be attributed to hydrogen bonding and dipole-dipole interactions between the sulfonic acid groups, and ion pair interactions between sulfonate and protonated amine groups. The higher temperature peak, on the other hand, should relate more to the relaxation of the entire SIPN structure. With the increase in the cross-linker length, the low-temperature peak became progressively broader and faded away gradually. This could be attributed to the dilution of the sulfonic acid groups per unit polymer volume, and hence the interactions between them, in networks with large mesh widths. This was accompanied by the increase in the high-temperature peak intensity (except for PPO-HMDA) – an indication of the growth in energy damping due to the increased viscous effects in a more flexible SIPN structure. PPO-HMDA is the outlier of this trend, which appears to be caused

by an unexplained high degree of ionic cross-linking which increased the rigidity of

the SIPN structure.
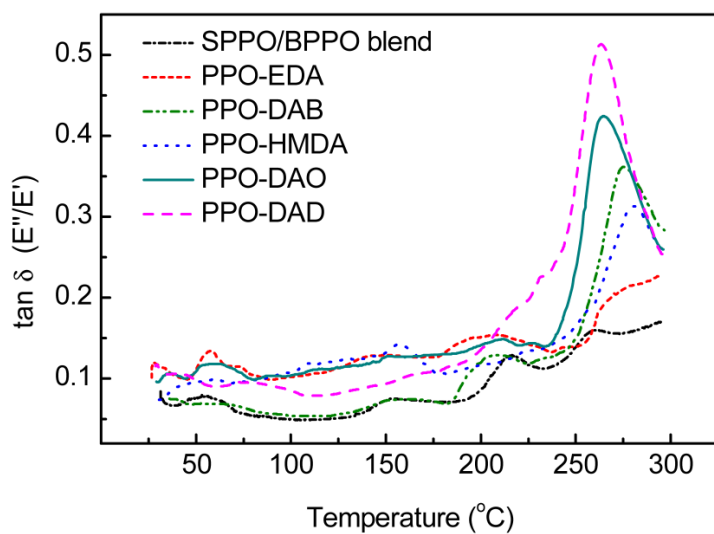
Figure 4.5 Temperature dependence of the loss factor (tanδ) of SIPN and SPPO/BPPO blend membranes.
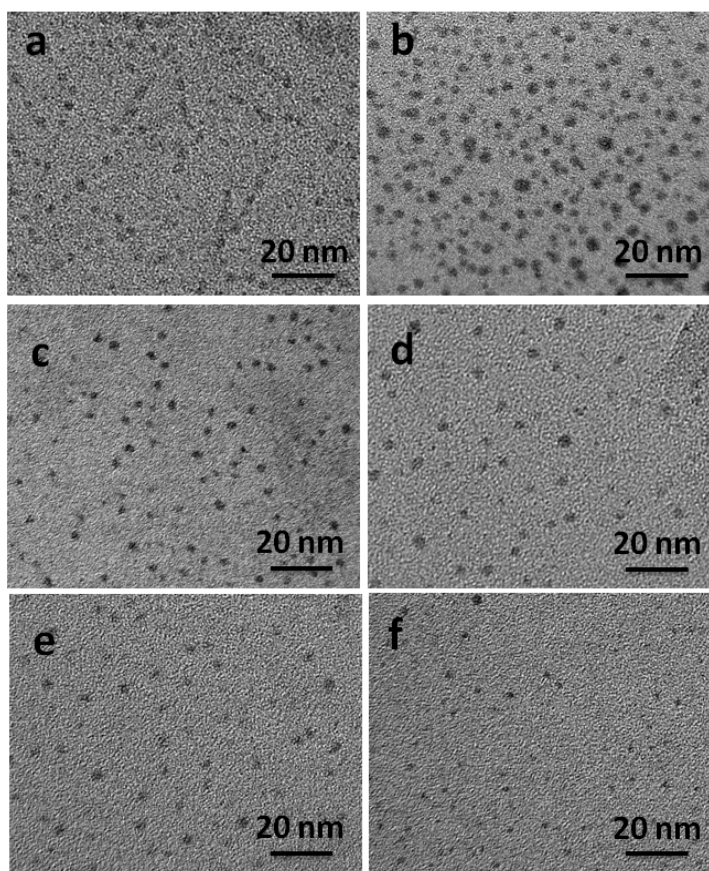
Figure 4.6 TEM micrographs of SIPN membranes: (a) SPPO/BPPO blend, (b) PPO-EDA, (c) PPO-DAB, (d) PPO-HMDA, (e) PPO-DAO, (f) PPO-DAD.

The effect of cross-linker length on membrane morphology is more evident in the direct examination of membrane morphology by TEM (Figure 4.6). The dark spots in the TEM images are hydrophilic domains where sulfonic acid clusters had been stained by the Pb^{2+} ions (as lead sulfonate) to improve the image contrast (Bae, B. *et al.* 2009). The density of these dark spots could be used to deduce the connectivity of the hydrophilic domains after water absorption. Due to the dilution of sulfonic acid groups in networks with a greater mesh width, the hydrophilic domains should become more scattered with the increase in the cross-linker length. Figure 4.6 reflects exactly this trend: fewer dark spots in the TEM images when the cross-linker length was increased from EDA to DAD. The other reason could be the hydrophobicity of the $-CH_2-$ segment in the cross-linker. Table 4.1 shows the calculated solubility parameters of α,ω-diamine cross-linkers decreasing from EDA to DAD, indicating the general increase in water rejection property due to the increase in the $-CH_2-$ segment. Consequently the clustering of sulfonic acid groups was constrained in networks cross-linked by large α,ω-diamine molecules due to the combination of these two factors (dilution of sulfonic acid groups and increase in hydrophobicity). Fewer contiguous hydrophilic channels were formed as suggested by the fewer number of Pb^{2+} stained sulfonic acid clusters. The high density of sulfonic acid clusters in the PPO-EDA membrane greatly increased the probability of forming interconnected hydrophilic domains upon hydration. The hydrophilic domain size in all SIPN membranes was in the range of 2~4 nm, much smaller than the values in the previous reports on SIPN membranes (Jain, S. H. *et al.* 2003) and Nafion[®] 117 (Figure 4.7). The small domain size is an advantage as it can more effectively suppress methanol crossover.
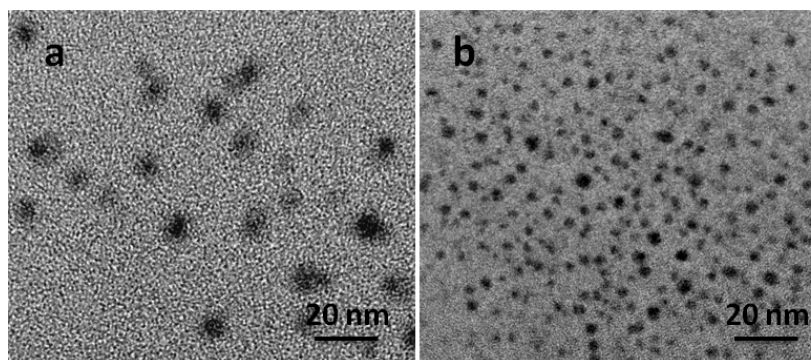
Figure 4.7 TEM micrographs of (a) Nafion[®] 117 and (b) PPO-EDA.

Table 4.1 Calculated solubility parameters of α,ω-diamine cross-linkers

	M (g mol^{-1})	ΣF^a[(MPa)$^{0.5}$ cm^3 mol^{-1}]	ρ(g cm^{-3})	δ^b [(MPa)$^{0.5}$]
EDA	60.1	1466	0.899	21.9
DAB	88.2	2004	0.877	19.9
HMDA	116.2	2542	0.890	19.5
DAO	144.3	3080	0.858	18.3
DAD	172.3	3618	0.857	18.0
Methanol	-	-	-	29.7[c]
Water	-	-	-	47.9[c]

[a] Total molar attraction constant can be estimated by simple addition of group contributions (Musale, D. A. *et al.* 2000). The effect of conformations was not taken into account.

[b] The solubility parameter can be calculated via $\delta = \rho\Sigma F / M$, where M is the molecular weight, ρ is the density.

[c] Data from handbook (Zeng, W., Du, Y., Xue, Y., Frisch, H. L. **2007**).

4.3.3 Effect of Aliphatic α,ω-Diamine Cross-linker Length on PEM-related Properties

IEC is a measure of the accessible sulfonic acid groups in a PEM membrane. It is an important parameter which closely affiliates with water uptake and proton conductivity. Table 4.2 shows the IEC values of various SIPN membranes investigated in this study. Here, the IEC dilution effect caused by the weights of the cross-linkers could be ignored because of the slight amount of cross-linkers in the

membranes (0.8%~2.2%). The good agreement between the measured and literature values of Nafion[®] 117 (0.91 mmol g^{-1}) (Tsang, E. M. W. *et al.* 2009) is a validation of the measurement method. The SPPO/BPPO blend without any cross-linker had the highest IEC value of 1.79 mmol g^{-1}. The IEC values of SIPN membranes were all lower because ionic cross-linking depleted some of the ion-exchangeable sulfonic acid groups. The decreasing IEC trend with increasing cross-linker length suggests decreased accessibility of the sulfonic acid groups caused by the increase in the number of isolated hydrophilic domains.

Table 4.2 IEC, proton conductivity and water uptake of SIPN and SPPO/BPPO blend membranes.

Membranes	IEC (mmol g^{-1})	σ (S cm^{-1})	WU (%)
SPPO/BPPO	1.79	0.084	53.2
PPO-EDA	1.63	0.082	43.6
PPO-DAB	1.53	0.077	45.2
PPO-HMDA	1.50	0.080	47.3
PPO-DAO	1.44	0.073	37.3
PPO-DAD	1.35	0.069	35.8
Nafion[®] 117	0.91	0.085	30.1

The proton conductivities (Table 4.2) follow a similar decreasing trend as the IEC. Nafion[®] 117 was also included for comparison. The decrease in proton conductivity could be attributed to generally more scattered hydrophilic domains and fewer contiguous interconnected hydrophilic channels in the membrane. The proton conductivity of the PPO-EDA membrane was therefore the highest among the SIPN membranes because of a high connectivity of its hydrophilic domains.

The water uptake by the membranes is also summarized in Table 4.2. As expected, the SPPO/BPPO blend membrane exhibited the highest water uptake of 53.2 wt%

because of its high free sulfonic acid content and un-constrained structure. The water uptake by the SIPN membranes was noticeably lower than the blend membrane. With the increase in the cross-linker length, the water uptake by SIPN membranes first increased and then decreased. This could be considered as the result of two competing effects. As discussed previously, the cross-linkers could increase the local volume between nearby polymer chains in the SIPN structure. Hence the free volume of the SIPN membrane should increase with the use of longer cross-linkers, resulting in more water accommodation. However, hydrophobicity consideration alone suggests lower water accommodation in longer cross-linkers because of the length of the $-CH_2$ segment. Hence maximum water uptake should occur at an intermediate cross-linker length due to the compensation of two opposing effects − it was the PPO-HMDA membrane in this case.

Table 4.3 Dimensional changes in SIPN and SPPO/BPPO blend membranes.

Membranes	In water			$V_{Methanol} :$ $V_{H2O}=1:3$			$V_{Methanol} :$ $V_{H2O}=1:1$		
	Δl	Δw	Δt	Δl	Δw	Δt	Δl	Δw	Δt
SPPO/BPPO	19.4	16.2	20.9	31.0	22.2	33.3	47.2	44.4	73.3
PPO-EDA	14.2	11.1	14.6	18.5	19.1	24.5	38.5	33.3	37.2
PPO-DAB	14.6	15.7	15.7	18.0	19.1	19.2	34.0	33.3	35.4
PPO-HMDA	15.3	15.7	16.6	23.3	21.3	19.3	42.5	44.4	44.1
PPO-DAO	12.6	15.7	14.2	16.0	19.1	19.6	33.5	22.2	33.7
PPO-DAD	11.2	11.1	14.2	16.0	19.1	17.4	31.0	27.7	39.3

Although water molecules in the membrane contribute to proton transport, a high water uptake could cause excessive membrane swelling (Eikerling, M. *et al.* 2001). Unbridled dimensional changes in the membrane can delaminate MEA at the membrane-electrode interface to compromise fuel cell durability (Bi, H. P. *et al.* 2010). Hence, smaller membrane dimensional changes are desirable for DMFC

operations. Table 4.3 shows the dimensional changes of the membranes in different concentrations of aqueous methanol solutions. All the SIPN membranes displayed general isotropic swelling behavior, suggesting uniform distribution of polymer constituents and density in the membrane matrix. They underwent smaller dimensional changes in length, width and thickness than the SPPO/BPPO blend membrane, confirming the positive contribution of a cross-linked network in restraining membrane swelling. The swellability of the SIPN membranes correlates positively with the changes in the water uptake by the membranes.
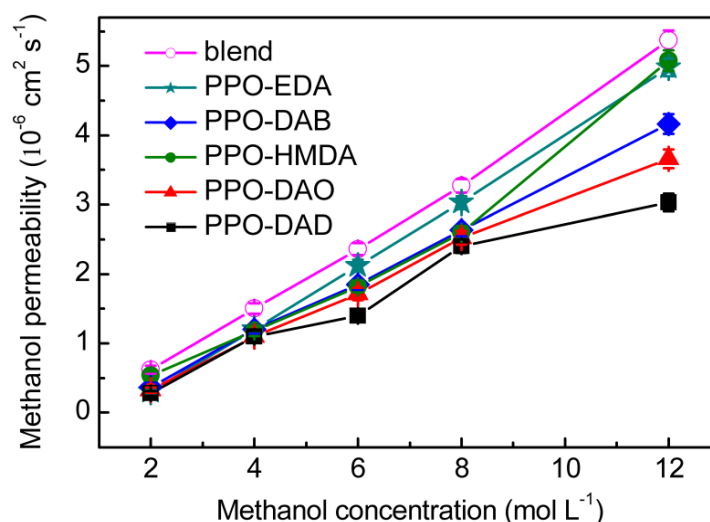
Figure 4.8 Methanol permeability of SIPN membranes and SPPO/BPPO blend.

The methanol permeabilities of the SIPN membranes as a function of methanol concentration are shown in Figure 4.8. At any given concentration, methanol permeability displays a similar decreasing trend with increasing cross-linker length as that of proton conductivity (Table 4.2). This is because methanol molecules, like protons and water molecules, were also transported through the hydrophilic channels in the membrane. Hence, the size and connectivity of the hydrophilic domains also affect the methanol permeability. In Figure 4.8, the SPPO/BPPO blend membrane shows the highest methanol permeability than any of the SIPN membranes. The SIPN

membranes exhibited a decreasing trend of methanol permeability in the order of PPO-EDA > PPO-DAB ≈ PPO-HMDA > PPO-DAO > PPO-DAD. The methanol permeability of Nafion® 117 in 2.0 M methanol solution (a common fuel concentration in DMFCs) was also measured and used as a reference, which was 2.01×10^{-6} cm^2 s^{-1}. In comparison with Nafion® 117, the methanol permeability of all SIPN membranes in 2M methanol solution was much lower, in the range of 6.2×10^{-7} ~2.7×10^{-7} cm^2 s^{-1}, which can be attributed to the smallness of the hydrophilic domains. The presence of cross-linking bridges ($-CH_2NH-R-NHCH_2-$) amid the hydrophilic domains of the sulfonic acid groups also impeded methanol transport. Figure 4.9 shows that the characteristic factors of the SIPN membranes were all higher than that of the SPPO/BPPO blend membrane. They followed a concave trend with the PPO-EDA membranes showing the highest characteristic factor of 2.7×10^5 S s cm^{-3}.
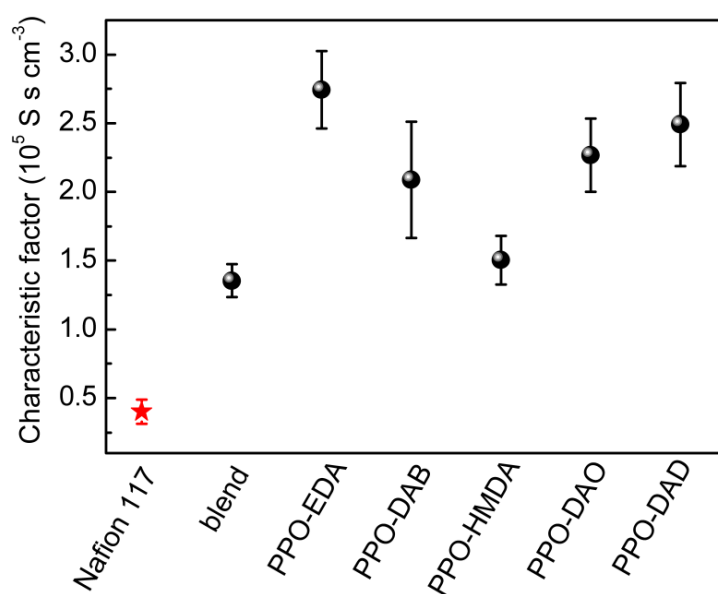
Figure 4.9 Characteristic factor of Nafion® 117 and SIPN membranes

4.3.4   Single Stack Fuel Cell Tests

The SIPN membranes were fabricated into MEAs and the performance of the latter was evaluated in a single stack DMFC and benchmarked against the performance of commercial Nafion® 117 MEA at 50 °C (Figure 4.10). The SIPN MEAs exhibited a decreasing trend of maximum power density in the order of PPO-DAO > PPO-EDA > PPO-DAB > PPO-HMDA > PPO-DAD, which is slightly different from the trend in the characteristic factor. Specifically, the highest maximum power density derivable from the PPO-DAO MEA was about 65.8 mW cm^{-2} at 292 mA cm^{-2} while the Nafion® 117 MEA delivered 62.5 mW cm^{-2} at 262 mA cm^{-2}. The open circuit voltage (OCV) was also higher for the PPO-DAO (0.796 V) MEA than the Nafion® 117 MEA (0.793 V). The PPO-EDA membrane had the highest characteristic factor, but its MEA only showed the second-highest performance at 62.5 mW cm^{-2}, which was comparable to the Nafion® 117 MEA. This discrepancy between characteristic factor and cell performance could be caused by electroosmotic drag on methanol crossover in the single cell test. It is expected that the electroosmotic contribution has a greater impact on membranes with a higher proton conductivity.

The good performance of the PPO-DAO MEA is testimony of the potential of SIPN membranes for the DMFC application. However, there are still practical issues to be overcome. In our experiments, we observed some interfacial incompatibility between the PPO-based SIPN membrane and the catalyst layers using Nafion® as the binder. The adhesion problem became more acute after extended runs at elevated temperatures where delamination of the membrane from the catalyst layers was found, causing an increase in the fuel cell internal resistance and consequently the degradation of the fuel cell performance. A defective electrode-membrane interface

could be the real limiting factor in the transport of protons across the PEM. Thus while all of the SIPN membranes have higher characteristic factors than Nafion[®] 117, only a handful of them could outperform a Nafion[®] 117 MEA, and only marginally at best (Figure 4.10). Further work is needed to improve the membrane-electrode adhesion, or new binder needs to be found to replace the Nafion[®] binder in MEA fabrication.
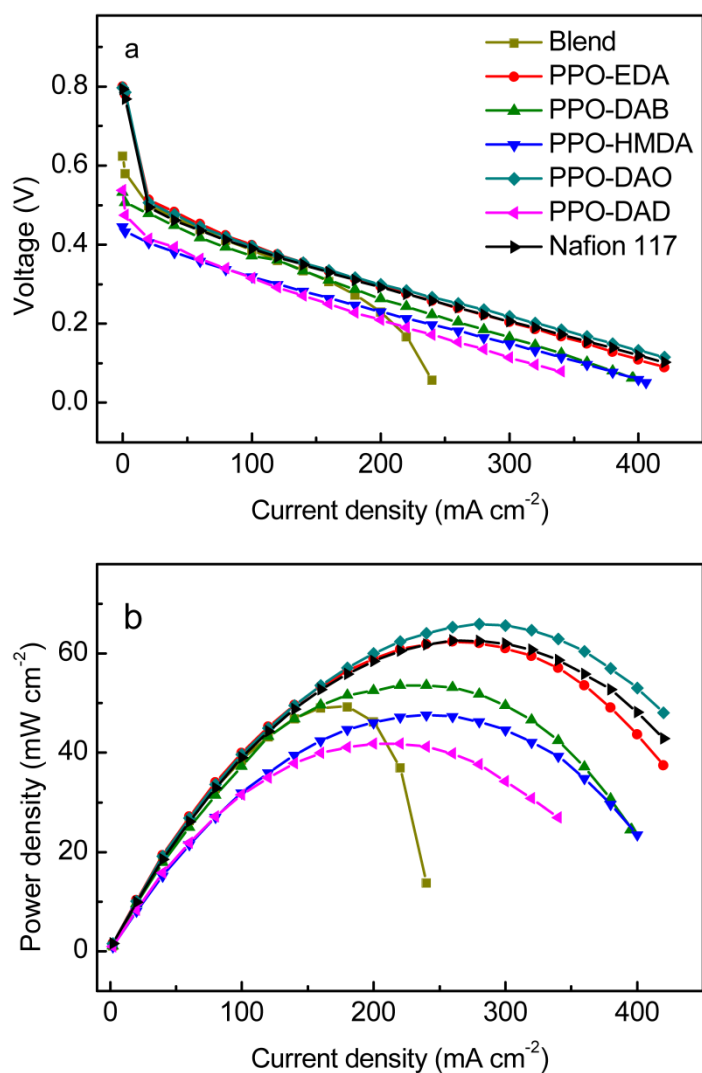
Figure 4.10 Single cell performance of Nafion[®] 117 and SIPN membranes at 50 $^\circ$C with 2.0 M methanol. (a) Voltage-current density plot. (b) Power density-current density plot.

4.4   Conclusion

In this part of the study, a series of SIPN membranes were fabricated by immobilizing linear SPPO in a covalently and ionically cross-linked BPPO/α,ω-diamine network. We investigated the effects of aliphatic α,ω-diamine cross-linker length on the formation of hydrophilic domains and the transport properties of the SIPN membranes. It was found that the aliphatic α,ω-diamine cross-linkers could increase the local volume between nearby polymer chains. The mesh width of the cross-linked network therefore increased with the cross-linker length, leading to a more unrestrained cross-linked network. In addition, the increase in the cross-linker $-CH_2-$ segment also increased the hydrophobicity of the cross-linked network. These effects combined to determine the formation of hydrophilic domains in the membrane. The increase in mesh width and hydrophobicity by the use of long cross-linkers resulted in the dilution of sulfonic acid groups and increase in water rejection properties. Consequently the hydrophilic domains were more scattered with fewer contiguous hydrophilic channels formed in the membrane. On the contrary, there were more hydrophilic domains formed in the SIPN membranes cross-linked by shorter α,ω-diamines, thereby increasing the probability of forming interconnected hydrophilic domains upon water absorption. The small size of the hydrophilic domains was most helpful to suppressing methanol crossover. The variations in the functional properties of the SIPN membranes for fuel cell applications could be understood by these basic understandings. Some of the SIPN membranes prepared here could perform better than Nafion[®] 117 in single stack DMFC.

CHAPTER 5

ION PAIR-REINFORCED SEMI-INTERPENETRATING POLYMER NETWORK FOR DIRECT METHANOL FUEL CELL APPLICATIONS: EFFECTS OF CROSS-LINK BULKINESS

5.1   Introduction

The earlier chapters have suggested ion pair-reinforced SIPN membranes as an approach to deliver the desired PEM morphology of well-connected hydrophilic channels. Due to the reinforcement by ion pair interactions, the hydrophilic and hydrophobic constituents are more intimately mixed (approaching molecular level) in an SIPN structure. The uniform dispersion of the hydrophilic constituent in a hydrophobic polymer network can increase the presence of connected hydrophilic domains. Smaller hydrophilic domains could also be formed at the same time. The hydrophilic channels could then be made narrower to more effectively inhibit methanol passage.

For the better control of membrane morphology and transport properties, we have investigated the effects of cross-linker length in Chapter 4 and found that: i) the use of shorter cross-linker increased the density of the sulfonic acid clusters in the SIPN membranes, thereby increasing the possibility of forming interconnected hydrophilic domains upon water absorption; ii) the use of long cross-linkers resulted in the dilution of sulfonic acid clusters with fewer contiguous hydrophilic channels formed in the SIPN membranes; and iii) both proton conductivity and methanol permeability

decreased with the increase in cross-linker length. These observations indicated that the proton to methanol transport selectivity cannot be realized merely by changing the cross-linker length. Other aspects of cross-linking need to be explored to achieve narrower and better connected hydrophilic channels.

Hence the effects of cross-link bulkiness on SIPN membrane morphology and transport properties were investigated in this part of the study. Several aliphatic and aromatic epoxides, namely 1,4-butanediol diglycidyl ether (BDE), resorcinol diglycidyl ether (RDE), bisphenol A diglycidyl ether (BADE) and poly(bisphenol A-co-epichlorohydrin) (PBAE), were used as model cross-linkers to represent a cross-section of molecular sizes. SIPN membranes were produced by thermally cross-linking the aminated BPPO with an epoxide cross-linker in the presence of SPPO. In the SIPN structure fabricated as such, the epoxide cross-linked aminated BPPO was the polymer network host providing the mechanical properties of the PEM while SPPO was the penetrant and the proton source. Morphology characterizations and electrochemical measurements revealed significant differences in the PEM morphology and transport properties due to the use of different cross-linkers. The systematic changes in cross-link bulkiness resulted in a better understanding of these PEM systems and the development of some rudimentary composition-morphology-property relationships for the PEM design.

5.2   Experimental Section

5.2.1   Materials

PPO (M_w=30000, T_g=211 ^{o}C), chlorosulfonic acid (99.0~99.4%), N-methyl-2-pyrrolidone (NMP, 99%), BDE, RDE, BADE and PBAE were purchased from

Sigma-Aldrich. BPPO (59.1% benzyl bromide and 40.9% aryl bromide as analyzed by ^{1}H NMR spectrometry) was supplied by Tianwei Membrane Corporation Ltd. of Shandong (People's Republic of China). Chloroform (99%), ammonia solution (32%) and methanol (99.8%) were purchased from Merck. Nafion® 117 films were provided by Sigma-Aldrich. SPPO with 29.8% degree of sulfonation (IEC = 2.07 mmol g^{-1}) was synthesized in Chapter 4.

5.2.2   Preparation of SIPN Membranes

PPO-based SIPN membranes were prepared by a thermal cross-linking method. The preparation of BDE0.25 where the figure '0.25' refers to the ratio of epoxy groups to bromomethyl groups (1.0 for complete cross-linking) is given below as an example. BPPO and SPPO were dissolved separately in NMP to a concentration of 30 mg mL^{-1} each. Excess ammonia was added to the solutions to neutralize SPPO and to aminate BPPO, respectively. A measured amount of BDE cross-linker was also added to the BPPO solution. After stirring for 1 h, the two solutions were mixed. The mixture was cast onto a glass petri dish, cured at 80 $^{\circ}$C for 48 h and then at 100 $^{\circ}$C for 2h in vacuum. The membrane formed as such was acidified in 1.0 M HCl for 24 h, washed several times with distilled water and then air-dried. A polymer blend membrane prepared was also prepared from neutralized SPPO and aminated BPPO without any cross-linker, and used as the control. All the membranes examined in this study were prepared with a –SO$_3$H/–CH$_2$Br molar ratio of 5/1, which was found by screening experiments to represent a good balance between various membrane properties such as dimensional swelling and proton conductivity.

5.2.3 Characterizations

Scanning transmission electron microscopy (STEM) and elemental mapping by energy dispersive X-ray (EDX) spectroscopy were conducted on a JEOL 2101F TEM. A Bruker DRX-400 MHz NMR spectrometer operating at 500 MHz was used for ^{13}C NMR measurements. The TEM, XPS, DSC, measurements of IEC, water uptake, dimensional swelling, methanol permeability, and single stack fuel cell performance followed the same procedures given in Chapter 3. Poroton conductivity was measured by an Autolab PGSTAT 12 (Netherlands) potentiostat/galvanostat fitted with a FRA2 frequency response analyzer. The tensile strengths and strains of the membranes were measured by an Instron 5544 universal tester at room temperature. For the measurements, a membrane was cut into a (3 × 1 cm) rectangle which was held in flat-faced grips and pulled apart at the crosshead speed of 1 mm min^{-1}.
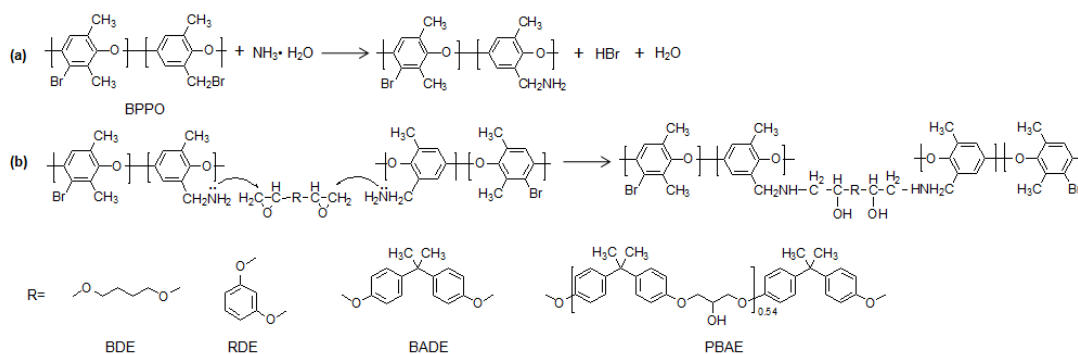
Figure 5.1 Schematic of (a) synthesis of aminated BPPO and (b) covalent cross-linking between aminated BPPO and epoxide cross-linkers.

5.3 Results and Discussion

5.3.1 Synthesis and Characterization of SIPN Structures

An SIPN structure was formed by mixing aminated BPPO, an epoxide cross-linker (BDE, RDE, BADE or PBAE) and neutralized SPPO, and keeping the mixture at an

elevated temperature to improve the reaction kinetics. Aminated BPPO was synthesized by the reaction of BPPO with excess ammonia (Figure 5.1a). XPS (Figure 5.2) and ^{13}C NMR spectroscopy (Figure 5.3) were used to confirm the successful completion of the synthesis. When ammonia was added to a BPPO solution, the bromomethyl (–CH$_2$Br) groups in BPPO were converted to aminomethyl (–CH$_2$NH$_2$) groups. The two peaks in the N1s XPS spectrum (Figure 5.2b) with binding energies at about 399.0 eV and 401.3 eV are characteristics of primary amines and ammonium cations, respectively (Cheng, Z. P. *et al.* 2006). In Figure 5.3b, the absence of a peak around 28 ppm characteristic of the aliphatic carbon in the bromomethyl group (peak 'a' in Figure 5.3a) suggests the complete conversion of –CH$_2$Br groups into –CH$_2$NH$_2$ groups (White, D. M. *et al.* 1990). When aminated BPPO was subsequently cross-linked by an epoxide cross-linker via the –CH$_2$NH$_2$ groups (Figure 5.1b), hydroxyl groups were formed in the inter-chain covalent cross-links, which were confirmed by comparing the ^{13}C NMR spectrum of a cross-linked sample (e.g., the RDE1.0 membrane) with a sample without the epoxide cross-linker (Figure 5.3b and c). Two new peaks emerged in the ^{13}C NMR spectrum of the cross-linked membrane RDE1.0, at 68.2 ppm (peak 'b') and 69.7 ppm (peak 'c'). Peaks 'b' and 'c' correspond well with carbon atoms next to a –OH group and a –O– group, respectively, indicating that the epoxide groups had reacted with the aminomethyl groups.

The neutralized SPPO was immobilized *in situ* by the cross-linked BPPO network during the covalent cross-linking. The pre-neutralization of the sulfonic acid (–SO$_3$H) groups in SPPO by ammonia was an essential step. It averted the precipitation of a polymeric salt in the reaction mixture due to ion pair formation between aminated BPPO and SPPO (protonated amine-sulfonate anion ion pairs) (Fu, R. Q. *et al.* 2008).

Four series of uniform, self-standing membranes cross-linked by different epoxides were obtained after the evaporation of the NMP solvent. Post-treatment of the membranes in HCl solution re-acidified the SPPO, finalizing the preparation of the SIPN membranes. Based on the $-SO_3H/-CH_2NH_2$ ratio used for membrane preparation, the acidic $-SO_3H$ groups were present in stoichiometric excess. Some of the $-SO_3H$ groups would develop ion pairs with unreacted $-CH_2NH_2$ groups or with the amine moieties formed by the covalent cross-linking reaction. The remaining $-SO_3H$ groups were free to sustain proton transport in the membrane.
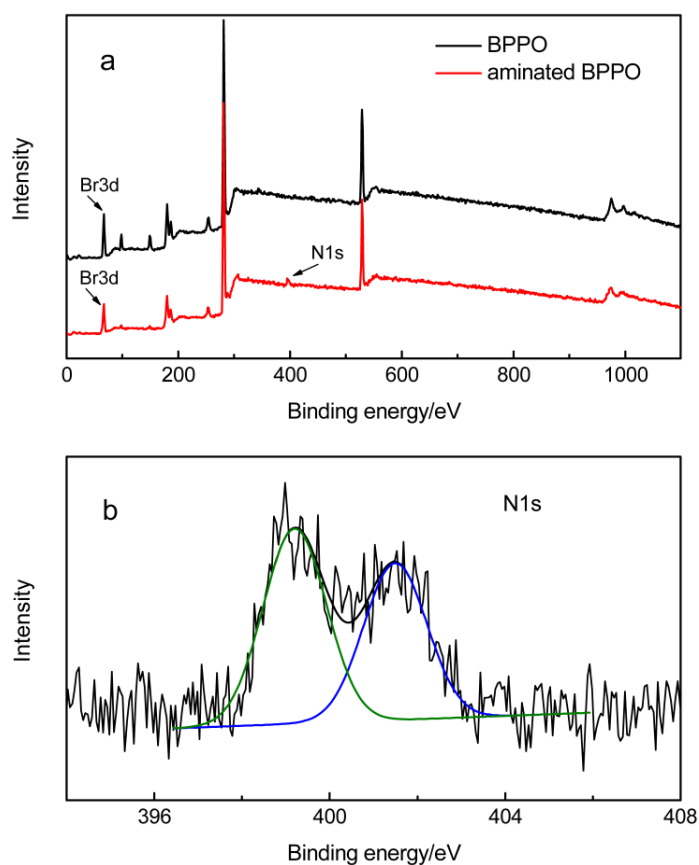
Figure 5.2 (a) XPS spectra of BPPO and aminated BPPO, (b) N1s core-level spectrum of aminated BPPO, where the green and blue peaks represent the primary amines and ammonium cations respectively.
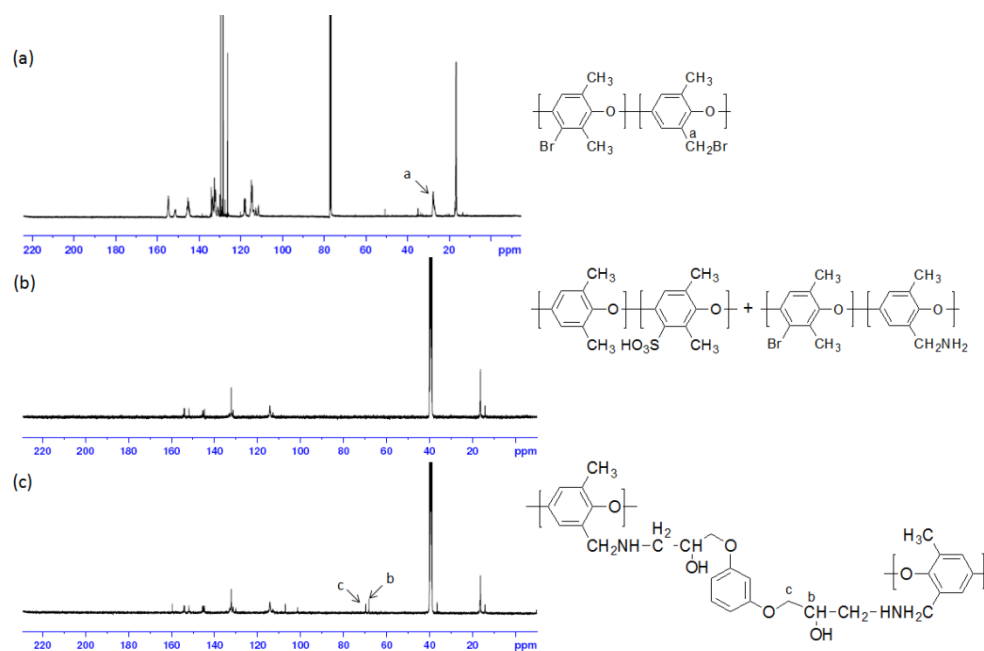
Figure 5.3 ^{13}C NMR spectra of (a) BPPO, (b) blend membrane of SPPO and aminated BPPO and (c) RDE1.0 membrane.

5.3.2 Composition-Morphology-Property Relationships

The chain structure and polarity of the constituent polymers have a strong influence on the membrane morphology (Kreuer, K. D. 2001; Kreuer, K. D. *et al.* 2004). In order to better understand the causative relationship, we examined the effects of cross-link size and solubility parameter, and the amount of cross-linker used, on membrane morphology (by TEM). The size (V, cm^3 mol^{-1}) and solubility parameter (δ, $(cal\ cm^3)^{0.5}$) of the cross-links between two epoxy groups were estimated by previously published methods (Coleman, M. M. *et al.* 1990; Musale, D. A. *et al.* 2000) and were summarized in Table 5.1. Both "V" and "δ" follow an increasing trend in the order of BDE < RDE < BADE < PBAE. A higher δ value indicates decreasing hydrophobicity of the cross-link.

Table 5.1 Calculated size and solubility parameters of cross-links between two epoxy groups.

	M (g mol^{-1})	V^a (cm^3 mol^{-1})	ρ (g cm^{-3})	ΣF ^{b} [(cal cm^3)$^{0.5}$ cm^3 mol^{-1}]	δ ^{c} [(cal cm^3)$^{0.5}$]
BDE	116.3	109.2	1.01	938	8.17
RDE	136.2	114.6	1.19	1064	9.31
BADE	254.4	209.6	1.21	2057	9.80
PBAE	291.0	329.2	0.88	3432	10.38
Methanol	-			-	14.51^d
Water	-			-	23.41^d

^{a} Data from the previous article (Coleman, M. M. *et al.* 1990).

^{b} Total molar attraction constant can be estimated by simple addition of group contributions (Musale, D. A. *et al.* 2000). The effect of conformations was not taken into account.

^{c} The solubility parameter can be calculated via $\delta = \rho \Sigma F / M$, where M is the molecular weight, ρ is the density.

^{d} Data from handbook (Zeng, W., Du, Y., Xue, Y., Frisch, H. L. **2007**).
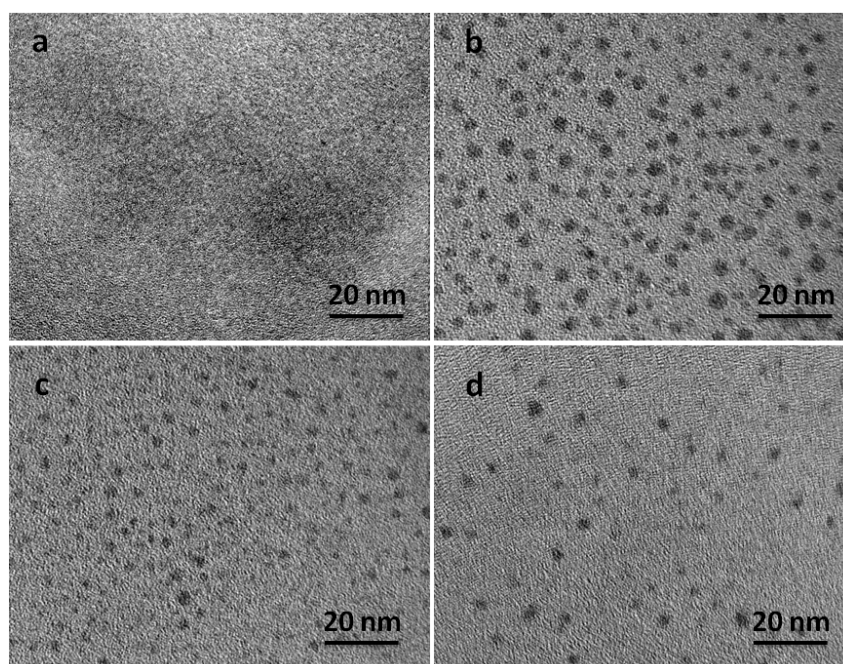
Figure 5.4 TEM images of SIPN membranes: (a) BDE0.5, (b) RDE0.5, (c) BADE0.5, (d) PBAE0.5.

The morphology of the SIPN membranes was examined by TEM. Four images of the 0.5 series SIPN membranes are used as comparative examples in Figure 5.4. The dark spots in the TEM images were hydrophilic domains where sulfonic acid clusters were stained by Pb^{2+} ions (Lee, M. *et al.* 2009). EDX elemental mapping confirmed the

simultaneous presence of Pb^{2+} and sulfur in these spots (Figure 5.5). Figures 5.5b and 5.5c are the element maps of S and Pb for the cross-section of a Pb^{2+} stained RDE0.75 membrane cross-section shown in Figure 5.5a. The bright spots in the EDX maps are in registration with each other, and correspond well with the dark spots in the TEM image (Figure 5.5a). The superimposability of these measurements confirmed that the dark spots were Pb^{2+} exchanged sulfonic acid groups.
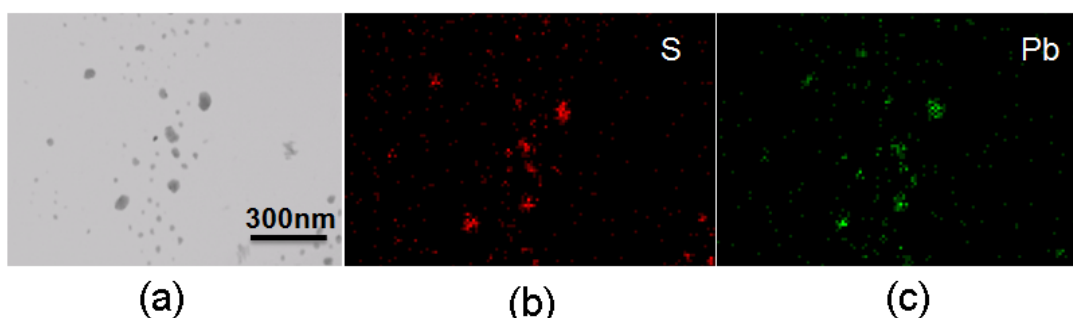
Figure 5.5 EDX elemental maps of S and Pb of a Pb^{2+} stained RDE0.75 membrane. (a) TEM image of the Pb^{2+} stained RDE0.75 membrane; (b) sulfur signal; (c) lead signal (shown as bright spots).
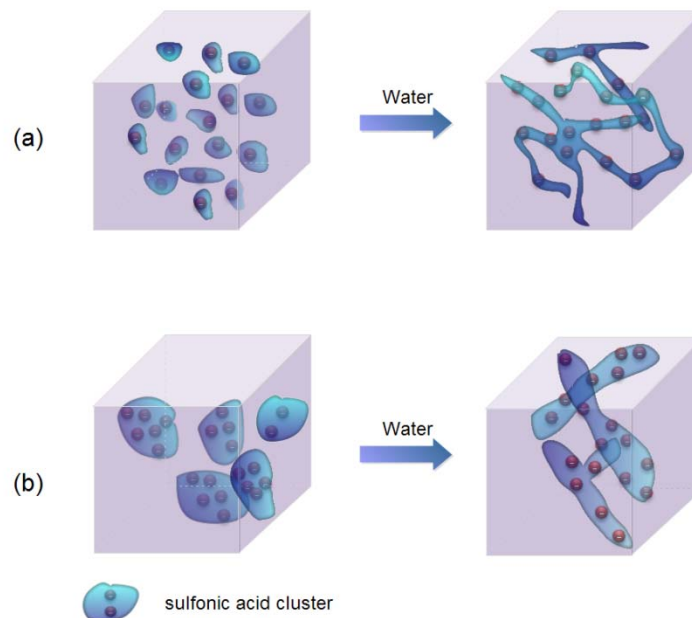
Figure 5.6 Illustrations showing the hydrophilic domains in SIPN membranes formed with different cross-links. (a) Small and more hydrophobic cross-links form small and numerous hydrophilic domains, which expand into narrow but well-connected hydrophilic channels upon hydroation. (b) Bulky and less hydrophobic cross-links form large but isolated hydrophilic domains, thus wide hydrophilic channels with more dead ends are formed upon hydration.
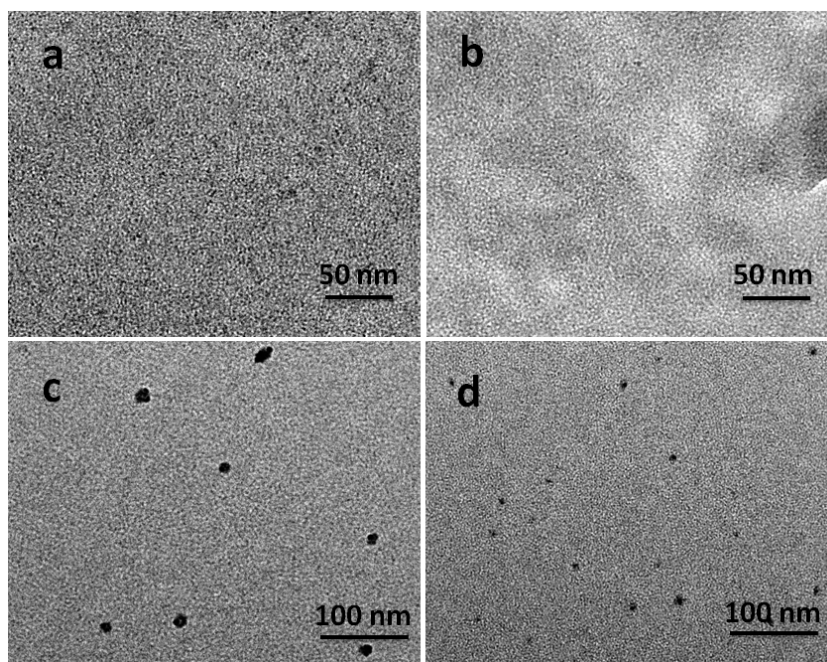
Figure 5.7 TEM images of SIPN membranes: (a) BDE0.25, (b) BDE0.5, (c) BDE0.75, (d) BDE1.0.

The TEM images in Figure 5.4 show a very different morphology of BDE0.5 from the other three SIPN membranes (i.e., RDE0.5, BADE0.5 and PBAE0.5): the hydrophilic domains were significantly smaller (< 1 nm) in BDE0.5. This is taken as an indication of a smaller extent of phase separation in this particular membrane matrix. The size and solubility parameter of the BDE cross-link are smaller than the other three cross-links (i.e., RDE, BADE and PBAE). This enabled the formation of a relatively dense hydrophobic membrane structure with good dimensional stability in the aqueous solution. The movement of SPPO was constrained to impede the aggregation of sulfonic acid groups into large clusters. The large number of sub-nanometer hydrophilic domains in BDE0.5 could increase the possibility of developing narrow and well-connected hydrophilic channels upon hydration, as shown in the illustration of Figure 5.6a. On the contrary, the bulkier RDE, BADE and PBAE cross-links would space out the cross-linked polymer chains, resulting in more freedom for the SPPO polymer segmental motion. In addition, the relatively high solubility parameters of

RDE, BADE and PBAE cross-links stimulated water permeation and consequently promoted the aggregation of sulfonic acid groups into large clusters. The larger hydrophilic domains in RDE0.5, BADE0.5 and PBAE0.5 were however more isolated, and the formation of wider but less connected hydrophilic channels was more likely to occur (Figure 5.6b).
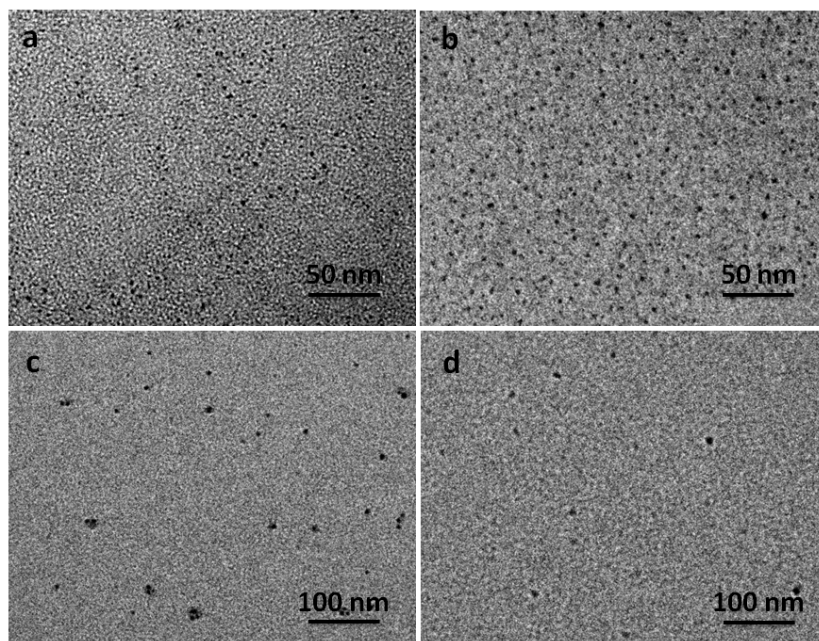
Figure 5.8 TEM images of SIPN membranes: (a) RDE0.25, (b) RDE0.5, (c) RDE0.75, (d) RDE1.0.

The effect of cross-linker amount on membrane morphology was investigated next. The BDE membranes will be used for discussion (Figure 5.7) as their results are typical of the other three SIPN membranes (see Figure 5.8-5.10). All four series of the SIPN membranes displayed the same trend of morphology variations: increasing isolation of the hydrophilic domains at high cross-linker content. This is because a high cross-linking degree would interrupt the continuity of the hydrophilic channels by forming dead-ends in the latter. Dead-ends are an impediment to the development of a contiguous network of hydrophilic channels. The TEM images mirrored the difficulty in Pb^{2+} staining due to the diffusion limitations of dense membranes.
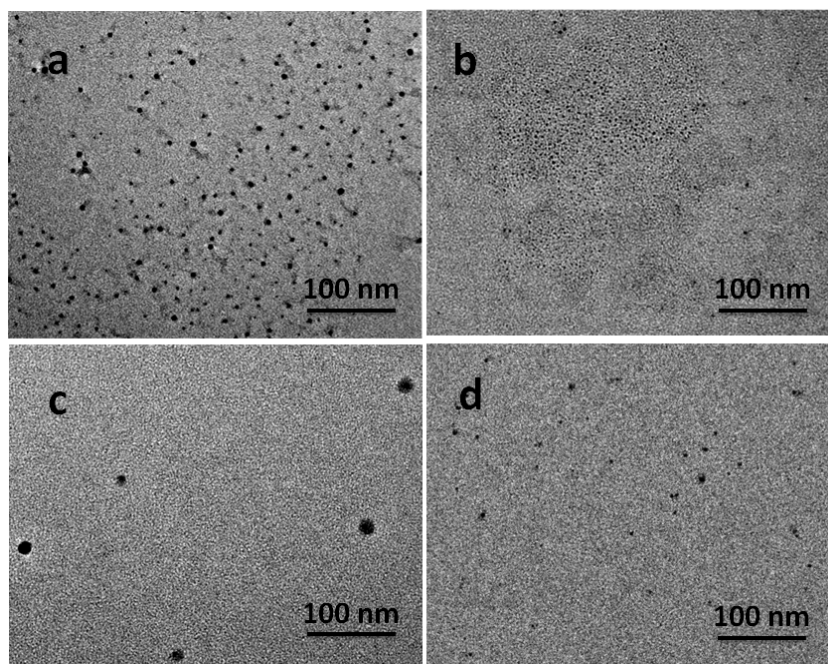
Figure 5.9 TEM images of SIPN membranes: (a) BADE0.25, (b) BADE0.5, (c) BADE0.75, (d) BADE1.0.
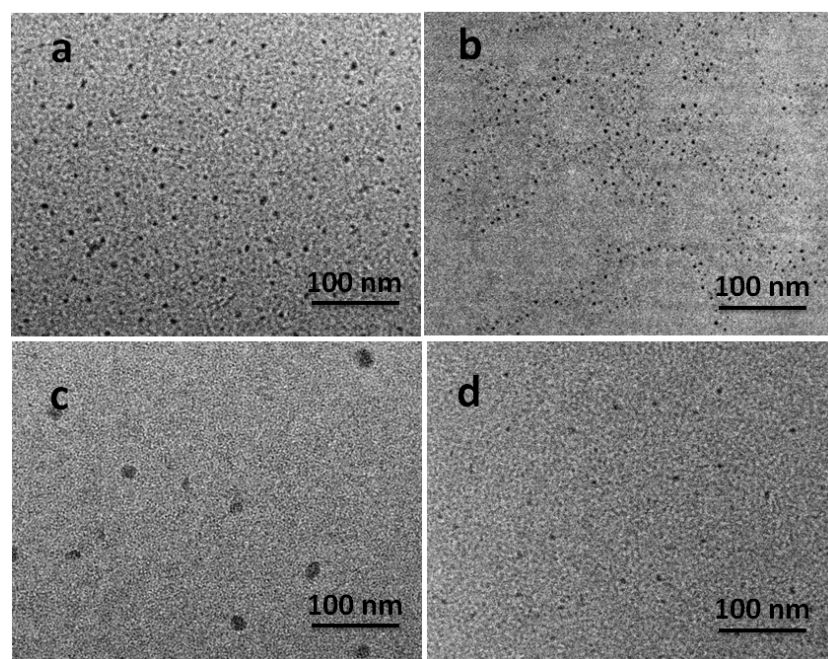
Figure 5.10 TEM images of SIPN membranes: (a) PBAE0.25, (b) PBAE0.5, (c) PBAE0.75, (d) PBAE1.0.
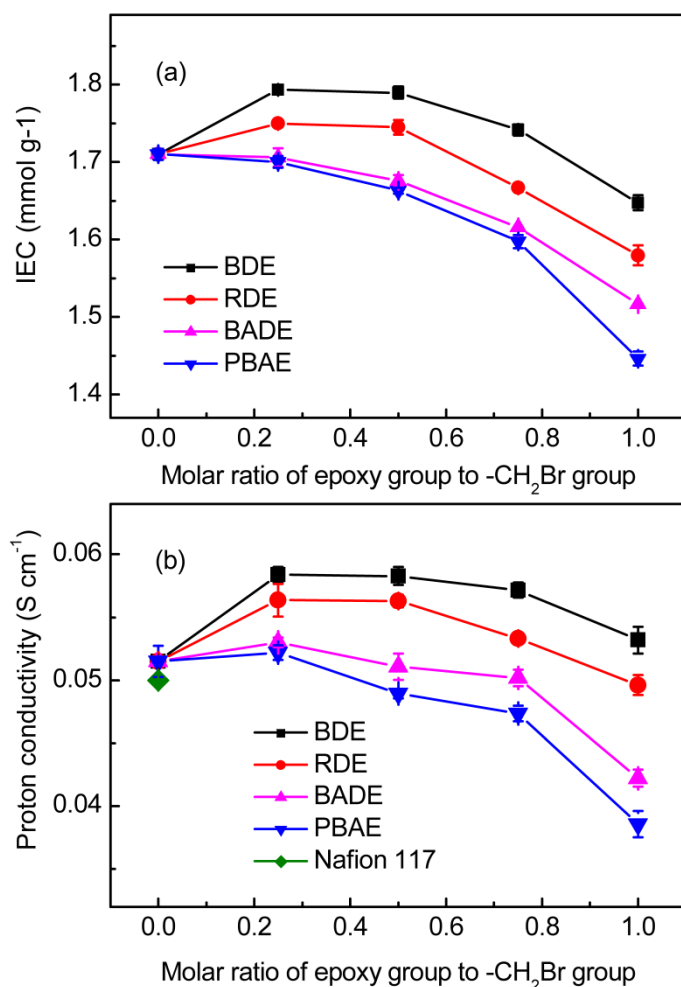
Figure 5.11 IEC (a) and proton conductivity (b) of SIPN membranes.

In order to determine the relation between membrane composition and transport properties, the IEC and proton conductivity of the membranes were measured and plotted against the epoxide to $–CH_2Br$ ratio in Figure 5.11. The measured proton conductivity of Nafion[®] 117 of 0.05 S cm^{-1} is also included in Figure 5.11b for reference. A decreasing trend of IEC and proton conductivity with increasing cross-linker amount was observed for all four series of the SIPN membranes. It is known that proton conduction depends on the accessibility of the ionic sites in aqueous solution. The increase in the number of dead-end channels with increasing cross-linking could reduce the number of accessible sulfonic acid groups and increased the tortuosity in proton transport to result in low IEC and conductivity values.

Comparison of the four series of SIPN membranes indicated generally higher proton conductivities than that of the Nafion[®] 117 membrane. The BDE membranes, in particular, had the highest proton conductivity of the SIPN membranes.

Table 5.2 The water uptake (WU, %), hydration number (λ, the number of water molecules per sulfonic acid groups in membranes), and mechanical properties of SIPN membranes.

Membrane	WU (%)	λ	Tensile strength (Mpa)	Maximum elongation (%)
SPPO/aminated BPPO	24.30	7.89	18.90	13.28
BDE0.25	28.41	8.82	18.83	17.53
BDE0.5	29.71	9.22	23.57	16.99
BDE0.75	26.31	8.40	26.94	13.16
BDE1.0	20.71	6.97	31.29	11.45
RDE0.25	24.30	7.89	18.03	19.63
RDE0.5	29.94	9.50	23.93	15.59
RDE0.75	30.31	9.68	26.16	13.19
RDE1.0	26.39	8.78	30.69	11.42
BADE0.25	24.30	7.89	17.33	18.36
BADE0.5	34.38	11.24	24.36	16.13
BADE0.75	35.94	11.96	27.65	15.24
BADE1.0	31.48	10.86	30.84	12.09
PBAE0.25	24.30	7.89	20.16	16.62
PBAE0.5	34.45	11.26	25.28	13.85
PBAE0.75	32.86	10.99	27.12	13.91
PBAE1.0	30.62	10.70	37.70	13.76
Nafion[®] 117	20.10	12.41	17.85	177.00

The high proton conductivity of the BDE membranes could be explained by membrane morphology. Generally, proton transport in PEMs can occur by three mechanisms depending on the water environment: Grotthuss mechanism, vehicular mechanism and surface mechanism. The relative contributions of these mechanisms are dependent on the hydration number λ (the number of water molecules per sulfonic acid group in the membrane), as shown in Chapter 2. The hydration numbers

λ of the SIPN membrane calculated from their IEC values and water uptake are given in Table 5.2. The λ values were all in the range indicative of moderate hydration, and hence the vehicular mechanisms should prevail. The rate of proton diffusion by the vehicular mechanism depends on the size and the connectivity of the hydrophilic channels. Relative to the BDE membranes, the other three series of SIPN membranes should have an edge in proton conduction because their wider hydrophilic channels would allow more protons to be transported together with water molecules. However, the advantage was compensated by the lower connectivity of the hydrophilic channels in RDE, BADE and PBAE membranes. The results of proton conductivity suggested that the connectivity effect outweighed the size effect on the proton transport in these membranes. Therefore the BDE membranes benefited from a highly connective network of hydrophilic channels where the vehicular diffusion of protons could contribute to high proton conductivity.
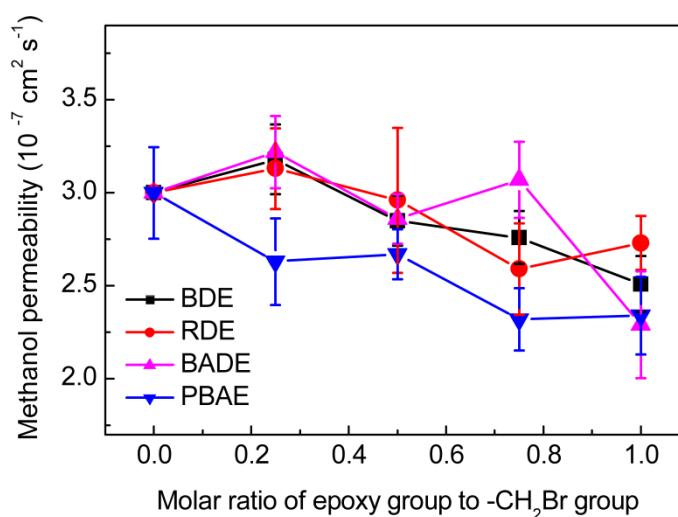
Figure 5.12 Methanol permeability of SIPN membranes.

Figure 5.12 shows that the methanol permeability of the membranes varied from 3.22×10^{-7} cm^2 s^{-1} (BADE0.25) to $\sim 2.29 \times 10^{-7}$ cm^2 s^{-1} (BADE1.0), which is an order of magnitude lower than the methanol permeability of Nafion$^{\circledR}$ 117 measured under the

same experimental conditions (2.01×10^{-6} cm^2 s^{-1}). Hence the SPIN membranes had generally good methanol barrier properties. The methanol permeabilities of BDE, RDE and BADE membranes were about the same, and were higher than the methanol permeability of the PBAE membranes. The good connectivity of the hydrophilic channels in the BDE membranes did not however cause an increase in methanol crossover because the small channel size impeded methanol diffusion. Relative to protons, the size effect affected methanol molecules more because of the larger (associated) cluster size of the latter (§2.2.3.1). The good methanol barrier properties of the RDE and BADE membranes, on the other hand, were more likely due to the increase in the tortuosity and dead-ends of the channels. The same reason could also explain the very low methanol permeability of the PBAE membranes formed by the extremely bulky PBAE cross-linker.

5.3.3 Dimensional Swelling, Mechanical Property and Oxidative Stability of SIPN Membranes

The dimensional swelling of the SIPN membranes was measured at 25 and 80 $^{\circ}$C, the two ends of the operating temperature typical for DMFCs (Figure 5.13). All SIPN membranes had smaller dimensional swelling than the uncross-linked SPPO/aminated BPPO blend membranes especially at the higher temperature. This is clearly due to the effectiveness of a cross-linked network in restraining swelling. The RDE, BADE and PBAE membranes underwent comparable or smaller dimensional changes than the BDE membranes, even though water uptake in the former was higher. The discrepancy between water uptake and membrane swelling could be explained by the larger free volume of the RDE, BADE and PBAE membranes. In these membranes, the cross-links served as spacers to keep the polymer chains at a greater distance. The

spacing-out effect resulted in more free volume for water absorption. However, the bulky cross-links inhibited the SPPO segmental motion, thus restraining the swelling of the SPPO polymers in water. Hence, the dimensional changes in RDE, BADE and PBAE SIPN membranes remained small.
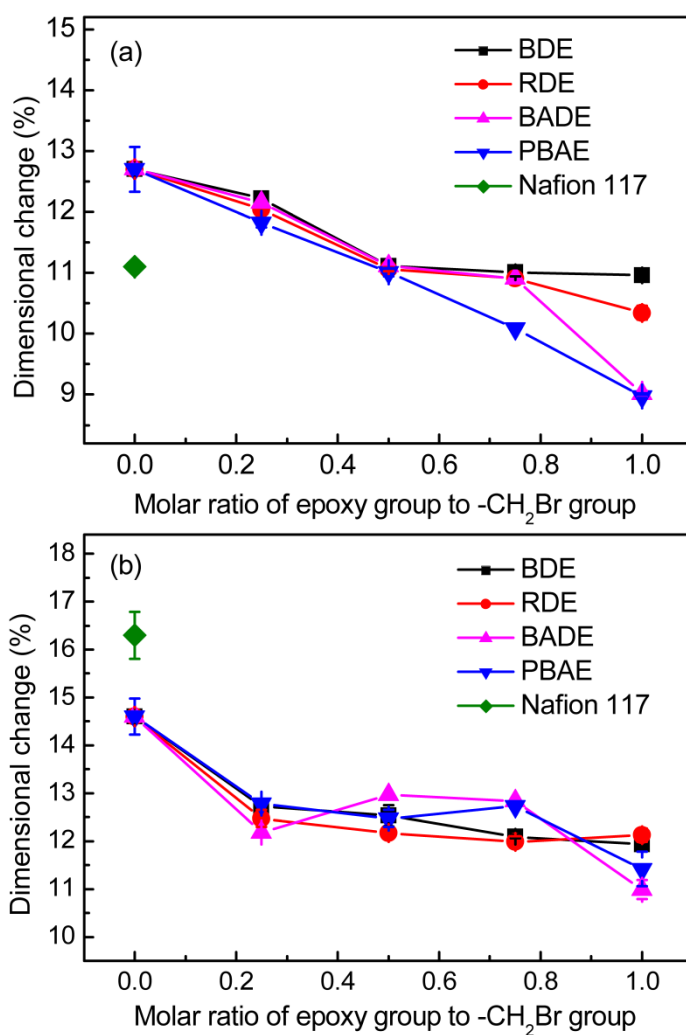
Figure 5.13 Dimensional swelling in Nafion® 117 and SIPN membranes at (a) 25 °C and (b) 80 °C.
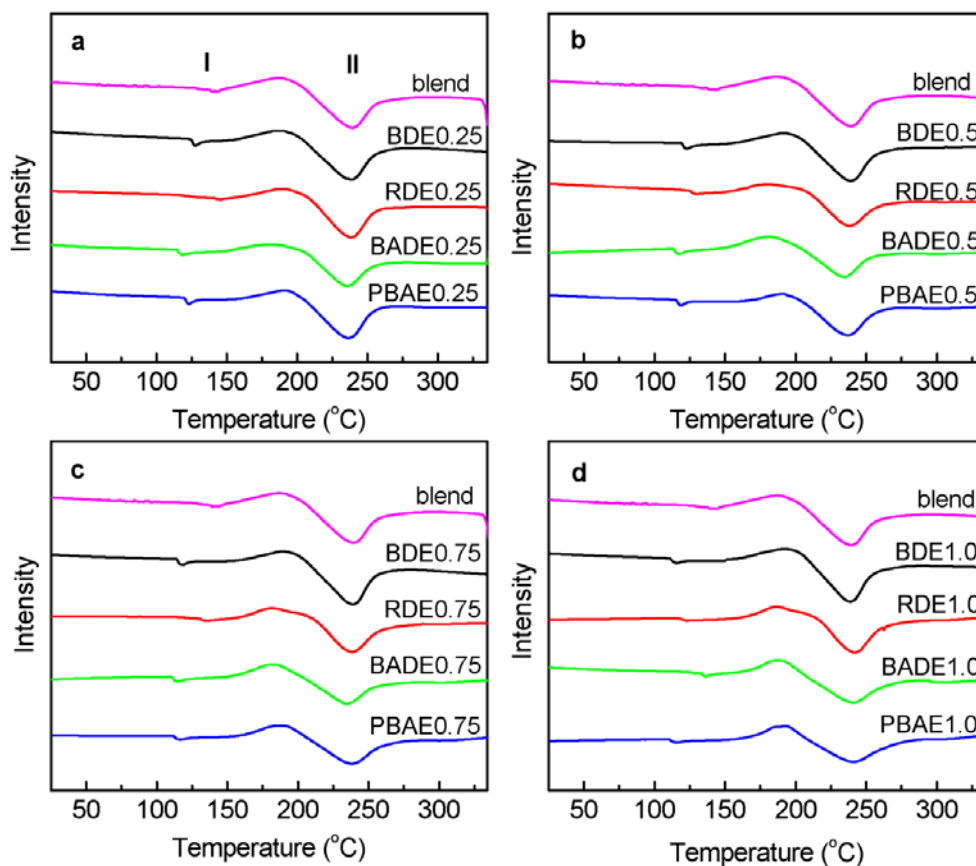
Figure 5.14 DSC curves of SIPN membranes.
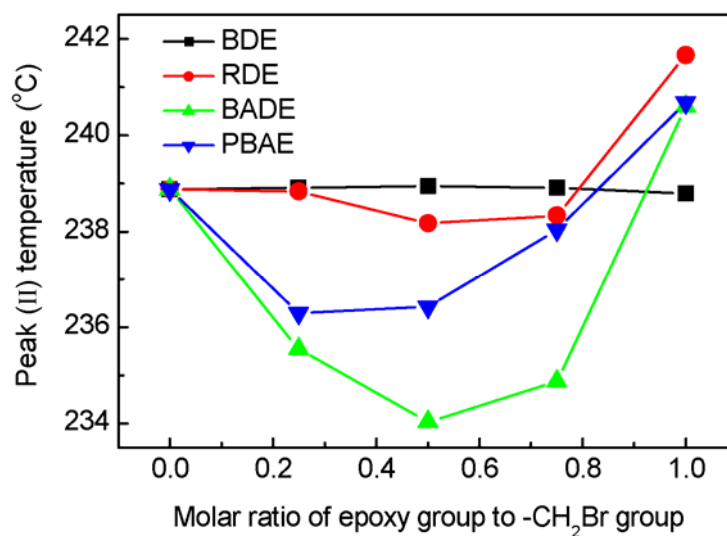
Figure 5.15 The peak (II) temperature of SIPN membranes.

The above effect of the cross-links was also reflected by DSC measurements. Two

endothermic peaks at around 125 $^\circ$C and 240 $^\circ$C were detected in the DSC curves of

the SIPN membranes (Figure 5.14). Although the assignment of the first peak (I) at lower temperature remains contestable (Goddard, R. J. *et al.* 1994; Page, K. A. *et al.* 2005), it is more likely associated with the rotation of the phenyl rings in short PPO segments. The high-temperature peak (II) should relate more to intermolecular attractions (i.e., dipole-dipole interactions between $-SO_3H$ groups and ion pair interactions) and polymer chain movements (Liu, B. J. *et al.* 2007). Generally, an endothermic peak at high temperature in the DSC curve is an indication of constrained polymer chain movements, and high energy barrier in phase transition. Consequently the second peak (II) in Figure 5.15 was carefully analyzed to provide some information on the SIPN membrane microstructure. The peak temperature was lower in the RDE, BADE and PBAE membranes than in the BDE membranes, suggesting less constrained motion of the polymer chains which is consistent with the spacing-out effect and larger free volume in membranes.

The results from the tensile strength measurements are summarized in Table 5.2. With the increase in the cross-linking extent, all four series of SIPN membranes showed higher tensile strengths and lower strains. The measured tensile strengths and maximum elongations of the BDE, RDE and BADE SIPN membranes were in the ranges of 17.33~31.29 MPa and 11.42%~19.63%, respectively. The PBAE SIPN membranes were the notable exception with much higher tensile strengths (20.16~37.70 MPa). This could be because the bulky PBAE cross-links inhibited the relative segmental motion of the polymer chains. For comparison, the tensile strength and maximum elongation of Nafion[®] 117 under the same test conditions were 17.85 MPa and 177.00%, respectively. Hence while the SIPN membranes were relatively rigid, they did possess sufficient mechanical strength to be used in DMFCs.

Table 5.3 Oxidative and hydrolytic stability of SIPN membranes.

Membrane	Oxidative stability	Hydrolytic stability	
	Weight loss in Fenton's test (after 24h) (%)	Proton conductivity (S cm^{-1})	
		before	after
SPPO/aminated	34.4	0.051	0.046
BDE0.25	21.6	0.058	0.056
BDE0.5	19.0	0.058	0.055
BDE0.75	14.6	0.057	0.055
BDE1.0	13.3	0.053	0.050
RDE0.25	21.2	0.056	0.053
RDE0.5	20.6	0.056	0.054
RDE0.75	19.5	0.053	0.051
RDE1.0	17.3	0.049	0.047
BADE0.25	25.4	0.053	0.049
BADE0.5	23.1	0.051	0.047
BADE0.75	25.5	0.050	0.047
BADE1.0	26.1	0.042	0.038
PBAE0.25	57.3	0.052	0.048
PBAE0.5	49.0	0.049	0.045
PBAE0.75	36.2	0.047	0.043
PBAE1.0	30.3	0.038	0.034
Nafion® 117	0.5	0.050	0.048

The oxidative and hydrolytic stability of the membranes were also measured and Table 5.3 is the summary of the measurements. The oxidative stability of the membranes was evaluated by the Fenton test (chemical stability in 3 wt% H_2O_2 aqueous solution containing 3 ppm $FeCl_2 \cdot 4H_2O$) at 80 ^{o}C (Tripathi, B. P. *et al.* 2010). All membranes were embrittled after 1 h in the Fenton solution. Detachment of small fragments occurred to result in over 10% of weight loss. Compared to a weight loss of 23.1%~57.3% for the BADE and PBAE membranes, the BDE and RDE membranes fared better, showing more oxidative stability. This is because the oxidative attack by radical species (HO• and HOO•) should occur mostly in or in the proximity of the hydrophilic domains (Asano, N. *et al.* 2006). The high water content of BADE and

PBAE membranes rendered them more susceptive to the radical attack. The hydrolytic stability of the membranes was evaluated by measuring the proton conductivity before and after equilibrium in 80 $^{\circ}$C water for two weeks. All membranes showed negligible loss of conductivity.

5.3.4   Single stack DMFC test
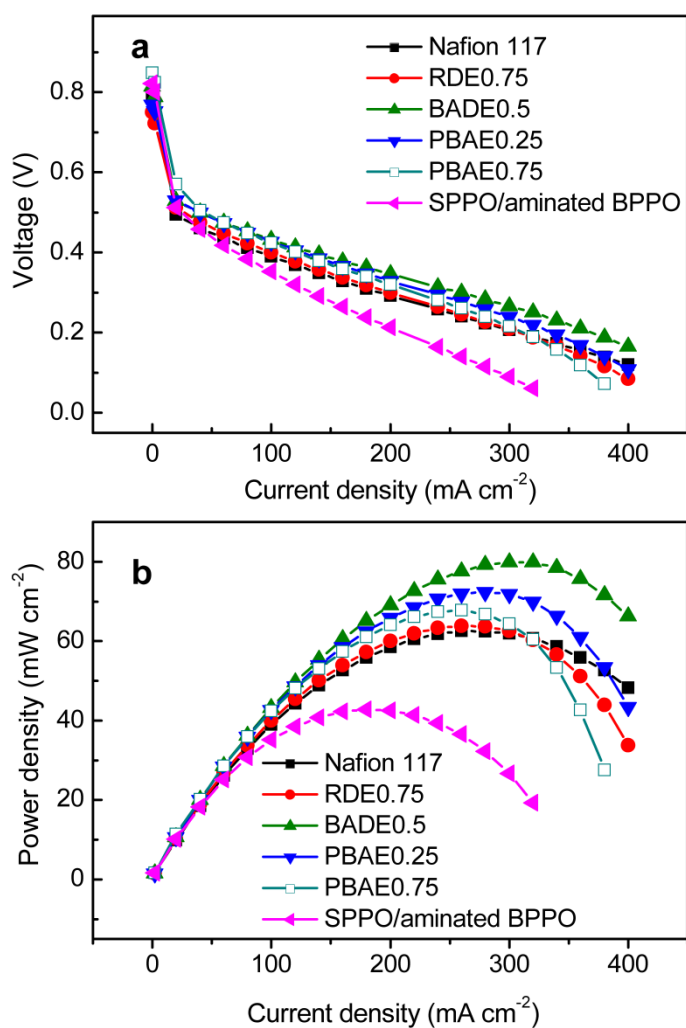
Figure 5.16 Single cell performances of SIPN membranes and Nafion$^{\circledR}$ 117: (a) Polarization curves, (b) power density curves.

The SIPN membranes and a SPPO/aminated BPPO blend were fabricated into MEAs and tested in single stack DMFCs. Power density and other fuel cell parameters were measured in order to evaluate the membrane performance under practical conditions.

Some of the membranes (i.e., RDE0.75, BADE0.5, PBAE0.25 and PBAE0.75) exhibited higher values of maximum power density than Nafion® 117 (Figure 5.16). For example the maximum power density of the BADE0.5 MEA was about 80.0 mW cm^{-2} at 310 mA cm^{-2}, about 30% higher than the Nafion® 117 MEA (62.6 mW cm^{-2} at 270 mA cm^{-2}). The OCV was also higher with the BADE0.5 MEA (0.814 V) than with the Nafion® 117 MEA (0.793 V). Compared with the four SIPN membranes, the cell performance of the SPPO/aminated BPPO blend membrane is relatively poor with a maximum power density of only 42.9 mW cm^{-2}. The improved performance of the SIPN membranes could be attributed to their low methanol permeability.
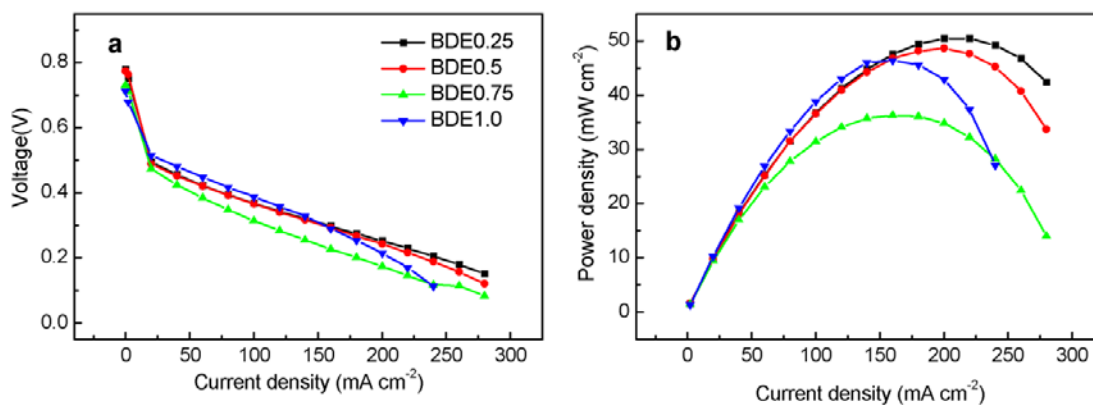
Figure 5.17 Single cell performances of BDE membranes: (a) Polarization curves, (b) power density curves.
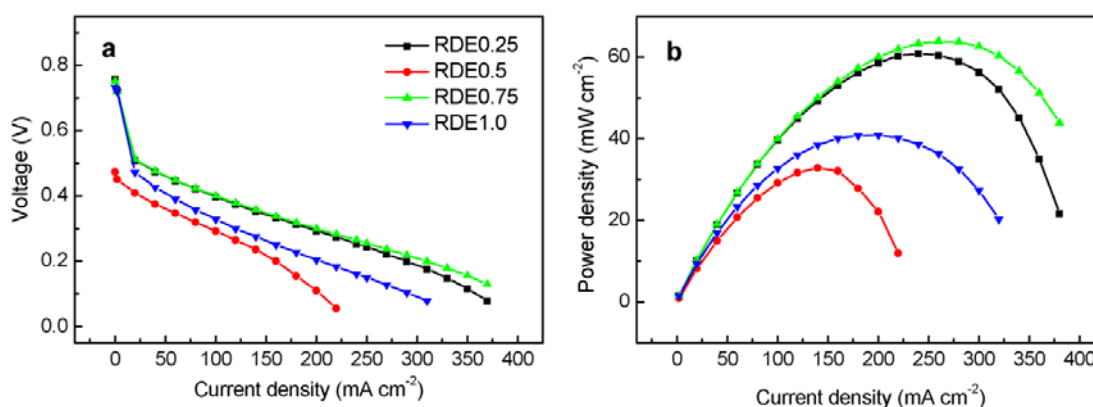
Figure 5.18 Single cell performances of RDE membranes: (a) Polarization curves, (b) power density curves.
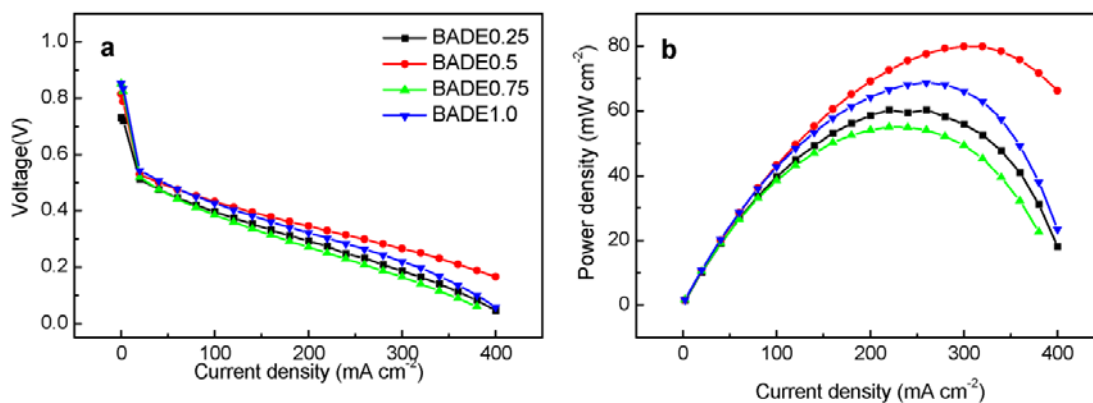
Figure 5.19 Single cell performances of BADE membranes: (a) Polarization curves, (b) power density curves.
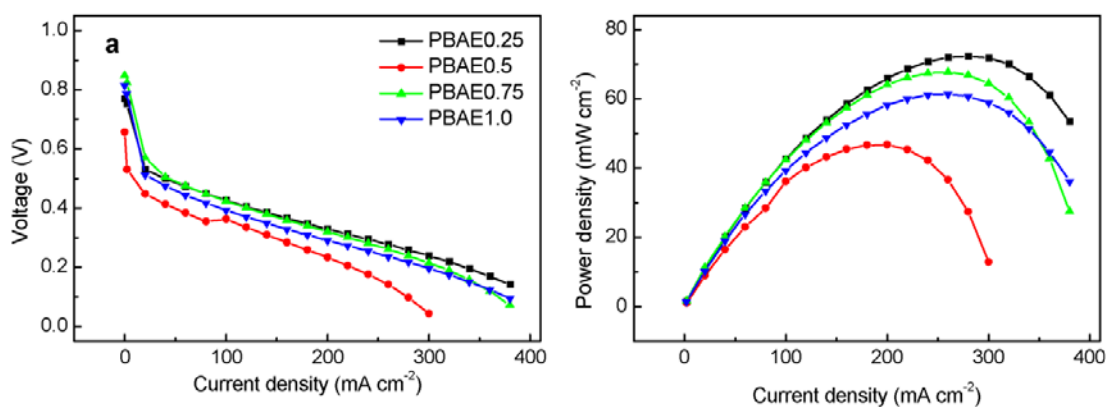
Figure 5.20 Single cell performances of PBAE membranes: (a) Polarization curves, (b) power density curves.

The polarization curves and power density plots for all of the SIPN membranes can be found in Figure 5.17-5.20. In general the single-cell performance of most RDE, BADE and PBAE membranes was better than that of the BDE membranes. While the proton conductivity of the BDE membranes was higher than the other three series of membranes, the BDE membranes did not perform as well at the MEA level. The reason remains unknown but the difference in current density between conductivity measurements (zero current density) and single cell tests (high current densities) could be a contributing factor (possible changes in polymer dynamics). This is an

indication of the importance of single cell tests for the objective evaluation of PEM performance.

5.4   Conclusion

SIPN membranes with narrow and well-connected hydrophilic channels were synthesized by thermally cross-linking BDE with aminated BPPO in the presence of linear SPPO. The resulting membranes exhibited higher proton conductivity and lower methanol permeability when compared with Nafion® 117. Three other series of SIPN membranes were also prepared using different cross-linkers (i.e., RDE, BDE, and PBAE). Comparison between these four series of membranes revealed the importance of the cross-link bulkiness on membrane morphology. Specifically, membranes formed with small and more hydrophobic cross-links (i.e., BDE) had smaller hydrophilic domains than membranes formed with bulky and less hydrophobic cross-links (i.e., RDE, BADE and PBAE). This difference was attributed to the dense structure and water rejection property in the former which impeded the aggregation of sulfonic acid groups into larger clusters. However, there were more small hydrophilic domains in the BDE membranes to increase the extent of channel connection upon hydration. The hydrophilic domains in RDE, BDE, and PBAE membranes were larger but more isolated, hence only wider but less-connected hydrophilic channels were formed after hydration. As a result of the difference in channel morphology, the BDE membranes yielded higher proton conductivity than the other three series of membranes. In comparison with the α,ω-diamine cross-linked SIPN membranes in Chapter 4, the sub-nanometer-sized hydrophilic domains in BDE cross-linked membranes are more conducive to the creation of narrow and well-connected hydrophilic channels. Some general composition-morphology-property

107

relationships were discovered which could be useful for the design of other SIPN

PEMs.

CHAPTER 6

PROTON TRANSFER THROUGH ACID-BASE COMPLEXES IN PROTON EXCHANGE MEMBRANES

6.1   Introduction

In our synthesized ion pair-reinforced SIPN membranes, the ion pairs between the acidic $-SO_3H$ groups and the basic amine moieties of the cross-linking reaction were used to enhance the attachment of linear SPPO to the host network and the uniform distribution of the former in the latter. One drawback of this strategy is the depletion of the free $-SO_3H$ groups by ion pair formation resulting in some decrease in the proton conductivity. The side effects of ion pair formation on proton conduction may be reduced without loss of other PEM benefits if the proton transport in acid-base cross-linked PEMs is better understood.

The dependence of proton transport on the PEM water content has been discussed in the earlier chapters. When a PEM is hydrated, phase separation occurs between the hydrophilic and hydrophobic constituents of the PEM. The sulfonic acid groups aggregate to form water-containing interconnected hydrophilic clusters where protons can pass through. The water in PEM may be classified by their thermal behaviour into three types: non-freezable tightly bound water, freezable loosely bound water; and free water (Kim, Y. S. *et al.* 2003). Non-freezable water is water which is tightly bound to the sulfonic acid groups and which does not display an endothermic melting peak in DSC. Freezable loosely bound water is water weakly bound to the ionic and polar parts of the polymer, which displays a relatively broad melting between -20~20

^{o}C. Free water is water which has no interaction with the polymer matrix and therefore displays the same phase change behavior as normal water (melting point: 0^oC) (Huang, C. H. *et al.* 2010). When there is only one melting peak in the DSC thermogram, it is customary to denote freezable loosely bound water and free water together as "free water".

Proton transport in the free water region of the PEM occurs by two main mechanisms: Grotthuss mechanism and vehicular mechanism. The proton transfer between acid and base molecules in aqueous solution also involves different reaction pathways and dynamics. The complexity of acid-base reactions in aqueous solution was analysed by Rini *et al.* where three different reaction pathways were identified (Rini, M. *et al.* 2003; Rini, M. *et al.* 2004). In tight acid-base complexes where the acid and base molecules are coordinated directly, proton transfer through them is ultrafast accompanied only by the rearrangement of surrounding water molecules. Proton transfer in loose complexes where the acid and base molecules are separated by water bridges is similar to the Grotthuss mechanism involving the reorientation of water molecules in the water bridges. The third mechanism applies only to the case of low acid and base concentrations where the acid and base molecules are initially separated by a large distance. The proton transport follows the three-step process shown in Figure 6.1. First, the acid and base molecules approach each other until they are separated by an optimal distance to form a water bridge between them. Next, protons are shuttled along the water bridge by the reorientation of water molecules. Finally, diffusive separation occurs (Rini, M. *et al.* 2003; Rini, M. *et al.* 2004; Mohammed, O. F. *et al.* 2005). The diffusion step is often rate-limiting in this case.
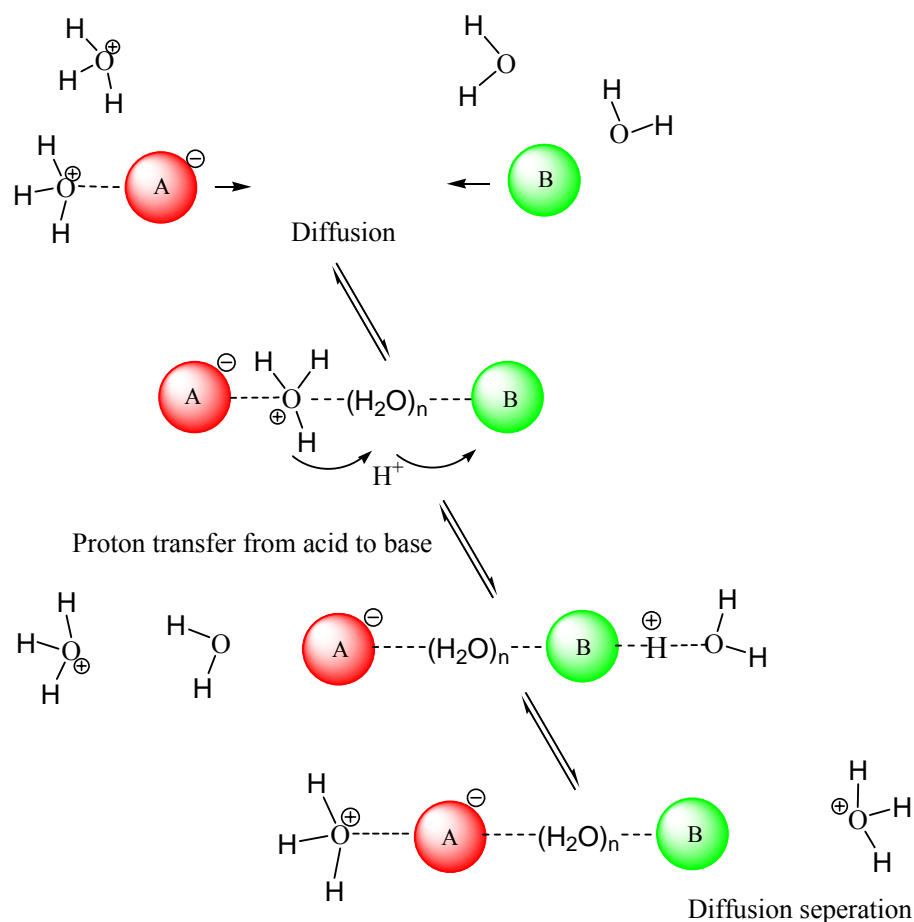
Figure 6.1 Proton transport mechanism when the acid and base molecules are initially separated by a large distance. The red sphere "A" and the green sphere "B" correspond to the acid and base molecules, respectively.

Generally, in acid-base cross-linked PEMs, the diffusion of acid and base polymers can be neglected because the polymer chains are intertwined to prohibit free movement. Therefore, the acid-base cross-links may be treated as tight or loose complexes. Hence, proton transport only involves water reorganization and the diffusive separation of the hydronium ions from the base sites.

The purpose in this part of the thesis study is to investigate acid-base cross-linking in sufficient details to provide some guidance in acid-base combinations with minimum adverse effect on proton conductivity. Hence several acid-base cross-linked

membranes were prepared using different aliphatic and heterocyclic amines as the base in a PPO blend polymer system. SPPO was selected as the acid polymer. The amine molecules were reacted with BPPO to generate different alkylated amine groups. An acid-base cross-linked membrane was then fabricated by blending the acid polymer (SPPO) and the base polymer (aminated BPPO). The proton transfer through acid-base complexes in the membrane was analysed by determining the membrane proton conductivity and the state of water; followed by the evaluation of these acid-base cross-linked membranes in DMFC operations.

6.2   Experimental Section

6.2.1   Materials

PPO (M_w=30000, T_g=211 ^{o}C), chloroform (99%), NMP (99%), sodium chloride (NaCl), propylamine (PA) and imidazole (ID) were purchased from Sigma-Aldrich. Diethylamine (DEA) was supplied by BDH Chemicals, methylimidazole (MID) by Alfa Aesar, BPPO (59.1% benzyl bromide and 40.9% aryl bromide according to ^{1}H NMR spectrometry) was supplied by Tianwei Membrane Corporation Ltd. of Shandong (People's Republic of China). Chlorosulfonic acid (99.0~99.4%), hydrochloric acid (37%), sodium hydroxide (NaOH) and methanol (99.8%) were purchased from Merck. Nafion[®] 117 films were provided by Sigma-Aldrich.

6.2.2   Preparation of SPPO and Cross-linked PPO Membranes

SPPO was synthesized by the procedures in Chapter 3. The IEC of the SPPO synthesized as such was 2.53 mmol g^{-1}, or 38.2% degree of sulfonation. Before use,

the synthesized SPPO was treated in 1M NaCl solution for 24 h to completely exchange its protons with Na$^+$. The Na$^+$-exchanged SPPO was washed with deionized water to remove residual salt and then over-dried at 80 ^{o}C.

Acid-base cross-linked PPO based membrane was fabricated by thermal cross-linking. The preparation of PPO-PA membrane is given below as an example. 0.3 g of the Na$^+$-exchanged SPPO and 0.045 g BPPO were dissolved in NMP separately to concentrations of 60 mg mL^{-1} and 9 mg mL^{-1} respectively. Excess PA was introduced to the BPPO solution and left to react for 2 h. The PA/BPPO mixture was then added to the NMP solution of Na$^+$-exchanged SPPO. The blend formed as such was clear without any solid deposit. It was cast into a membrane in a glass petri dish at 80 ^{o}C (in an oven) over a period of 48 h. The PPO-DEA, PPO-ID, and PPO-MID membranes were similarly prepared by using DEA, ID, and MID as the cross-linkers.

The dried membranes were acidified in 1.0 M HCl for 24 h to allow them to be re-protonated into the H$^+$ form, washed several times with distilled water and then air-dried. A blank membrane prepared from an SPPO-BPPO blend without any cross-linker was used as the experimental control. All the membranes investigated in this study were prepared with an SPPO:BPPO weight ratio of 20:3 ($-SO_3H/-CH_2Br = 5.8/1$), which was found to provide the best balance of membrane properties for fuel cells such as dimensional swelling and proton conductivity.

6.2.3   Characterizations

The XPS characterization, measurements of IEC, water uptake, dimensional swelling, methanol permeability, and single stack fuel cell performance followed the same

procedures given in Chapter 3. Poroton conductivity was measured by an Autolab PGSTAT 12 (Netherlands) potentiostat/galvanostat fitted with a FRA2 frequency response analyzer. The different states of water in the membrane were characterized by DSC, using a Mettler Toledo DSC 822e calorimeter and N_2 atmosphere. The measurements involved holding the samples at -50 ^{o}C for 0.5 h and then heating at the rate of 10 ^{o}C min^{-1} to to 50 ^{o}C. The proportion of free water, f_{free} was calculated by comparing the measured enthalpy with the heat of melting of pure water (334.0 J g^{-1}) (So, S. Y. *et al.* 2010). The number of water molecules can then be computed from equations (1) to (3) below where $n_{H2O,total}$ (mmol), $n_{H2O,free}$ (mmol) and $n_{H2O,bound}$ (mmol) are the amounts of total, free and bound water molecules respectively.

$$n_{H2O,total} = (W_{wet} - W_{dry})/18 \tag{1}$$

$$n_{H2O,free} = n_{H2O,total} \times f_{free} \tag{2}$$

$$n_{H2O,bound} = n_{H2O,total} - n_{H2O,free} \tag{3}$$

The maximum number of bound water molecules per free $-SO_3H$ is six according to electronic structure calculations (Kreuer, K. D. *et al.* 2004). Hence we may assume that every oxygen atom in a $-SO_3H$ group binds to two water molecules through hydrogen bonds.
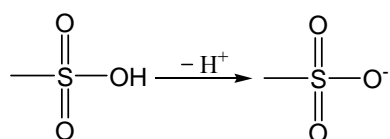
The oxygen atom in the $-O^-$ group is taken up by ionic cross-linking and can no longer accommodate water molecules due to steric hindrance. Hence the maximum number of bound water molecules per $-SO_3^-$ after acid-base cross-linking could be reduced to four. The number of bound water molecules in the water bridge in an acid-base complex can then be calculated as follows. Firstly, the total number of bound

water, $n_{H2O, bound}$ was determined. The numbers of water molecules bound to free –SO$_3$H and –SO$_3^-$ (after acid-base cross-linking), calculated by the aforementioned assumptions, were then subtracted from the total number of bound water to yield the number of bound water molecules in the water bridge, $n_{H2O,acid-base}$ (mmol).

6.3   Results and Discussion

6.3.1   Synthesis and Characterization of Acid-Base Cross-linked PPO Membranes
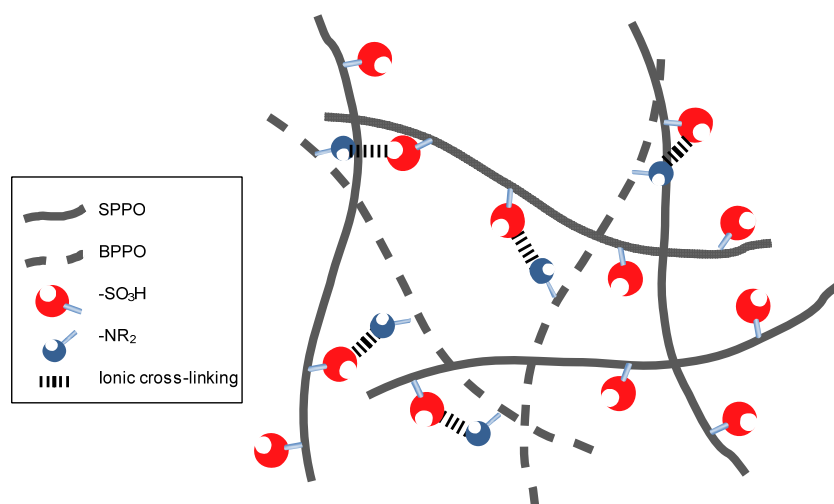
Figure 6.2 Acid-base cross-linked PPO membranes

The acid-base cross-linked PPO membranes shown in Figure 6.2 were formed by mixing aminated BPPO (a polymer base) with SPPO (a polymer acid). Aminated BPPO was obtained by the reaction between BPPO and amine molecules thereby converting the –CH$_2$Br groups in alkylated amine moieties. For example, the reaction between –CH$_2$Br and primary amine PA and secondary amine DEA would form secondary and tertiary amines respectively. The reactions of ID and MID with the –

CH$_2$Br group are shown in Figure 6.3. The occurrence of these reactions could be confirmed by XPS spectroscopy.

(a)
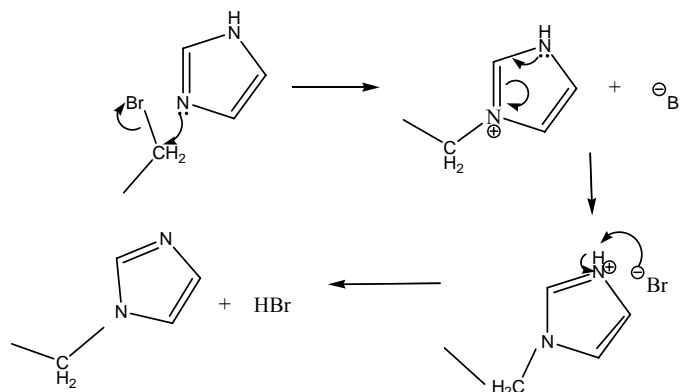
(b)
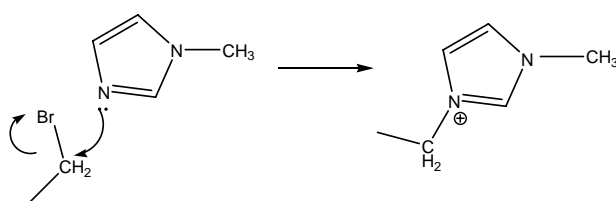
Figure 6.3 (a) Tautomerization in the S$_{N2}$ reaction of ID with BPPO, (b) the substitution reaction between MID and BPPO.

Figure 6.4 shows the XPS spectra of two batches of membrane samples: untreated membranes and membranes treated by NaOH solution. The purpose of the base treatment was to break up the acid-base cross-links and return the protonated secondary/tertiary amine groups to secondary/tertiary amines in PPO-PA and PPO-DEA membranes. By this method we could avoid the interference from unreacted amines and identify the extent of reaction (please refer to Chapter 3 for more details). The peaks with binding energies at about 399.6 eV, 400.0 eV, and 401.6 eV in the N1s XPS spectra agree well with those of secondary amines, tertiary amines and N$^+$ species respectively. The structures of the N$^+$ species deduced by referencing to

previously reported XPS spectra (Jansen, R. J. J. *et al.* 1995; Jousseaume, V. *et al.* 2003; Caporali, S. *et al.* 2006) are also shown in Figure 6.4. The existence of acid-base cross-links was therefore confirmed by the presence of the N$^+$ peaks in Figure 6.4a-d. From Figure 6.4e-h, the completeness of the reaction between amine molecules and BPPO could be confirmed by the absence of primary, secondary amine and pyrrolic N peaks in NaOH treated PPO-PA, PPO-DEA and PPO-ID, and the presence of the N$^+$ peak in NaOH treated PPO-MID, respectively, similar to the reasons given in § 3.3.1
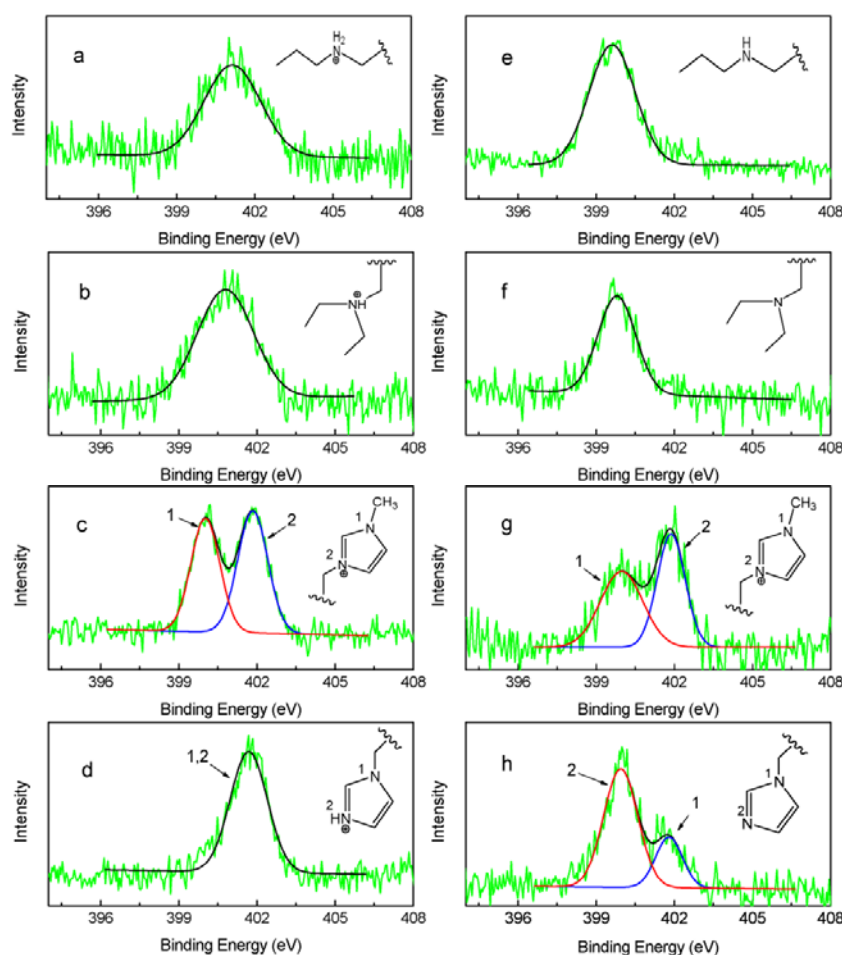
Figure 6.4 N1s core-level spectra of the cross-linked membranes: (a) PPO-PA membrane, (b) PPO-DEA membrane, (c) PPO-MID membrane, (d) PPO-ID membrane, (e) base-treated PPO-PA membrane, (f) base-treated PPO-DEA membrane, (g) base-treated PPO-MID membrane and (h) base-treated PPO-ID membrane.

The purpose of converting the sulfonic acid groups ($-SO_3H$) in SPPO into $-SO_3^-Na^+$ was to prevent the precipitation of a polymer salt when SPPO and aminated-BPPO solutions were mixed. Since SPPO and aminated BPPO contain the same parent polymer (PPO), the two polymers mixed very well in NMP, forming (four) uniform membranes after solvent evaporation. The post-treatment of the membranes in HCl solution re-acidified the SPPO, finalizing the preparation of acid-base cross-linked PPO membranes.

6.3.2   Effects of Acid-Base Cross-links on Proton Transport

The effects of acid-base cross-links on proton transport in the membrane were assessed by measurements of IEC, water content and the states of water in the membrane. IEC is a quantification of the free (ion-exchangeable) sulfonic acid groups in the membrane. The measured IEC values of the PPO membranes are shown in Figure 6.5. The IEC values of the acid-base cross-linked membranes were lower than that of the un-cross-linked blank membrane, understandably so because of fewer free sulfonic acid groups after the formation of acid-base cross-links. The measured IEC values of the cross-linked membranes varied noticeably for the same amount of amine used in the preparation even though XPS suggested complete amination of the bromomethyl groups. The discrepancy is an indication of possible disturbance to the acid-base cross-links. When the interactions between acid and base groups was relatively weak, the acid-base cross-links could be destabilized by the Na^+ ions in NaCl solution, leading to proton release from the acid-base complexes. The measured IEC values were therefore higher. This was the case for the PPO-MID and PPO-ID membranes.
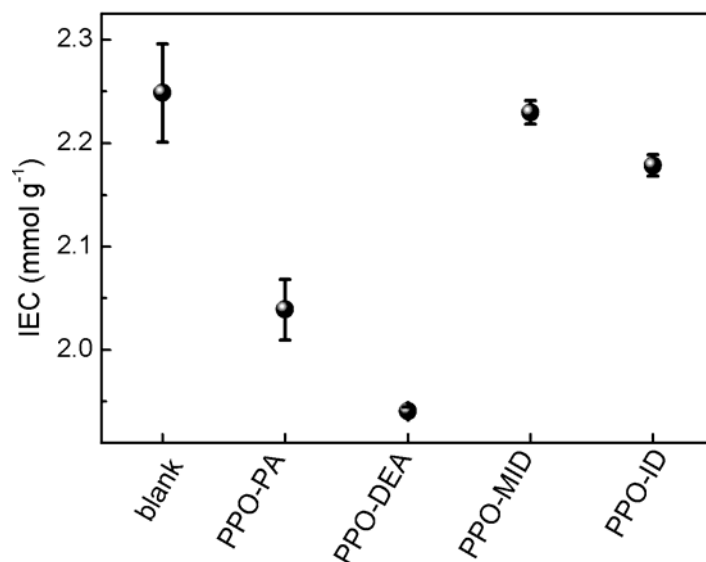
Figure 6.5 IEC of blank and cross-linked membranes.
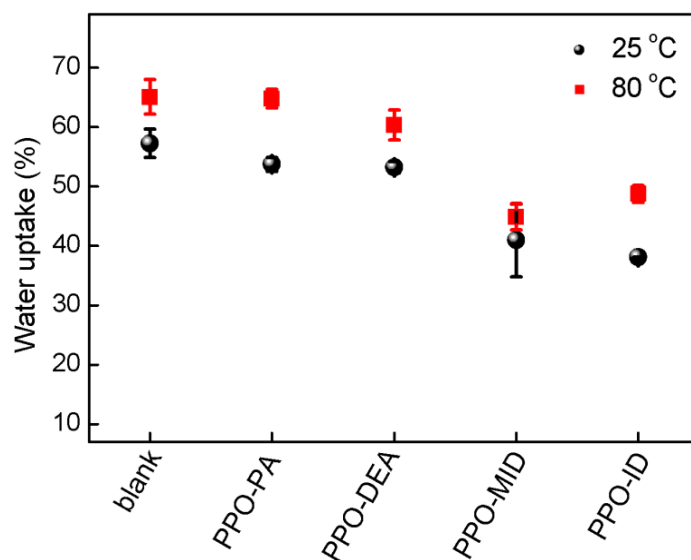
Figure 6.6 Water uptakes by blank and cross-linked membranes.

The water content in the membrane is closely related to the IEC and the free volume in the membrane – an increase in the free $-SO_3H$ groups and a larger free volume would increase water absorption. The highest water uptake of the un-cross-linked blank membrane could be understood as such (Figure 6.6). The formation of acid-base cross-links densified the membrane structure and resulted in fewer free $-SO_3H$ groups, hence the water uptake was correspondingly reduced. Despite a similar cross-

linking degree through the use of the same amount of amine molecules and their complete reaction with the –SO$_3$H groups of SPPO, water uptake was different for different cross-linked membranes. This difference suggests a possible influence from the basicity of the N$^+$ moieties on the hydrophilicity of the cross-linked polymer. The higher basicity of the secondary amine (pKa = 10.57) and tertiary amine groups (pKa = 10.75) of PPO-PA of and PPO-DEA membranes could lead to hydrophilicity increase and consequently their capacity for water absorption. Therefore, the water uptakes of PPO-PA and PPO-DEA membranes were almost as high as that of the blank membrane despite the low IEC values of the former. PPO-ID and PPO-MID membranes, on the contrary, showed lower water uptake because of the lower basicity of the imidazolium cations (pKa = 6.95 for ID and pKa = 7.06 for MID) (Catalan, J. *et al.* 1984). The increase in the water update by all membranes with temperature increase was caused by the thermal weakening of the intermolecular forces resulting in a greater free volume for water accommodation.
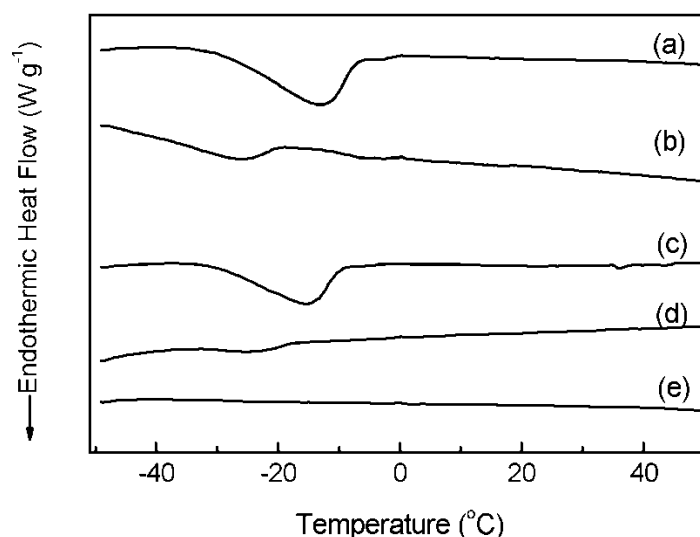
Figure 6.7 DSC heating curves of the PPO membranes: (a) blank membrane, (b) PPO-PA membrane, (c) PPO-DEA membrane, (d) PPO-MID membrane, (e) PPO-ID membrane.
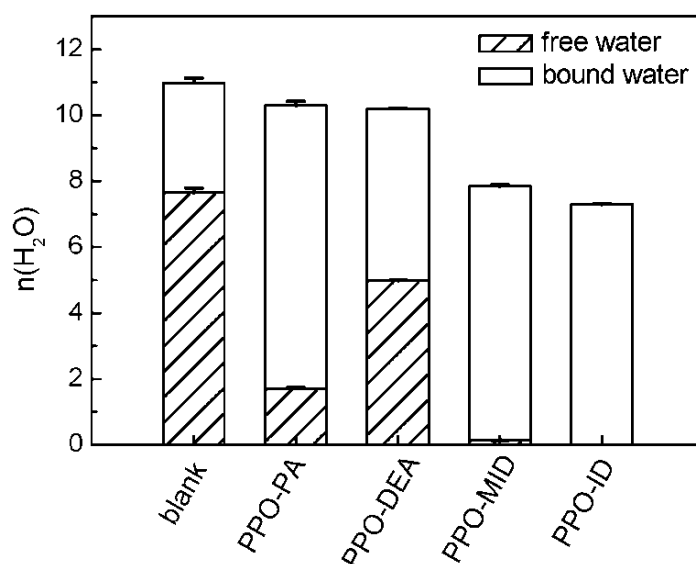
Figure 6.8 Numbers of bound and free water in the cross-linked membranes.

Table 6.1 Numbers of bound water, free water in membranes and number of water in acid-base complexes, and activation energies of the cross-linked membranes from Arrhenius plots.

Membrane	$n_{H2O,total}$ (mmol)	$n_{H2O,free}$ (mmol)	$n_{H2O,bound}$ (mmol)	$n_{H2O,acid-base}$ (mmol)	E_a (kJ mol^{-1})
blank	10.98	7.66	3.31	-	11.11
PPO-PA	10.29	1.72	8.57	4.28	11.82
PPO-DEA	10.20	4.99	5.21	0.92	10.09
PPO-MID	7.84	0.14	7.70	2.99	11.07
PPO-ID	7.29	0	7.29	3.41	10.34

The proportions of free and bound water contents were calculated from the DSC analysis. PPO-ID membrane aside, the free water in the other four membranes produced a broad endothermic peak around -10 ^{o}C in the DSC heating curves (Figure 6.7). The values of $n_{H2O,bound}$ and $n_{H2O,free}$ calculated from equations (1)-(3) are summarized in Table 6.1 and Figure 6.8. All acid-base cross-linked membranes contained more bound water than the blank membrane. Since there were more free sulfonic acid groups in the blank membrane, the finding suggests the existence of water bridges which behaved like bound water in acid-base complexes. The number

of water in acid-base complexes ($n_{H2O, \text{acid-base}}$) calculated by the procedure in § 6.2.3 is also given in Table 6.1.
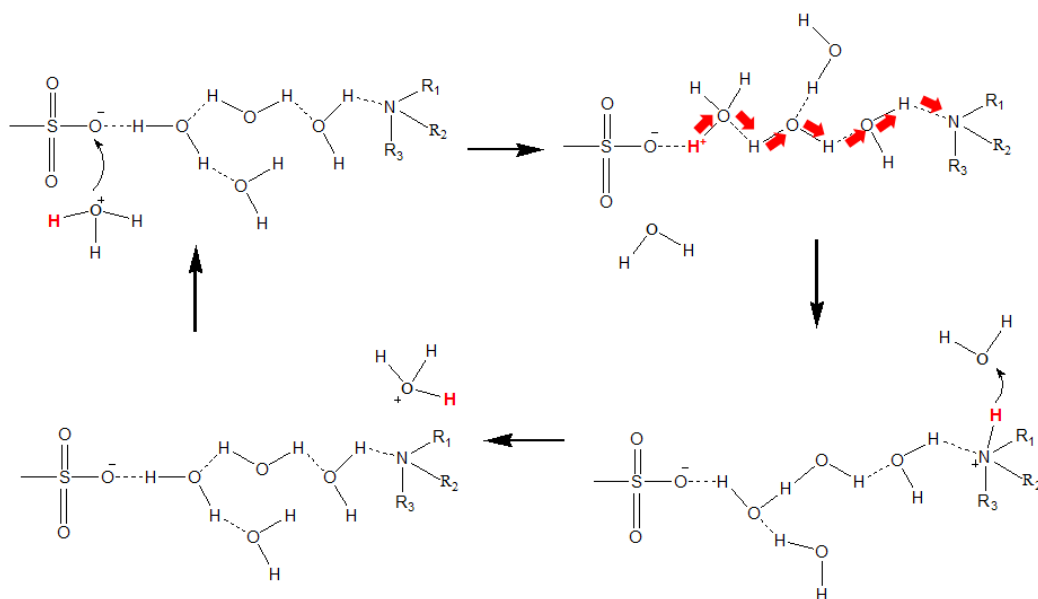
Figure 6.9 Schematic illustration of proton transfer along the water bridges in an acid-base complex. Red arrows represent the direction of proton transfer.

In a previous report (Wu, L. *et al.* 2009), the acid and base groups and the water bridges between them formed a loose complex, an example of which is shown in Figure 6.9. Proton transfer along the water bridges involves three steps. A proton in H_3O^+ first interacts with the $-SO_3^-$ group in an acid-base complex by hydrogen bonding, and is then transferred along the water bridges through a series of hydrogen bond formation and splitting to arrive at the base site, and finally moves out of the acid-base complex by hydrogen bonding with a free water molecule outside the water bridge. The transfer rate of protons through acid-base complexes should then vary with the length of the water bridges. However, the exact number of water molecules in each water bridge cannot be determined since the number of water bridges in acid-base complexes is an unknown. Nonetheless an average length can be estimated by

comparing the number of water molecules in acid-base complexes. Generally, a larger number would correspond to a longer water bridge and vice versa.

The Siwick group discovered that the rate of proton transfer is determined by the number of water molecules between the acid and the base sites (Siwick, B. J. *et al.* 2007). The fastest transfer from the acid to the base site occurs in the direct-contact complexes (< 150 fs). They found that the proton transfer between acid and base sites is only important when the acid-base sites are separated by 1-5 water molecules. Beyond that the diffusion of acid and base would have to occur to bring them together first before proton transfer can take place. From the results of Table 6.1, it can be inferred that proton transfer was the fastest in the PPO-DEA membrane because it had the shortest water bridge in acid-based complexes. On the contrary, the length of the water bridge in the PPO-PA membrane would most probably be too long and hence the proton transfer rate through the acid-base complexes should be the slowest.

The above conclusions were also supported by the measurement of the activation energy (E_a, kJ mol^{-1}) of proton transport. In general the activation energy indicates the amount of energy barrier in breaking a hydrogen bond in water, which is often the rate limiting step in the Grotthuss mechanism. Therefore, activation energy measurements may be used to gauge the importance of the Grotthuss mechanism to the proton transport in the cross-linked membranes. The activation energies calculated from the Arrhenius plot (ln σ vs. 1/T, Figure 6.10) are listed in Table 6.1.
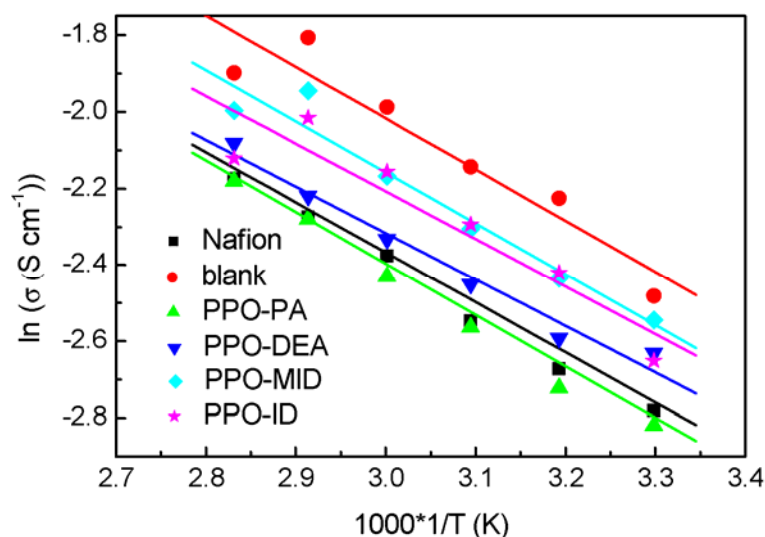
Figure 6.10 Arrhenius plots of proton conductivity of membrane samples.
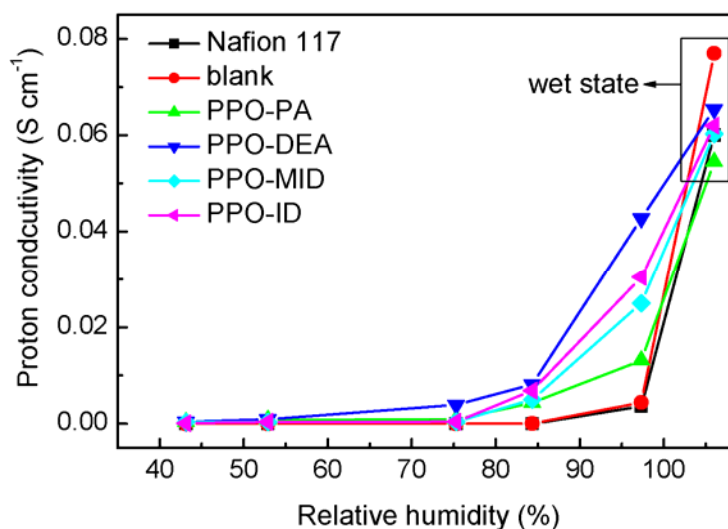
Figure 6.11 Proton conductivity of Nafion[®] 117 and the cross-linked PPO membranes at different relative humidities.

Experimental measurements yielded an E_a=11.18 kJ mol^{-1} for Nafion[®] 117 which is consistent with the literature value (Pei, H. Q. *et al.* 2006). It is generally accepted that the proton transport in Nafion[®] membranes is dominated by the Grotthuss mechanism (Colomban, P. *et al.* 1992). Vehicular mechanism, on the other hand, requires a higher activation energy to overcome the barrier to an *en masse* diffusion (Choi, P. *et al.* 2005). The measured activation energies of all of the PPO membranes

were similar to that of Nafion$^{®}$ 117 (Table 6.1), which can be used to infer similarly the predominance of the Grotthuss mechanism in proton transport through the PPO membranes. Proton conductivity measurements carried out at different levels of relative humidity (Figure 6.11) corroborated this inference. Since the number of free -SO$_3$H groups was the same in all acid-base cross-linked membranes, the difference in conductivity at each relative humidity level had to be attributed to the proton transfer rate through the acid-base complexes. While the increase in humidity generally increased the proton conductivity of the membranes, the rates of increase were different for different membranes. The PPO-PA membrane showed the lowest rate of increase resulting in the lowest proton conductivity at 97% relative humidity. This could be attributed to the long water bridges in PPO-PA which impeded the proton transfer. On the contrary, the PPO-DEA membrane with the shortest water bridge in the acid-base complexes had the highest conductivity among all acid-base cross-linked membranes at all humidity levels. High conductivity was also noted for the PPO-ID membrane because it too had a small number of water molecules in the acid-base complexes.

6.3.3   Dimensional Swelling, Methanol Permeability and Single Stack Fuel Cell Performance of the Cross-linked Membranes

The dimensional stability of the PPO membranes was evaluated by measuring membrane swelling at 25 ^{o}C and 80 ^{o}C representing the two ends of the common operating temperature range. From the results in Figure 6.12, all cross-linked membranes underwent smaller dimensional changes than the blank membrane. This was clearly the consequence of a lower water uptake due to the reduction in the number of free sulfonic acid groups and a denser membrane structure after cross-

linking. The membranes swelled notably more at the higher temperature (80 $^{\circ}$C). Except for PPO-PA, dimensional changes in the other three cross-linked membranes were comparable with or lower than that of Nafion$^{\circledR}$ 117, indicating the effective restraint on swelling at elevated temperatures by the acid-base cross-links in the membrane. The exception of PPO-PA was probably due to its long water bridge in the acid-base complexes, which led to weak acid-base interactions.
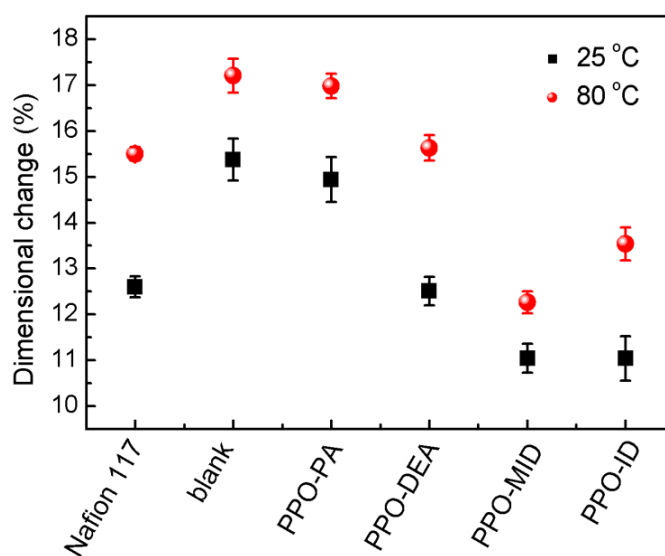
Figure 6.12 Dimensional changes of Nafion$^{\circledR}$ 117 and cross-linked membranes at 25 and 80 $^{\circ}$C.
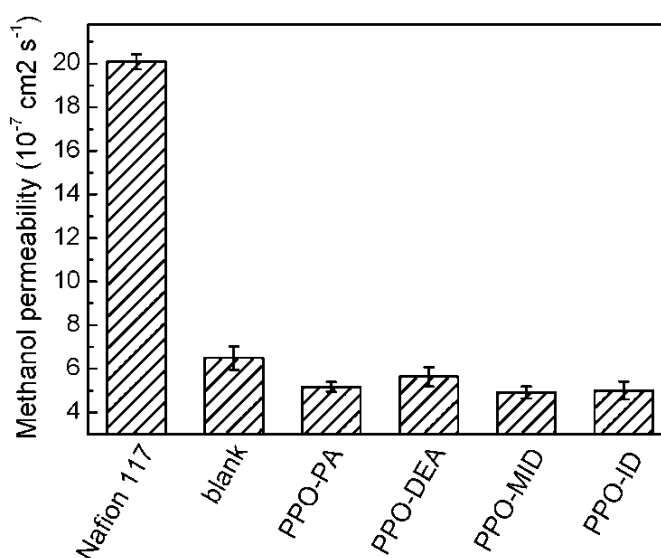
Figure 6.13 Methanol permeability of Nafion$^{\circledR}$ 117 and the cross-linked membranes.
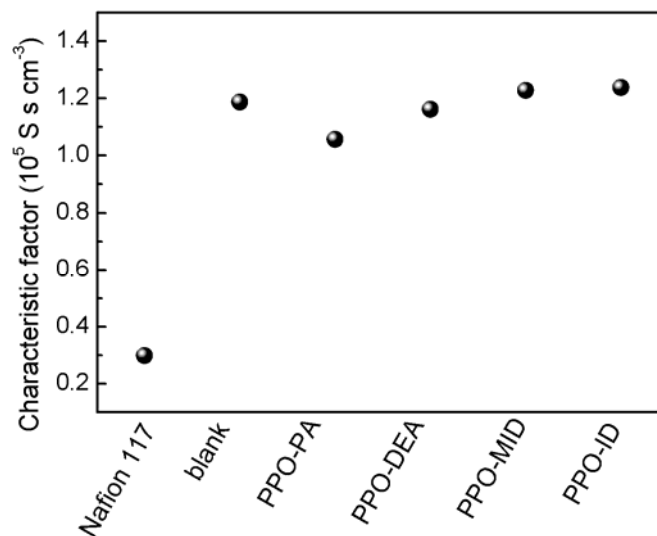
Figure 6.14 Characteristic factors of Nafion® 117 and the cross-linked membranes

Since the PPO membranes are intended for the DMFCs, measurements of methanol permeability were carried out and compared in Figure 6.13. It is apparent that the methanol permeability of the acid-base cross-linked membranes was lower than that of the blank membrane and much lower than that of Nafion® 117. This was clearly a contribution from acid-base cross-linking leading to the densification of the membrane structure and an increased barrier to methanol passage. Methanol transport in PEM typically follows the vehicular mechanism and hence the rate is higher if the hydrophilic channels in the membrane are continuous and wide. As the amount of free water was the largest for PPO-PA and PPO-DEA membranes, it is reasonable to assume that more continuous hydrophilic channels were formed in these two membranes benefiting indirectly the methanol transport. The higher methanol permeability of PO-PA and PPO-DEA membranes was therefore within expectations. The overall effect of proton conductivity and methanol permeability is generally measured by the characteristic factor. The characteristic factors of the cross-linked membranes as shown in Figure 6.14 were all higher than that of Nafion® 117 (PPO-

PA < PPO-DEA < PPO-MID < PPO-ID) showing that the cross-linked membranes

were more selective to proton transport (compared with methanol) than Nafion[®] 117.
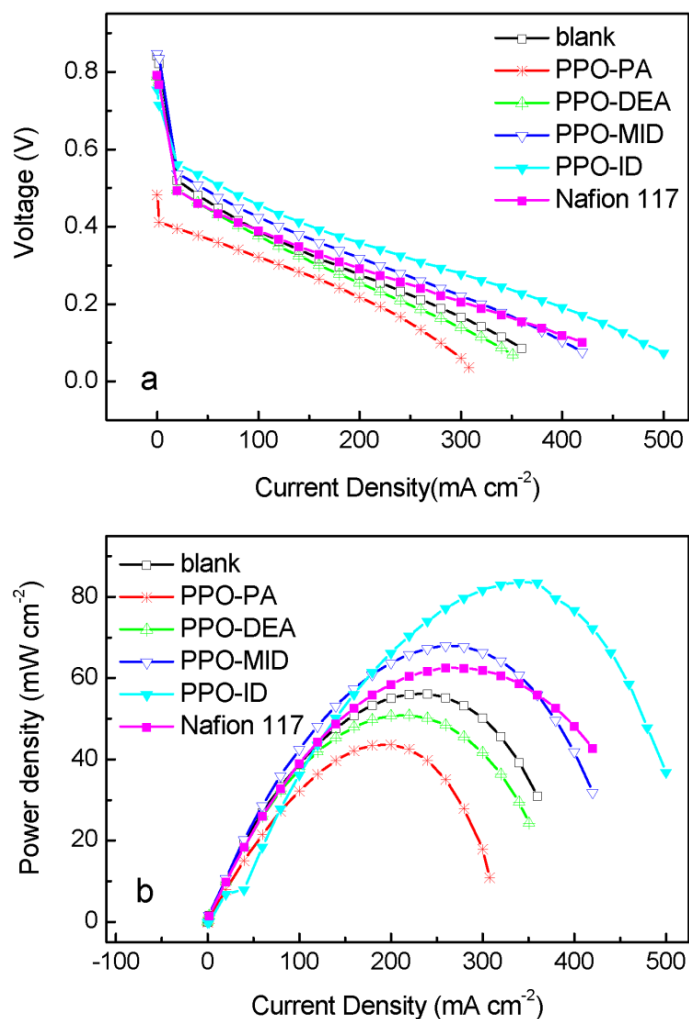
Figure 6.15 Single cell performance of Nafion[®] 117 and cross-linked membranes at 50[o]C with a 2.0 M methanol feed. (a) Voltage-current density plots. (b) Power density-current density plots.

Figure 6.15 shows the single cell performance of MEAs fabricated from the acid-base

cross-linked membranes in comparison with the performance of a Nafion[®] 117 MEA

at 50 [o]C. In comparison with Nafion[®] 117 MEA which delivered a maximum power

density of 62.5 mW cm^{-2} at 262 mA cm^{-2}, the maximum power density was even

higher in two of the acid-base cross-linked membranes: 83.7 mW cm^{-2} at 320 mA cm[-]

[2] from the PPO-ID membrane, and 68 mW cm^{-2} at 260 mA cm^{-2} from the PPO-MID

membrane. The MEAs of the cross-linked membranes displayed the following decreasing trend of maximum power density: PPO-ID > PPO-MID > PPO-DEA > PPO-PA, which mirrored the trend of characteristic factors. The maximum power density of the blank membrane MEA was lower than those of PPO-MID and PPO-ID membranes. This was probably due to interfacial incompatibility between the membrane and the catalyst layers caused by the poorer dimensional stability of the blank membrane.

6.4   Conclusion

This chapter investigated the proton transport mechanisms in acid-base cross-linked membranes through measurements of proton conductivity and the state of water at different temperatures and relatively humidity levels. The proton transport in the acid-base cross-linked membranes was found to be dominated by the Grotthuss mechanism both in the free water region and along the water bridges in acid-base complexes. Four inferences could be made based on the experimental results, i) water uptake was primarily affected by the basicity of the amine group; ii) at low water content the rate of proton transfer was determined by the average length of the water bridges in acid-base complexes; iii) proton transfer was faster along shorter water bridges; iv) the acid-heterocyclic amine cross-linked membranes could provide a better fuel cell performance than the acid-aliphatic amine cross-linked membranes. However, more detailed studies are still required to discover if there are ramifications in these early results.

CHAPTER 7

CONCLUSIONS AND RECOMMENDATIONS FOR FUTURE
WORK

7.1   Conclusions

The objective of this thesis was to develop PEMs with narrow and well-connected hydrophilic channels to mitigate the classical tradeoff between proton conductivity and methanol permeability. An SIPN configuration was adopted for the design since the network polymer (which provides structure and stability) and the guest polymer (which provides the desired transport properties) can be assimilated in one pot. A high level of homogenization can be achieved to suppress component phase separation. By changing the length, bulkiness and hydrophobicity of the cross-links in the host network, the size and the connectivity of the hydrophilic domains could also be tuned to support continuous hydrophilic channels at the nanoscale. The resultant membranes, when properly designed and fabricated, could deliver proton conductivity no less than that of Nafion$^{®}$ 117 without the high methanol permeability of the latter. Their good performance was also confirmed at the single stack level in DMFC test cells. The major findings of this PhD study include the following:

1. The retraction of the mobile linear polymer from the host network of an SIPN structure is known to occur under certain conditions, especially when the constituents differ greatly in polarity. The stability of an SIPN then depends on the minimization of component incompatibility. PPO, a low-cost engineering

polymer, was therefore deployed as both the host and guest polymers in our implementation of an SIPN design for the PEMs of DMFCs. Specifically a series of SIPN membranes were fabricated by thermally cross-linking EDA and BPPO in the presence of linear SPPO. The cross-linking reactions produced a variety of amine moieties (i.e., secondary, tertiary amines and protonated amines) which reinforced the attachment of SPPO to the BPPO network by ion pair formation (with the sulfonic acid groups of SPPO); in addition to the usual mechanical interlocking mechanism. Ion pair formation also increased the uniformity of SPPO distribution in the cross-linked BPPO network, and hence the likelihood to form a continuous network of connected hydrophilic domains for proton transport upon water absorption. The amine-containing cross-links were hydrophilic, and could compensate for some of the decrease in proton conductivity due to ion pair formation to lessen the classical tradeoff between methanol permeability and proton conductivity. The membranes fabricated as such displayed good mechanical strength, good dimensional stability and adequate functionalities for a DMFC operation; thereby establishing the case of using SIPNs for the design of DMFC PEMs.

2. The effects of cross-linker length in the ion pair-reinforced SIPN membranes were examined next. A series of aliphatic α,ω-diamine cross-linkers were used to provide variability in the cross-link hydrophobicity and mesh width (the average distance between two cross-linked polymers) of the cross-linked network host. The effects of these adjustments on the host cross-linked network structure were evaluated by membrane morphology examinations and transport property (proton conductivity and methanol permeability) measurements. It was found that long

cross-linkers increased the network mesh width and hydrophobicity resulting in more scattered hydrophilic domains and fewer contiguous connections. On the contrary, the hydrophilic domains in networks with short cross-linkers were closer and more completely connected to facilitate proton transport. Methanol crossover in the SIPN membranes was suppressed by decreasing the size of the hydrophilic domains. Overall water uptake and dimensional swelling of the membranes were also affected by the cross-linker length. Some of these SIPN membranes also outperformed the Nafion[®] 117 membrane in single stack fuel cell tests.

3. In addition to the cross-linker length, the cross-linker size (bulkiness) was also used to vary the SIPN membrane properties. A comparison of the membranes fabricated from four epoxide cross-linkers with different bulkiness and hydrophobicity (i.e., BDE, RDE, BADE, and PBAE) revealed the importance of the bulkiness of the cross-links and reiterated the significance of the hydrophobicity of the network host on membrane morphology. Specifically small (less bulky) and more hydrophobic cross-links allowed narrower and more connected hydrophilic channels to be formed relative to bulky and less hydrophobic cross-links. The BDE membranes had the highest proton conductivity of the SIPN membranes without any noticeable compensatory effect in other PEM properties, such as dimensional stability and methanol permeability.

4. The ion pairs between acidic $-SO_3H$ groups and basic amine groups in the SIPN membranes clearly contributed to the membrane dimensional stability. However, such improvement was realized at the expense of some loss of proton

conductivity. The proton transport mechanism in PPO-based membranes with only acid-base cross-links was therefore investigated in order to identify the acid-base combinations that could minimize the conductivity loss in future membrane synthesis. The PPO-based membranes here were cross-linked by acid-base interactions only. Different acid-base complexes, including the acid-heterocyclic amine (i.e., ID and MID) complexes and acid-aliphatic amine (i.e., PA and DEA) complexes, were used to infer some systemic trends. Proton transfer through these complexes occurred via the water bridges between the acid and base sites by the Grotthuss mechanism. The length of the water bridge had a significant influence on the proton transfer rate. Among the four acid-base cross-linked PPO membranes, higher proton conductivities were obtained in membranes ionically cross-linked with DEA or ID. This could be understood in terms of the shorter water bridges in sulfonic acid-DEA and sulfonic acid-ID complexes, where proton transfer was more efficient. However, the DEA-cross-linked membrane also retained more free water in the matrix, leading to methanol permeability higher than the ID-cross-linked membrane. Single cell tests confirmed that the sulfonic acid-ID cross-linked membrane had the best overall fuel cell performance.

7.2   Recommendations for Future Work

7.2.1   Heterocyclic Amine-Containing Ion Pair-Reinforced SIPN Membranes

Chapters 3-5 showed that membranes with good DMFC performance could be produced by an ion pair-reinforced SIPN design. The combination of ion pairs and an SIPN structure was effective in homogenizing the distribution of the hydrophilic

linear polymer in the hydrophobic polymer network host. Narrower and better-connected hydrophilic channels were formed as a result. This is a desirable membrane morphology which can support high proton conductivity and low methanol permeability simultaneously. The results in Chapter 6 further suggest that the ionic-crosslinking in SIPN membrane may be tuned to reduce the adverse effects of ion pair formation on proton conductivity. Specifically the heterocyclic amine ID was found to have the least negative impact. Hence there is high likelihood that the proton-to-methanol transport selectivity may be improved by using imidazolium molecules as cross-linker *cum* amination agent in the synthesis of ion pair-reinforced SIPN membranes.

7.2.2 Optimization of MEA Fabrication

The results of single cell tests in Chapter 3-6 clearly demonstrated that a good alternative PEM does not necessarily make a better MEA than Nafion® 117. The major reason for the disappointing performance of several "promising" membranes in single fuel cell tests was the low quality of the membrane-catalyst interface caused by material incompatibility. The minimization of interfacial incompatibility in MEA fabrication is therefore an important consideration in the development of hydrocarbon-based PEMs. We need good adhesion of the membrane with the catalyst layers with no gaps between them in order to keep the interfacial resistance to a minimum.

All MEAs in this project were fabricated by hot-pressing where the PEMs were sandwiched between two commercial catalyst electrodes. At the beginning, only dry

membranes were used for the MEA fabrication but single cell tests soon revealed significant membrane-electrode interfacial resistance resulting in poor power densities. The adhesion between the membrane and electrodes was improved after hydrated membranes were used in lieu of the dry membranes – there were notable improvements in interfacial contacts and consequently the fuel cell performance. However, the delamination problem was not completely eradicated. In single cell tests, some SIPN membranes with intrinsic transport properties better than those of Nafion$^{®}$, such as the BDE series of SIPN membranes, failed to surpass Nafion$^{®}$ at the MEA level. Hence the translation of SIPN membranes to high quality MEA is still a current problem. The compatibility between the PEM and the electrodes can in principle be improved by the following: i) the optimization of MEA fabrication parameters such as hot-pressing temperature, pressure and duration, ii) chemical modifications of the PEM surface for greater process compatibility, iii) the use of molecular "gules" (compatilizers), and iv) by replacing Nafion binder with other polymer binders.

7.2.3 New Performance Indicator for the Evaluation of PEM Fuel Cell Performance

A good PEM for DMFCs is expected to fulfil a number of operational requirements, such as high proton conductivity, low methanol permeability, good chemical and dimensional stability, and a few others. In principle a PEM should be synthesized to optimize all of these properties but tradeoffs between some of these properties often exist to make the decision-making process complex and difficult (e.g., high methanol resistance at the expense of low proton conductivity). Currently the ratio of proton

conductivity to methanol permeability, known as the characteristic factor, is used as a performance indicator of PEMs. A high characteristic factor, however, does not guarantee good fuel cell performance because the actual value of proton conductivity may be too low to be of practical use. A more comprehensive indicator which combines all of the measures of PEM performance should theoretically be more useful. A possible formula is suggested here: $I = aX_1^2 + bX_2^2 + cX_3^2 + ...$ where I is the composite indicator that correlates positively with power density, X_i is the figure of merit of a functional membrane property relative to the Nafion$^{®}$ membrane, and a, b and c are the weighting factors. A good PEM is therefore one that yields the maximum I value. Other formulas may also be proposed based on the practical needs (e.g., I may be used to correlate positively with membrane durability).

REFERENCES

Ainla, A.; Brandell, D., Nafion (R)-polybenzimidazole (PBI) composite membranes for DMFC applications. *Solid State Ionics* **2007,** 178, 581-585.

Antolini, E., Catalysts for direct ethanol fuel cells. *Journal of Power Sources* **2007,** 170, 1-12.

Argun, A. A.; Ashcraft, J. N.; Hammond, P. T., Highly conductive, methanol resistant polyelectrolyte multilayers. *Advanced Materials* **2008,** 20, 1539-1543.

Arico, A. S.; Srinivasan, S.; Antonucci, V., DMFCs: from fundamental aspects to technology development. *Fuel Cells* **2001,** 1, 133-161.

Asano, N.; Aoki, M.; Suzuki, S.; Miyatake, K.; Uchida, H.; Watanabe, M., Aliphatic/aromatic polyimide Ionomers as a proton conductive membrane for fuel cell applications. *Journal of the American Chemical Society* **2006,** 128, 1762-1769.

Bae, B.; Miyatake, K.; Watanabe, M., Effect of the hydrophobic component on the properties of sulfonated poly(arylene ether sulfone)s. *Macromolecules* **2009,** 42, 1873-1880.

Bai, Y.; Wu, J.; Xi, J.; Wang, J.; Zhu, W.; Chen, L.; Qiu, X., Electrochemical oxidation of ethanol on Pt-ZrO2/C catalyst. *Electrochemistry Communications* **2005,** 7, 1087-1090.

Bai, Z. W.; Houtz, M. D.; Mirau, P. A.; Dang, T. D., Structures and properties of highly sulfonated poly(arylenethioethersulfone)s as proton exchange membranes. *Polymer* **2007,** 48, 6598-6604.

Bi, H. P.; Wang, J. L.; Chen, S. W.; Hu, Z. X.; Gao, Z. L.; Wang, L. J.; Okamoto, K., Preparation and properties of cross-linked sulfonated poly(arylene ether sulfone)/sulfonated polyimide blend membranes for fuel cell application. *Journal of Membrane Science* **2010,** 350, 109-116.

Binsu, V. V.; Nagarale, R. K.; Shahi, V. K., Phosphonic acid functionalized aminopropyl triethoxysilane-PVA composite material: organic-inorganic hybrid proton-exchange membranes in aqueous media. *Journal of Materials Chemistry* **2005,** 15, 4823-4831.

Bonfanti, C.; Lanzini, L.; Roggero, A.; Sisto, R., Chemical modification of poly(2,6-dimethyl-1,4-phenylene oxide) by bromination-alkynylation. *Journal of Polymer Science Part A: Polymer Chemistry* **1994,** 32, 1361-1369.

Borup, R.; Meyers, J.; Pivovar, B.; Kim, Y. S.; Mukundan, R.; Garland, N.; Myers, D.; Wilson, M.; Garzon, F.; Wood, D.; Zelenay, P.; More, K.; Stroh, K.; Zawodzinski, T.; Boncella, J.; McGrath, J. E.; Inaba, M.; Miyatake, K.; Hori, M.; Ota, K.; Ogumi, Z.; Miyata, S.; Nishikata, A.; Siroma, Z.; Uchimoto, Y.; Yasuda, K.; Kimijima, K. I.;

Iwashita, N., Scientific aspects of polymer electrolyte fuel cell durability and degradation. *Chemical Reviews* **2007,** 107, 3904-3951.

Caporali, S.; Bardi, U.; Lavacchi, A., X-ray photoelectron spectroscopy and low energy ion scattering studies on 1-buthyl-3-methyl-imidazolium bis(trifluoromethane) sulfonimide. *Journal of Electron Spectroscopy and related Phenomena* **2006,** 151, 4-8.

Carbone, A.; Pedicini, R.; Portale, G.; Longo, A.; D'Ilario, L.; Passalacqua, E., Sulphonated poly(ether ether ketone) membranes for fuel cell application: Thermal and structural characterisation. *Journal of Power Sources* **2006,** 163, 18-26.

Carrette, L.; Friedrich, K. A.; Stimming, U., Fuel cells - fundamentals and applications. *Fuel Cells* **2001,** 1, 5-39.

Catalan, J.; Elguero, J., Basicity of azoles.4. empirical relationships between basicity and ionization-potential for aromatic 5 membered rings containing nitrogen or oxygen. *Journal of Heterocyclic Chemistry* **1984,** 21, 269-270.

Chang, H. Y.; Lin, C. W., Proton conducting membranes based on PEG/SiO2 nanocomposites for direct methanol fuel cells. *Journal of Membrane Science* **2003,** 218, 295-306.

Cheng, Z. P.; Zhu, X. L.; Shi, Z. L.; Neoh, K. G.; Kang, E. T., Polymer microspheres with permanent antibacterial surface from surface-initiated atom transfer radical polymerization of 4-vinylpyridine and quaternization. *Surface Review and Letters* **2006,** 13, 313-318.

Chiang, W.-Y.; Chen, C.-L., Separation of water--alcohol mixture by using polymer membranes--6. Water--alcohol pervaporation through terpolymer of PVA grafted with hydrazine reacted SMA. *Polymer* **1998,** 39, 2227-2233.

Chikh, L.; Delhorbe, V.; Fichet, O., (Semi-)Interpenetrating polymer networks as fuel cell membranes. *Journal of Membrane Science* **2011,** 368, 1-17.

Cho, J. H.; Kim, J. M.; Prabhuram, J.; Hwang, S. Y.; Ahn, D. J.; Ha, H. Y.; Kim, S. K., Fabrication and evaluation of membrane electrode assemblies by low-temperature decal methods for direct methanol fuel cells. *Journal of Power Sources* **2009,** 187, 378-386.

Cho, K. Y.; Jung, H. Y.; Shin, S. S.; Choi, N. S.; Sung, S. J.; Park, J. K.; Choi, J. H.; Park, K. W.; Sung, Y. E., Proton conducting semi-IPN based on Nafion and crosslinked poly(AMPS) for direct methanol fuel cell. *Electrochimica Acta* **2004,** 50, 589-593.

Choi, P.; Jalani, N. H.; Datta, R., Thermodynamics and proton transport in Nafion - II. Proton diffusion mechanisms and conductivity. *Journal of the Electrochemical Society* **2005,** 152, E123-E130.

Coleman, M. M.; Serman, C. J.; Bhagwagar, D. E.; Painter, P. C., A practical guide to polymer miscibility. *Polymer* **1990,** 31, 1187-1203.

Colomban, P.; Novak, A. Proton Conductors: Classification and Conductivity. In *Proton Conductors: Solids, Membranes and Gels - Materials and Devices* P. Colomban, Ed.; Press Syndicate of the University of Cambridge, 1992, pp 38-78.

Deluca, N. W.; Elabd, Y. A., Polymer electrolyte membranes for the direct methanol fuel cell: A review. *Journal of Polymer Science Part B-Polymer Physics* **2006,** 44, 2201-2225.

Di Noto, V.; Boaretto, N.; Negro, E.; Pace, G., New inorganic-organic proton conducting membranes based on Nafion and hydrophobic fluoroalkylated silica nanoparticles. *Journal of Power Sources* **2010,** 195, 7734-7742.

Di Vona, M. L.; Marani, D.; D'Epifanio, A.; Traversa, E.; Trombetta, M.; Licoccia, S., A covalent organic/inorganic hybrid proton exchange polymeric membrane: synthesis and characterization. *Polymer* **2005,** 46, 1754-1758.

Dimitrova, P.; Friedrich, K. A.; Vogt, B.; Stimming, U., Transport properties of ionomer composite membranes for direct methanol fuel cells. *Journal of Electroanalytical Chemistry* **2002,** 532, 75-83.

Ding, J. F.; Chuy, C.; Holdcroft, S., Solid polymer electrolytes based on ionic graft polymers: Effect of graft chain length on nano-structured, ionic networks. *Advanced Functional Materials* **2002,** 12, 389-394.

Dunwoody, D. C.; Chung, H.; Haverhals, L.; Leddy, J. Current Status of Direct Methanol Fuel-Cell Technology. In *Alcoholic Fuels*; S. D. Minteer, Ed.; Taylor & Francis Group, LLC, 2006, pp 273.

Easton, E. B.; Astill, T. D.; Holdcroft, S., Properties of gas diffusion electrodes containing sulfonated poly(ether ether ketone). *Journal of the Electrochemical Society* **2005,** 152, A752-A758.

Eikerling, M.; Kornyshev, A. A.; Kuznetsov, A. M.; Ulstrup, J.; Walbran, S., Mechanisms of proton conductance in polymer electrolyte membranes. *Journal of Physical Chemistry B* **2001,** 105, 3646-3662.

Elabd, Y. A.; Hickner, M. A., Block Copolymers for Fuel Cells. *Macromolecules* **2011,** 44, 1-11.

Elabd, Y. A.; Napadensky, E.; Sloan, J. M.; Crawford, D. M.; Walker, C. W., Triblock copolymer ionomer membranes Part I. Methanol and proton transport. *Journal of Membrane Science* **2003,** 217, 227-242.

Essafi, W.; Gebel, G.; Mercier, R., Sulfonated polyimide ionomers: A structural study. *Macromolecules* **2004,** 37, 1431-1440.

Fang, C.; Julius, D.; Tay, S. W.; Hong, L.; Lee, J. Y., Ion Pair Reinforced Semi-Interpenetrating Polymer Network for Direct Methanol Fuel Cell Applications. *Journal of Physical Chemistry B* **2012,** 116, 6416-6424.

Feng, S.; Shang, Y.; Wang, Y.; Liu, G.; Xie, X.; Dong, W.; Xu, J.; Mathur, V. K., Synthesis and crosslinking of hydroxyl-functionalized sulfonated poly(ether ether ketone) copolymer as candidates for proton exchange membranes. *Journal of Membrane Science* **2010,** 352, 14-21.

Feng, S. G.; Shang, Y. M.; Wang, S. B.; Xie, X. F.; Wang, Y. Z.; Wang, Y. W.; Xu, J. M., Novel method for the preparation of ionically crosslinked sulfonated poly(arylene ether sulfone)/polybenzimidazole composite membranes via in situ polymerization. *Journal of Membrane Science* **2010,** 346, 105-112.

Fu, R. Q.; Julius, D.; Hong, L.; Lee, J. Y., PPO-based acid-base polymer blend membranes for direct methanol fuel cells. *Journal of membrane Science* **2008,** 322, 331-338.

Fu, T. Z.; Liu, J.; Cui, Z. M.; Ni, J.; Zhang, G.; Yu, H. B.; Zhao, C. J.; Shi, Y. H.; Na, H.; Xing, W., Sulphonated Tetramethyl Poly(ether ether ketone)/Epoxy/Sulphonated Phenol Novolac Semi-IPN Membranes for Direct Methanol Fuel Cells. *Fuel Cells* **2009,** 9, 570-578.

Gebel, G., Structural evolution of water swollen perfluorosulfonated ionomers from dry membrane to solution. *Polymer* **2000,** 41, 5829-5838.

Gebel, G.; Aldebert, P.; Pineri, M., Swelling study of perfluorosulphonated ionomer membranes. *Polymer* **1993,** 34, 333-339.

Gebel, G.; Moore, R. B., Small-angle scattering study of short pendant chain perfuorosulfonated ionomer membranes. *Macromolecules* **2000,** 33, 4850-4855.

Gierke, T. D.; Munn, G. E.; Wilson, F. C., The morphology in Nafion perfluorinated membrane products, as determined by wide-angle and small-angle X-ray studies. *Journal of Polymer Science Part B: Polymer Physics* **1981,** 19, 1687-1704.

Gitsov, I.; Zhu, C., Novel functionally grafted pseudo-semi-interpenetrating networks constructed by reactive linear-dendritic copolymers. *Journal of the American Chemical Society* **2003,** 125, 11228-11234.

Goddard, R. J.; Grady, B. P.; Cooper, S. L., The room-temperature annealing peak in ionomers - ionic crystallites or water-absorption. *Macromolecules* **1994,** 27, 1710-1719.

Gosalawit, R.; Chirachanchai, S.; Shishatskiy, S.; Nunes, S. P., Sulfonated montmorillonite/sulfonated poly(ether ether ketone) (SMMT/SPEEK) nanocomposite membrane for direct methanol fuel cells (DMFCs). *Journal of Membrane Science* **2008,** 323, 337-346.

Guan, Y. S.; Pu, H. T.; Pan, H. Y.; Chang, Z. H.; Jin, M., Proton conducting membranes based on semi-interpenetrating polymer network of Nafion (R) and polybenzimidazole. *Polymer* **2010,** 51, 5473-5481.

Guo, M. M.; Liu, B. J.; Liu, Z.; Wang, L. F.; Jiang, Z. H., Novel acid-base molecule-enhanced blends/copolymers for fuel cell applications. *Journal of Power Sources* **2009,** 189, 894-901.

Gurau, B.; Smotkin, E. S., Methanol crossover in direct methanol fuel cells: a link between power and energy density. *Journal of Power Sources* **2002,** 112, 339-352.

Harrison, W. L.; Hickner, M. A.; Kim, Y. S.; McGrath, J. E., Poly(arylene ether sulfone) copolymers and related systems from disulfonated monomer building blocks: Synthesis, characterization, and performance - A topical review. *Fuel Cells* **2005,** 5, 201-212.

Herring, A. M., Inorganic-polymer composite membranes for proton exchange membrane fuel cells. *Polymer Reviews* **2006,** 46, 245-296.

Hickner, M. A.; Ghassemi, H.; Kim, Y. S.; Einsla, B. R.; McGrath, J. E., Alternative Polymer Systems for Proton Exchange Membranes (PEMs). *Chemical Reviews* **2004,** 104, 4587-4612.

Hickner, M. A.; Ghassemi, H.; Kim, Y. S.; Einsla, B. R.; McGrath, J. E., Alternative polymer systems for proton exchange membranes (PEMs). *Chemical Reviews* **2004,** 104, 4587-4611.

Hickner, M. A.; Pivovar, B. S., The chemical and structural nature of proton exchange membrane fuel cell properties. *Fuel Cells* **2005,** 5, 213-229.

Higa, M.; Sugita, M.; Maesowa, S. I.; Endo, N., Poly(vinyl alcohol)-based polymer electrolyte membranes for direct methanol fuel cells. *Electrochimica Acta* **2010,** 55, 1445-1449.

Higashihara, T.; Matsumoto, K.; Ueda, M., Sulfonated aromatic hydrocarbon polymers as proton exchange membranes for fuel cells. *Polymer* **2009,** 50, 5341-5357.

Hsu, W. Y.; Gierke, T. D., Elastic theory for ionic clustering in perfluorinated ionomers. *Macromolecules* **1982,** 15, 101-105.

Hsu, W. Y.; Gierke, T. D., Ion-transport and clustering in Nafion perfluorinated membranes. *Journal of Membrane Science* **1983,** 13, 307-326.

Hsu, W. Y.; Gierke, T. D., Ion transport and clustering in nafion perfluorinated membranes. *Journal of Membrane Science* **1983,** 13, 307-326.

Hu, Z. X.; Ogou, T.; Yoshino, M.; Yamada, O.; Kita, H.; Okamoto, K. I., Direct methanol fuel cell performance of sulfonated polyrimide membranes. *Journal of Power Sources* **2009,** 194, 674-682.

Huang, C. H.; Wu, H. M.; Chen, C. C.; Wang, C. W.; Kuo, P. L., Preparation, characterization and methanol permeability of proton conducting membranes based on sulfonated ethylene-vinyl alcohol copolymer. *Journal of Membrane Science* **2010,** 353, 1-9.

Huang, R. Y. M.; Kim, J. J., Synthesis and transport-properties of thin-film composite membranes. 1. synthesis of poly(phenylene oxide) polymer and its sulfonation. *Journal of Applied Polymer Science* **1984,** 29, 4017-4027.

Huang, Y. F.; Chuang, L. C.; Kannan, A. M.; Lin, C. W., Proton-conducting membranes with high selectivity from cross-linked poly(vinyl alcohol) and poly(vinyl pyrrolidone) for direct methanol fuel cell applications. *Journal of Power Sources* **2009,** 186, 22-28.

Jagur-Grodzinski, J., Polymeric materials for fuel cells: concise review of recent studies. *Polymers for Advanced Technologies* **2007,** 18, 785-799.

Jain, S. H.; Murata, K.; Anazawa, T., Nanostructures developed from semi-interpenetrating polymer network structures. *Macromolecular Chemistry and Physics* **2003,** 204, 893-902.

Jang, W.; Sundar, S.; Choi, S.; Shul, Y. G.; Han, H., Acid-base polyimide blends for the application as electrolyte membranes for fuel cells. *Journal of Membrane Science* **2006,** 280, 321-329.

Jansen, R. J. J.; Vanbekkum, H., XPS of nitrogen-containing functional-groups on activated carbon. *Carbon* **1995,** 33, 1021-1027.

Jha, A. K.; Chen, L.; Offeman, R. D.; Balsara, N. P., Effect of nanoscale morphology on selective ethanol transport through block copolymer membranes. *Journal of Membrane Science* **2011,** 373, 112-120.

Jousseaume, V.; Morsli, M.; Bonnet, A., XPS study of aged polyaniline films. *Journal of Applied Polymer Science* **2003,** 90, 3730-3736.

Jung, H. Y.; Park, J. K., Long-term performance of DMFC based on the blend membrane of sulfonated poly(ether ether ketone) and poly(vinylidene fluoride). *International Journal of Hydrogen Energy* **2009,** 34, 3915-3921.

Kamarudin, S. K.; Achmad, F.; Daud, W. R. W., Overview on the application of direct methanol fuel cell (DMFC) for portable electronic devices. *International Journal of Hydrogen Energy* **2009,** 34, 6902-6916.

Kang, M. S.; Kim, J. H.; Won, J.; Moon, S. H.; Kang, Y. S., A highly charged proton exchange membranes prepared by using water soluble polymer blends for fuel cells. *Journal of Membrane Science* **2005,** 247, 127-135.

Kerres, J., Covalent-ionically cross-linked poly(etheretherketone)-basic polysulfone blend ionomer membranes. *Fuel Cells* **2006,** 6, 251-260.

Kerres, J.; Hein, M.; Zhang, W.; Graf, S.; Nicoloso, N., Development of new blend membranes for polymer electrolyte fuel cell applications. *Journal of New Materials for Electrochemical Systems* **2003,** 6, 223-229.

Kerres, J.; Zhang, W.; Jorissen, L.; Gogel, V., Application of different types of polyaryl-blend-membranes in DMFC. *Journal of New Materials for Electrochemical Systems* **2002,** 5, 323-323.

Kerres, J. A., Development of ionomer membranes for fuel cells. *Journal of Membrane Science* **2001,** 185, 3-27.

Kerres, J. A., Blended and cross-linked ionomer membranes for application in membrane fuel cells. *Fuel Cells* **2005,** 5, 230-247.

Kim, D. S.; Kim, Y. S.; Guiver, M. D.; Ding, J. F.; Pivovar, B. S., Highly fluorinated comb-shaped copolymer as proton exchange membranes (PEMs): Fuel cell performance. *Journal of Power Sources* **2008,** 182, 100-105.

Kim, H.; Chang, H., Organic/inorganic hybrid membranes for direct methanol fuel cells. *Journal of Membrane Science* **2007,** 288, 188-194.

Kim, H.; Prakash, S.; Mustain, W. E.; Kohl, P. A., Sol-gel based sulfonic acid-functionalized silica proton conductive membrane. *Journal of Power Sources* **2009,** 193, 562-569.

Kim, Y. S.; Dong, L. M.; Hickner, M. A.; Glass, T. E.; Webb, V.; McGrath, J. E., State of water in disulfonated poly(arylene ether sulfone) copolymers and a perfluorosulfonic acid copolymer (nafion) and its effect on physical and electrochemical properties. *Macromolecules* **2003,** 36, 6281-6285.

Kim, Y. S.; Kim, S. C., Properties of polyetherimide/dicyanate semi-interpenetrating polymer network having the morphology spectrum. *Macromolecules* **1999,** 32, 2334-2341.

Kosmala, B.; Schauer, J., Ion-exchange membranes prepared by blending sulfonated poly(2,6-dimethyl-1,4-phenylene oxide) with polybenzimidazole. *Journal of Applied Polymer Science* **2002,** 85, 1118-1127.

Kreuer, K. D., On the development of proton conducting materials for technological applications. *Solid State Ionics* **1997,** 97, 1-15.

Kreuer, K. D., On the development of proton conducting polymer membranes for hydrogen and methanol fuel cells. *Journal of Membrane Science* **2001,** 185, 29-39.

Kreuer, K. D.; Ise, M.; Fuchs, A.; Maier, J., Proton and water transport in nano-separated polymer membranes. *Journal De Physique Iv* **2000,** 10, 279-281.

Kreuer, K. D.; Paddison, S. J.; Spohr, E.; Schuster, M., Transport in proton conductors for fuel-cell applications: Simulations, elementary reactions, and phenomenology. *Chemical Reviews* **2004,** 104, 4637-4678.

Kreuer, K. D.; Paddison, S. J.; Spohr, E.; Schuster, M., Transport in Proton Conductors for Fuel-Cell Applications: Simulations, Elementary Reactions, and Phenomenology. *Chemical Reviews* **2004,** 104, 4637-4678.

Kreuer, K. D.; Rabenau, A.; Weppner, W., Vehicle Mechanism, a New Model for the Interpretation of the Conductivity of Fast Proton Conductors. *Angewandte Chemie-International Edition in English* **1982,** 21, 208-209.

Krishnan, P.; Park, J.-S.; Yang, T.-H.; Lee, W.-Y.; Kim, C.-S., Sulfonated poly(ether ether ketone)-based composite membrane for polymer electrolyte membrane fuel cells. *Journal of Power Sources* **2006,** 163, 2-8.

Krishnan, P.; Park, J. S.; Yang, T. H.; Lee, W. Y.; Kim, C. S., Sulfonated poly(ether ether ketone)-based composite membrane for polymer electrolyte membrane fuel cells. *Journal of Power Sources* **2006,** 163, 2-8.

Kruczek, B.; Matsuura, T., Development and characterization of homogeneous membranes de from high molecular weight sulfonated polyphenylene oxide. *Journal of Membrane Science* **1998,** 146, 263-275.

Kumar, G. G.; Lee, D. N.; Kim, P.; Nahm, K. S.; Nimmaelizabeth, R., Poly(Vinylidene fluoride-co-hexa fluoropropylene)/Poly vinyl alcohol porous membranes for the application of fuel cells. *Journal of Polymer Research* **2009,** 16, 55-61.

Kundu, P. P.; Kim, B. T.; Ahn, J. E.; Han, H. S.; Shul, Y. G., Formation and evaluation of semi-IPN of nafion 117 membrane for direct methanol fuel cell - 1. Crosslinked sulfonated polystyrene in the pores of nafion 117. *Journal of Power Sources* **2007,** 171, 86-91.

Kundu, P. P.; Kim, B. T.; Ahn, J. E.; Han, H. S.; Shul, Y. G., Formation and evaluation of semi-IPN of nafion 117 membrane for direct methanol fuel cell: 1. Crosslinked sulfonated polystyrene in the pores of nafion 117. *Journal of Power Sources* **2007,** 171, 86-91.

Kwon, Y. H.; Kim, S. C.; Lee, S. Y., Nanoscale Phase Separation of Sulfonated Poly(arylene ether sulfone)/Poly(ether sulfone) Semi-IPNs for DMFC Membrane Applications. *Macromolecules* **2009,** 42, 5244-5250.

Lamy, C.; Belgsir, E. M.; Leger, J. M., Electrocatalytic oxidation of aliphatic alcohols: Application to the direct alcohol fuel cell (DAFC). *Journal of Applied Electrochemistry* **2001,** 31, 799-809.

Lee, G.; Lee, H.; Kwon, D., Interfacial characterization of catalyst coating on electrolyte polymer through microscratch analysis in DMFC. *Electrochimica Acta* **2007,** 52, 4215-4221.

Lee, M.; Park, J. K.; Lee, H. S.; Lane, O.; Moore, R. B.; McGrath, J. E.; Baird, D. G., Effects of block length and solution-casting conditions on the final morphology and properties of disulfonated poly(arylene ether sulfone) multiblock copolymer films for proton exchange membranes. *Polymer* **2009,** 50, 6129-6138.

Li, Q. F.; He, R. H.; Jensen, J. O.; Bjerrum, N. J., Approaches and recent development of polymer electrolyte membranes for fuel cells operating above 100 degrees C. *Chemistry of Materials* **2003,** 15, 4896-4915.

Li, T.; Zhong, G.; Fu, R.; Yang, Y., Synthesis and characterization of Nafion/cross-linked PVP semi-interpenetrating polymer network membrane for direct methanol fuel cell. *Journal of Membrane Science* **2010,** 354, 189-197.

Li, T.; Zhong, G. M.; Yang, Y., Methanol-Blocking Perfluorosulfonic Acid Composite Membranes in Direct Methanol Fuel Cells. *Progress in Chemistry* **2010,** 22, 522-536.

Li, W.; Manthiram, A., Sulfonated poly(arylene ether sulfone) as a methanol-barrier layer in multilayer membranes for direct methanol fuel cells. *Journal of Power Sources* **2010,** 195, 962-968.

Li, W.; Manthiram, A.; Guiver, M. D., Acid-base blend membranes consisting of sulfonated poly(ether ether ketone) and 5-amino-benzotriazole tethered polysulfone for DMFC. *Journal of Membrane Science* **2010,** 362, 289-297.

Li, W. L.; Gao, Y. M.; Wang, S. M., Gel polymer electrolyte with semi-IPN fabric for polymer lithium-ion battery. *Journal of Applied Polymer Science* **2012,** 125, 1027-1032.

Liang, Z. X.; Zhao, T. S.; Prabhuram, J., A glue method for fabricating membrane electrode assemblies for direct methanol fuel cells. *Electrochimica Acta* **2006,** 51, 6412-6418.

Lin, C. K.; Kuo, J. F.; Chen, C. Y., Preparation of nitrated sulfonated poly(ether ether ketone) membranes for reducing methanol permeability in direct methanol fuel cell applications. *Journal of Power Sources* **2009,** 187, 341-347.

Lin, C. W.; Huang, Y. F.; Kannan, A. M., Cross-linked poly(vinyl alcohol) and poly(styrene sulfonic acid-co-maleic anhydride)-based semi-interpenetrating network as proton-conducting membranes for direct methanol fuel cells. *Journal of Power Sources* **2007,** 171, 340-347.

Lin, H. D.; Zhao, C. J.; Ma, W. J.; Li, H. T.; Na, H., Layer-by-layer self-assembly of in situ polymerized polypyrrole on sulfonated poly(arylene ether ketone) membrane with extremely low methanol crossover. *International Journal of Hydrogen Energy* **2009,** 34, 9795-9801.

Liu, B. J.; Hu, W.; Robertson, G. P.; Guiver, M. D., Poly(aryl ether ketone)s with carboxylic acid groups: synthesis, sulfonation and crosslinking. *Journal of Materials Chemistry* **2008,** 18, 4675-4682.

Liu, B. J.; Robertson, G. P.; Kim, D. S.; Guiver, M. D.; Hu, W.; Jiang, Z. H., Aromatic poly(ether ketone)s with pendant sulfonic acid phenyl groups prepared by a mild sulfonation method for proton exchange membranes. *Macromolecules* **2007,** 40, 1934-1944.

Liu, C. H.; Chen, Y. Q.; Chen, J. G., Synthesis and characteristics of pH-sensitive semi-interpenetrating polymer network hydrogels based on konjac glucomannan and poly(aspartic acid) for in vitro drug delivery. *Carbohydrate Polymers* **2010,** 79, 500-506.

Liu, F. Q.; Yi, B. L.; Xing, D. M.; Yu, J. R.; Zhang, H. M., Nafion/PTFE composite membranes for fuel cell applications. *Journal of Membrane Science* **2003,** 212, 213-223.

Liu, J. G.; Zhou, Z. H.; Zhao, X. X.; Xin, Q.; Sun, G. Q.; Yi, B. L., Studies on performance degradation of a direct methanol fuel cell (DMFC) in life test. *Physical Chemistry Chemical Physics* **2004,** 6, 134-137.

Lumelsky, Y.; Zoldan, J.; Levenberg, S.; Silverstein, M. S., Porous polycaprolactone-polystyrene semi-interpenetrating polymer networks synthesized within high internal phase emulsions. *Macromolecules* **2008,** 41, 1469-1474.

Mann, J.; Yao, N.; Bocarsly, A. B., Characterization and analysis of new catalysts for a direct ethanol fuel cell. *Langmuir* **2006,** 22, 10432-10436.

Matsuguchi, M.; Takahashi, H., Methanol permeability and proton conductivity of a semi-interpenetrating polymer networks (IPNs) membrane composed of Nafion® and cross-linked DVB. *Journal of Membrane Science* **2006,** 281, 707-715.

Mauritz, K. A.; Moore, R. B., State of understanding of Nafion. *Chemical Reviews* **2004,** 104, 4535-4585.

Moghaddam, S.; Pengwang, E.; Jiang, Y. B.; Garcia, A. R.; Burnett, D. J.; Brinker, C. J.; Masel, R. I.; Shannon, M. A., An inorganic-organic proton exchange membrane for fuel cells with a controlled nanoscale pore structure. *Nature Nanotechnology* **2010,** 5, 230-236.

Mohammed, O. F.; Pines, D.; Dreyer, J.; Pines, E.; Nibbering, E. T. J., Sequential proton transfer through water bridges in acid-base reactions. *Science* **2005,** 310, 83-86.

Mundargi, R. C.; Shelke, N. B.; Babu, V. R.; Patel, P.; Rangaswamy, V.; Aminabhavi, T. M., Novel Thermo-Responsive Semi-Interpenetrating Network Microspheres of Gellan Gum-Poly(N-isopropylacrylamide) for Controlled Release of Atenolol. *Journal of Applied Polymer Science* **2010,** 116, 1832-1841.

Musale, D. A.; Kumar, A., Solvent and pH resistance of surface crosslinked chitosan/poly(acrylonitrile) composite nanofiltration membranes. *Journal of Applied Polymer Science* **2000,** 77, 1782-1793.

Nakagawa, N.; Sekimoto, K.; Masdar, M. S.; Noda, R., Reaction analysis of a direct methanol fuel cell employing a porous carbon plate operated at high methanol concentrations. *Journal of Power Sources* **2009,** 186, 45-51.

Nasef, M. M.; Zubir, N. A.; Ismail, A. F.; Dahlan, K. Z. M.; Saidi, H.; Khayet, M., Preparation of radiochemically pore-filled polymer electrolyte membranes for direct methanol fuel cells. *Journal of Power Sources* **2006,** 156, 200-210.

Neburchilov, V.; Martin, J.; Wang, H.; Zhang, J., A review of polymer electrolyte membranes for direct methanol fuel cells. *Journal of Power Sources* **2007,** 169, 221-238.

Neburchilov, V.; Martin, J.; Wang, H. J.; Zhang, J. J., A review of polymer electrolyte membranes for direct methanol fuel cells. *Journal of Power Sources* **2007,** 169, 221-238.

Nguyen, T. H.; Wang, C.; Wang, X., Pore-filling membrane for direct methanol fuel cells based on sulfonated poly(styrene-ran-ethylene) and porous polyimide matrix. *Journal of Membrane Science* **2009,** 342, 208-214.

Paddison, S. J.; Paul, R.; Kreuer, K. D., Theoretically computed proton diffusion coefficients in hydrated PEEKK membranes. *Physical Chemistry Chemical Physics* **2002,** 4, 1151-1157.

Page, K. A.; Cable, K. M.; Moore, R. B., Molecular origins of the thermal transitions and dynamic mechanical relaxations in perfluorosulfonate ionomers. *Macromolecules* **2005,** 38, 6472-6484.

Pan, H.; Pu, H.; Chang, Z.; Jin, M.; Wan, D., Effects of crosslinkers on semi-interpenetrating polymer networks of Nafion (R) and fluorine-containing polyimide. *Electrochimica Acta* **2010,** 55, 8476-8481.

Pan, H.; Pu, H.; Wan, D.; Jin, M.; Chang, Z., Proton exchange membranes based on semi-interpenetrating polymer networks of fluorine-containing polyimide and Nafion®. *Journal of Power Sources* **2010,** 195, 3077-3083.

Pan, H. Y.; Pu, H. T.; Jin, M.; Wan, D. C.; Chang, Z. H., Semi-interpenetrating polymer networks of Nafion (R) and fluorine-containing polyimide with crosslinkable vinyl group. *Polymer* **2010,** 51, 2305-2312.

Peckham, T. J.; Holdcroft, S., Structure-Morphology-Property Relationships of Non-Perfluorinated Proton-Conducting Membranes. *Advanced Materials* **2010,** 22, 4667-4690.

Pei, H. Q.; Hong, L.; Lee, J. Y., Polymer electrolyte membrane based on 2-acrylamido-2-methyl propanesulfonic acid fabricated by embedded polymerization. *Journal of Power Sources* **2006,** 160, 949-956.

Pivovar, B. S.; Wang, Y. X.; Cussler, E. L., Pervaporation membranes in direct methanol fuel cells. *Journal of Membrane Science* **1999,** 154, 155-162.

Qi, Z.; Kaufman, A., Open circuit voltage and methanol crossover in DMFCs. *Journal of Power Sources* **2002,** 110, 177-185.

Qian, W. M.; Wilkinson, D. P.; Shen, J.; Wang, H. J.; Zhang, J. J., Architecture for portable direct liquid fuel cells. *Journal of Power Sources* **2006,** 154, 202-213.

Ren, X.; Springer, T. E.; Zawodzinski, T. A.; Gottesfeld, S., Methanol Transport Through Nation Membranes. Electro-osmotic Drag Effects on Potential Step Measurements. *Journal of The Electrochemical Society* **2000,** 147, 466-474.

Rini, M.; Magnes, B. Z.; Pines, E.; Nibbering, E. T. J., Real-time observation of bimodal proton transfer in acid-base pairs in water. *Science* **2003,** 301, 349-352.

Rini, M.; Pines, D.; Magnes, B. Z.; Pines, E.; Nibbering, E. T., Bimodal proton transfer in acid-base reactions in water. *The Journal of chemical physics* **2004,** 121, 9593-9610.

Rini, M.; Pines, D.; Magnes, B. Z.; Pines, E.; Nibbering, E. T. J., Bimodal proton transfer in acid-base reactions in water. *Journal of Chemical Physics* **2004,** 121, 9593-9610.

Roelofs, K. S.; Hirth, T.; Schiestel, T., Sulfonated poly(ether ether ketone)-based silica nanocomposite membranes for direct ethanol fuel cells. *Journal of Membrane Science* **2010,** 346, 215-226.

Rohman, G.; Grande, D.; Laupretre, F.; Boileau, S.; Guerin, P., Design of porous polymeric materials from interpenetrating polymer networks (IPNs): Poly(DL-lactide)/poly(methyl methacrylate)-based semi-IPN systems. *Macromolecules* **2005,** 38, 7274-7285.

Roy, A.; Yu, X.; Dunn, S.; McGrath, J. E., Influence of microstructure and chemical composition on proton exchange membrane properties of sulfonated–fluorinated, hydrophilic–hydrophobic multiblock copolymers. *Journal of Membrane Science* **2009,** 327, 118-124.

Saarinen, V.; Himanen, O.; Kallio, T.; Sundholm, G.; Kontturi, K., Current distribution measurements with a free-breathing direct methanol fuel cell using PVDF-g-PSSA and Nafion (R) 117 membranes. *Journal of Power Sources* **2007,** 163, 768-776.

Sahu, A. K.; Bhat, S. D.; Pitchumani, S.; Sridhar, P.; Vimalan, V.; George, C.; Chandrakumar, N.; Shukla, A. K., Novel organic-inorganic composite polymer-electrolyte membranes for DMFCs. *Journal of Membrane Science* **2009,** 345, 305-314.

Saimani, S.; Dal-Cin, M. M.; Kumar, A.; Kingston, D. M., Separation performance of asymmetric membranes based on PEGDa/PEI semi-interpenetrating polymer network in pure and binary gas mixtures of CO2, N-2 and CH4. *Journal of Membrane Science* **2010,** 362, 353-359.

Saito, M.; Tsuzuki, S.; Hayamizu, K.; Okada, T., Alcohol and Proton Transport in Perfluorinated Ionomer Membranes for Fuel Cells. *J. Phys. Chem. B* **2006,** 110, 24410-24417.

Sankir, M.; Kim, Y. S.; Pivovar, B. S.; McGrath, J. E., Proton exchange membrane for DMFC and H-2/air fuel cells: Synthesis and characterization of partially fluorinated disulfonated poly(arylene ether benzonitrile) copolymers. *Journal of Membrane Science* **2007,** 299, 8-18.

Sarneski, J. E.; Surprenant, H. L.; Molen, F. K.; Reilley, C. N., Chemical-shifts and protonation shifts in C-13 Nuclear Magnetic-Resonance studies of aqueous amines. *Analytical Chemistry* **1975,** 47, 2116-2124.

Schmidt-Rohr, K.; Chen, Q., Parallel cylindrical water nanochannels in Nafion fuel-cell membranes. *Nature Materials* **2008,** 7, 75-83.

Sgreccia, E.; Chailan, J. F.; Khadhraoui, M.; Di Vona, M. L.; Knauth, P., Mechanical properties of proton-conducting sulfonated aromatic polymer membranes: Stress-strain tests and dynamical analysis. *Journal of Power Sources* **2010,** 195, 7770-7775.

Shah, M.; Basak, P.; Manorama, S. V., Polymer Nanocomposites as Solid Electrolytes: Evaluating Ion Polymer and Polymer-Nanoparticle Interactions in PEG-PU/PAN Semi-IPNs and Titania Systems. *Journal of Physical Chemistry C* **2010,** 114, 14281-14289.

Shuqin, S.; Vasiliki, M.; Panagiotis, T., How Far Are Direct Alcohol Fuel Cells From Our Energy Future? *Journal of Fuel Cell Science and Technology* **2007,** 4, 203-209.

Si, Y. C.; Lin, J. C.; Kunz, H. R.; Fenton, J. M., Trilayer membranes with a methanol-barrier layer for DMFCs. *Journal of the Electrochemical Society* **2004,** 151, A463-A469.

Silva, V. S.; Weisshaar, S.; Reissner, R.; Ruffmann, B.; Vetter, S.; Mendes, A.; Madeira, L. M.; Nunes, S., Performance and efficiency of a DMFC using non-fluorinated composite membranes operating at low/medium temperatures. *Journal of Power Sources* **2005,** 145, 485-494.

Singha, N. R.; Ray, S. K., Separation of Toluene-Methanol Mixtures by Pervaporation Using Semi-IPN Polymer Membranes. *Separation Science and Technology* **2010,** 45, 2298-2307.

Siwick, B. J.; Bakker, H. J., On the role of water in intermolecular proton-transfer reactions. *Journal of the American Chemical Society* **2007,** 129, 13412-13420.

So, S. Y.; Hong, Y. T.; Kim, S. C.; Lee, S. Y., Control of water-channel structure and state of water in sulfonated poly(arylene ether Sulfone)/diethoxydimethylsilane in situ hybridized proton conductors and its influence on transport properties for DMFC membranes. *Journal of Membrane Science* **2010,** 346, 131-135.

Sone, Y.; Ekdunge, P.; Simonsson, D., Proton conductivity of Nafion 117 as measured by a four-electrode AC impedance method. *Journal of the Electrochemical Society* **1996,** 143, 1254-1259.

Song, S.; Zhou, W.; Tian, J.; Cai, R.; Sun, G.; Xin, Q.; Kontou, S.; Tsiakaras, P., Ethanol crossover phenomena and its influence on the performance of DEFC. *Journal of Power Sources* **2005,** 145, 266-271.

Song, S. Q.; Tsiakaras, P., Recent progress in direct ethanol proton exchange membrane fuel cells (DE-PEMFCs). *Applied Catalysis B-Environmental* **2006,** 63, 187-193.

Staiti, P.; Arico, A. S.; Baglio, V.; Lufrano, F.; Passalacqua, E.; Antonucci, V., Hybrid Nafion-silica membranes doped with heteropolyacids for application in direct methanol fuel cells. *Solid State Ionics* **2001,** 145, 101-107.

References

Tang, H. L.; Wang, S. L.; Pan, M.; Jiang, S. P.; Ruan, Y. Z., Performance of direct methanol fuel cells prepared by hot-pressed MEA and catalyst-coated membrane (CCM). *Electrochimica Acta* **2007,** 52, 3714-3718.

Tay, S. W.; Zhang, X.; Liu, Z.; Hong, L.; Chan, S. H., Composite Nafion (R) membrane embedded with hybrid nanofillers for promoting direct methanol fuel cell performance. *Journal of Membrane Science* **2008,** 321, 139-145.

Tricoli, V.; Carretta, N.; Bartolozzi, M., A comparative investigation of proton and methanol transport in fluorinated ionomeric membranes. *Journal of the Electrochemical Society* **2000,** 147, 1286-1290.

Tripathi, B. P.; Chakrabarty, T.; Shahi, V. K., Highly charged and stable cross-linked 4,4 '-bis(4-aminophenoxy) biphenyl-3,3 '-disulfonic acid (BAPBDS)-sulfonated poly(ether sulfone) polymer electrolyte membranes impervious to methanol. *Journal of Materials Chemistry* **2010,** 20, 8036-8044.

Tsai, C. E.; Lin, C. W.; Hwang, B. J., A novel crosslinking strategy for preparing poly(vinyl alcohol)-based proton-conducting membranes with high sulfonation. *Journal of Power Sources* **2010,** 195, 2166-2173.

Tsang, E. M. W.; Zhang, Z. B.; Yang, A. C. C.; Shi, Z. Q.; Peckham, T. J.; Narimani, R.; Frisken, B. J.; Holdcroft, S., Nanostructure, Morphology, and Properties of Fluorous Copolymers Bearing Ionic Grafts. *Macromolecules* **2009,** 42, 9467-9480.

Vigier, F.; Rousseau, S.; Coutanceau, C.; Leger, J. M.; Lamy, C., Electrocatalysis for the direct alcohol fuel cell. *Topics in Catalysis* **2006,** 40, 111-121.

Wan, C. H.; Lin, C. H., A composite anode with reactive methanol filter for direct methanol fuel cell. *Journal of Power Sources* **2009,** 186, 229-237.

Wang, C. H.; Chen, C. C.; Hsu, H. C.; Du, H. Y.; Chen, C. R.; Hwang, J. Y.; Chen, L. C.; Shih, H. C.; Stejskal, J.; Chen, K. H., Low methanol-permeable polyaniline/Nafion composite membrane for direct methanol fuel cells. *Journal of Power Sources* **2009,** 190, 279-284.

Wang, H.; Xu, C. W.; Cheng, F. L.; Jiang, S. P., Pd nanowire arrays as electrocatalysts for ethanol electrooxidation. *Electrochemistry Communications* **2007,** 9, 1212-1216.

Wang, L.; Yi, B. L.; Zhang, H. M.; Liu, Y. H.; Xing, D. M.; Shao, Z. G.; Cai, Y. H., Sulfonated polyimide/PTFE reinforced membrane for PEMFCs. *Journal of Power Sources* **2007,** 167, 47-52.

Wang, S.; Sun, G. Q.; Wang, G. X.; Zhou, Z. H.; Zhao, X. S.; Sun, H.; Fan, X. Y.; Yi, B. L.; Xin, Q., Improvement of direct methanol fuel cell performance by modifying catalyst coated membrane structure. *Electrochemistry Communications* **2005,** 7, 1007-1012.

White, D. M.; Nye, S. A., C-13 NMR-study of poly(2,6-dimethyl-1,4-phenylene oxide)s-sites of amine incorporation. *Macromolecules* **1990,** 23, 1318-1329.

Wojciech, K.; Quang Trong, N.; Jean, N., Infrared investigations of sulfonated ionomer membranes. I. Water-alcohol compositions and counterions effects. *Journal of Applied Polymer Science* **1992,** 44, 951-958.

Wu, D.; Fu, R. Q.; Xu, T. W.; Wu, L.; Yang, W. H., A novel proton-conductive membrane with reduced methanol permeability prepared from bromomethylated poly(2,6-dimethyl-1,4-phenylene oxide) (BPPO). *Journal of Membrane Science* **2008,** 310, 522-530.

Wu, D.; Wu, L.; Woo, J. J.; Yun, S. H.; Seo, S. J.; Xu, T. W.; Moon, S. H., A simple heat treatment to prepare covalently crosslinked membranes from sulfonated poly(2,6-dimethyl-1,4-phenylene oxide) for application in fuel cells. *Journal of Membrane Science* **2010,** 348, 167-173.

Wu, D.; Xu, T. W.; Wu, L.; Wu, Y. H., Hybrid acid-base polymer membranes prepared for application in fuel cells. *Journal of Power Sources* **2009,** 186, 286-292.

Wu, H.; Zheng, B.; Zheng, X. H.; Wang, J. T.; Yuan, W. K.; Jiang, Z. Y., Surface-modified Y zeolite-filled chitosan membrane for direct methanol fuel cell. *Journal of Power Sources* **2007,** 173, 842-852.

Wu, L.; Huang, C.; Woo, J.-J.; Wu, D.; Yun, S.-H.; Seo, S.-J.; Xu, T.; Moon, S.-H., Hydrogen Bonding: A Channel for Protons to Transfer through Acid−Base Pairs. *Journal of Physical Chemistry B.* **2009,** 113, 12265–12270.

Wu, X.; He, G.; Gu, S.; Hu, Z.; Yao, P., Novel interpenetrating polymer network sulfonated poly (phthalazinone ether sulfone ketone)/polyacrylic acid proton exchange membranes for fuel cell. *Journal of Membrane Science* **2007,** 295, 80-87.

Xu, T. W.; Wu, D.; Wu, L., Poly(2,6-dimethyl-1,4-phenylene oxide) (PPO)-A versatile starting polymer for proton conductive membranes (PCMs). *Progress in Polymer Science* **2008,** 33, 894-915.

Xue, Y.; Fu, R.; Wu, C.; Lee, J. Y.; Xu, T., Acid-base hybrid polymer electrolyte membranes based on SPEEK. *Journal of Membrane Science* **2010,** 350, 148-153.

Yamaguchi, T.; Kuroki, H.; Miyata, F., DMFC performances using a pore-filling polymer electrolyte membrane for portable usages. *Electrochemistry Communications* **2005,** 7, 730-734.

Yamaguchi, T.; Miyata, F.; Nakao, S., Polymer electrolyte membranes with a pore-filling structure for a direct methanol fuel cell. *Advanced Materials* **2003,** 15, 1198-1201.

Yamaguchi, T.; Zhou, H.; Nakazawa, S.; Hara, N., An extremely low methanol crossover and highly durable aromatic pore-filling electrolyte membrane for direct methanol fuel cells. *Advanced Materials* **2007,** 19, 592-596.

Yamauchi, A.; Ito, T.; Yamaguchi, T., Low methanol crossover and high performance of DMFCs achieved with a pore-filling polymer electrolyte membrane. *Journal of Power Sources* **2007,** 174, 170-175.

Yang, C. C.; Chien, W. C.; Li, Y. J. J., Direct methanol fuel cell based on poly(vinyl alcohol)/titanium oxide nanotubes/poly(styrene sulfonic acid) (PVA/nt-TiO2/PSSA) composite polymer membrane. *Journal of Power Sources* **2010,** 195, 3407-3415.

Ye, Y. S.; Yen, Y. C.; Cheng, C. C.; Chen, W. Y.; Tsai, L. T.; Chang, F. C., Sulfonated poly(ether ether ketone) membranes crosslinked with sulfonic acid containing benzoxazine monomer as proton exchange membranes. *Polymer* **2009,** 50, 3196-3203.

Zapata, P.; Mountz, D.; Meredith, J. C., High-Throughput Characterization of Novel PVDF/Acrylic Polyelectrolyte Semi-Interpenetrated Network Proton Exchange Membranes. *Macromolecules* **2010,** 43, 7625-7636.

Zeng, W., Du, Y., Xue, Y., Frisch, H. L. In *Physical properties of polymers handbook*; 2nd ed.; J. E. Mark, Ed.; Springer: New York, **2007**, Vol. 16, pp 289-303.

Zhang, G.; Li, H. T.; Ma, W. J.; Zhang, L. Y.; Lew, C. M.; Xu, D.; Han, M. M.; Zhang, Y.; Wu, J.; Na, H., Cross-linked membranes with a macromolecular cross-linker for direct methanol fuel cells. *Journal of Materials Chemistry* **2011,** 21, 5511-5518.

Zhang, G. W.; Zhou, Z. T.; Li, C. Q.; Chu, H., Proton conducting composite membranes from sulfonated polyether ether ketone and SiO2. *Journal of Wuhan University of Technology-Materials Science Edition* **2009,** 24, 95-99.

Zhang, Y.; Wan, Y.; Zhang, G.; Shao, K.; Zhao, C. J.; Li, H. T.; Na, H., Preparation and properties of novel cross-linked sulfonated poly(arylene ether ketone) for direct methanol fuel cell application. *Journal of Membrane Science* **2010,** 348, 353-359.

Zhong, S. L.; Cui, X. J.; Dou, S.; Liu, W. C., Preparation and characterization of self-crosslinked organic/inorganic proton exchange membranes. *Journal of Power Sources* **2010,** 195, 3990-3995.

APPENDIX

PUBLICATIONS

Publications

<u>C. L. Fang</u>, D. Julius, S. W. Tay, L. Hong, and J. Y. Lee, "Ion pair reinforced semi-interpenetrating polymer network for direct methanol fuel cell application." *The Journal of Physical Chemistry B*, 2012, 116, 6416-6426.

<u>C. L. Fang</u>, D. Julius, S. W. Tay, L. Hong, and J. Y. Lee, "Preparation of semi-interpenetrating polymer networks with adjustable mesh width and hydrophobicity." *Polymer*, 2013, 54, 134-142.

<u>C. L. Fang</u>, X. N. Toh, Q. F. Yao, D. Julius, L. Hong, and J. Y. Lee, "Semi-interpenetrating polymer network proton exchange membranes with narrow and well-connected hydrophilic channels." *Journal of Power Sources*, 2013, 226, 289-298.

Y. Ma, <u>C. L. Fang</u>, G. Ji, B. Ding, J. Y. Lee, "Rational Design of Fe-doped Macro/Mesoporous Mn_xO_y with Extended Cycle Stability for Battery Applications." In preparation.